DEPOSITIONAL AND PALEOENVIRONMENTAL SETTINGS OF CRETACEOUS LIMESTONES IN THE GREATER ANTILLES

by

Alvin J. Bonilla-Rodríguez

Submitted to the Department of Geology and the Faculty of the Graduate School of The University of Kansas in partial fulfillment of the requirements for the degree of Doctor of Philosophy

Advisory Committee:

Luis A. González, Chair

Robert H. Goldstein

Douglas Walker

Bruce S. Lieberman

Edith L. Taylor

Date Defended: 09/08/2014

The dissertation committee for Alvin J. Bonilla-Rodríguez certifies
that this is the approved version of the following dissertation:

DEPOSITIONAL AND PALEOENVIRONMENTAL SETTINGS OF CRETACEOUS LIMESTONES IN THE GREATER ANTILLES

Advisory Committee:

Luis A. González, Chair

Date Approved: 09/08/2014

ABSTRACT

Alvin J. Bonilla-Rodríguez, Ph.D.
Department of Geology, September 2014
The University of Kansas

The first part of this research examines uncertainties surrounding the middle Cretaceous Antillean rudist biostratigraphy from fossiliferous limestones in the Greater Antilles and adds chemostratigraphic controls to constrain their stratigraphic ranges. In particular, this study shows the practical uses of strontium isotope stratigraphy in tectonically complex areas that lack good biostratigraphic controls. Our results show similar strontium isotope ($^{87}Sr/^{86}Sr$) derived ages from the middle Cretaceous rudist specimens collected in Puerto Rico (112.43Ma), the Dominican Republic (112.62 Ma) and Jamaica (112.68 Ma). Moreover, these derived ages agree with the presumed depositional age of related rudist taxa from the Gulf of Mexico (114.03-111.55 Ma). Strontium isotope stratigraphy is also used to constrain the depositional age of the Late Cretaceous rudist assemblage from southwestern Puerto Rico. The $^{87}Sr/^{86}Sr$ derived numerical ages (84.45Ma) from these rudist specimens are consistent with the inferred stratigraphic range of related rudist taxa from Jamaica. In this study we present the first Aptian/Albian Antillean carbon isotope ($\delta^{13}C$) chemostratigraphy from the Hatillo Limestone in the Dominican Republic with age control provided by $^{87}Sr/^{86}Sr$ derived ages, published ammonite, rudist, and foraminiferal biostratigraphy, and U/Pb zircon dates. The Antillean $\delta^{13}C$ profiles provide insights into middle Cretaceous ocean circulation within the Caribbean and Circum-Caribbean regions.

The second part of this research examines the uncertainties surrounding the response of tropical oceans to Cretaceous greenhouse conditions and the effects of enhanced evaporation to calcite $\delta^{18}O$ signatures. For this study, the analyzed material consisted of Late Cretaceous rudist

specimens collected in southwestern Puerto Rico. Fluid inclusions from marine cements precipitated within the inner cavities of rudists were used to derive paleosalinities (35.3 to 41.2 ppt). The effect of these salinities on the calcite $\delta^{18}O$ values was evaluated using temperature and salinity reconstructions based on the Railsback et al. (1989) model. The scenarios used to calculate sea surface temperatures resulted in paleotemperatures of up to 6°C higher than present day conditions. These results suggest that enhanced evaporative conditions dominated the paleotropics, and agree with global circulation and mass balance models, which predict warmer and saline conditions for tropical and sub-tropical regions during the Cretaceous.

The final chapter of this dissertation explores the socioeconomic effect of Caribbean reef degradation and utilizes the knowledge gained in this and other studies to provide ideas for mitigation. During the Cretaceous, reef ecosystems experienced a major ecological shift that included domination by rudist bivalves and scleractinian corals during the Early Cretaceous and by rudist bivalves during the middle to Late Cretaceous. The Cretaceous ecological shift, however, took approximately 30 Ma to happen, while the current warming rates for tropical oceans suggest that the temperature tolerance of corals will be exceeded within a few decades. Because the timing for genetic adaptation is longer than the rate of climate change and global warming, the genetic mapping of corals and bivalve should be a priority in order to create heat resistant coral stocks.

ACKNOWLEDGMENTS

I would like to thank Dr. Hernán Santos and Dr. Wilson Ramírez at the University of Puerto Rico for their valuable feedback toward the design of this research and their logistic assistance during my fieldwork seasons in Puerto Rico and the Dominican Republic. I would give special thanks to my friend and colleague Dr. Jorge Velez-Juarbe at the Florida Museum of Natural History for his field assistance in Puerto Rico and the Dominican Republic, and his valuable feedback in the improvement of part of this manuscript. Thanks to Dr. Greg A. Ludvigson and Wayne Dickerson for their assistance with the Cathodoluminescence microscope at the Kansas Geological Survey. I would like to thank Greg Cane and Masato Ueshima at the University of Kansas KECK Paleoenvironmental and Environmental Stable Isotope Laboratory (K-PESIL) for their assistance generating the stable isotope ($\delta^{13}C$ and $\delta^{18}O$) and trace element (Sr, Mn and Fe) data presented in this dissertation. Thanks to Dr. Robert Goldstein for his valuable feedback on the overall research project and his assistance generating the fluid inclusion data presented in Chapter 4. I would like to thanks Dr. J. Douglas Walker and Josh Feldman at the University of Kansas Isotope Geochemistry Laboratories for their valuable help generating the strontium isotope ($^{87}Sr/^{86}Sr$) data presented in Chapters 2 and 4. Thanks to Dr. Bradley D. Cramer at the University of Iowa and my friend Diana Ortega-Ariza, PhD Candidate at the University of Kansas for their valuable input to improve part of this manuscript. I would like to thank the staff at the University of Kansas, Department of Geology, especially to Yolanda Davis and Ian Rowell for their help throughout my years at the University of Kansas. To my advisor Dr. Luis A. González, whose collaboration and support made this research possible, thank you for your patience, guidance and opportunity to grow as a professional.

Thanks to the Dominican Republic National Geological Survey (SGN), especially to Engineer Santiago J. Muñoz-Tapia (SGN director) for their logistical assistance during our field season in the Dominican Republic. Thanks to Hugo Domínguez (Everton Minera Dominicana) for his field logistical assistance also in the Dominican Republic. I would like to thank the BarrickGold Corporation, Méjico Angeles (Director of Government Affairs Barrick Gold Corporation – Pueblo Viejo) and José Polanco (Geology Division) for their assistance in the Barrick Gold mining grounds in the Dominican Republic. Thanks to the staff at the University of the West Indies Geological Museum, the organizing committee of the Ninth International Congress on Rudist Bivalves, and specially to Dr. Simon Mitchell for the opportunity of expanding this study to Jamaica.

I would also like to express my appreciation to the institutions that provided financial support for this research: the University of Kansas, Kansas Interdisciplinary Carbonate Consortium (KICC), 2011 ENCANA scholarship, the 2010 Geological Society of America (GSA) Graduate Student Research Grant, the 2010 America Association of Petroleum Geologist (AAPG) Grant-in-aid - Alexander and Geraldine Wanek Memorial Grant, the 2010 Society for Sedimentary Geology (SEPM) Student Assistance Grant - Robert J. and Ruth A. Weimer Student Research Grant, the KU Department of Geology and the KU Keck Paleoenvironmental and Environmental Stable Isotope Laboratory (KPESIL). Thanks to the University of Kansas's Climate Change Humans and Nature in the Global Environment (C-CHANGE), part of the National Science Foundation (NFS) Integrative Graduate Education and Research Traineeship (IGERT) program, for their financial support for two years

I would like to thank my parents, Alvin A. Bonilla and Doris Rodríguez, for the support and encouragement along this journey. To all the friends made at the University of Kansas,

especially to Wes Gap, Dr. Zhaoqi Li, Dr. Celina Suarez, Dr. Marina Suarez, Dr. Julie Retrum, Dr. Brian Platt, Diana Ortega-Ariza, Alejandra Rodríguez, Luis G. Montalvo, Jose A. Velez and Edgardo J. Pujols-Vazquez, thank you for your help and advice throughout all these years. Last, but not least, special thanks to my family, my wife Lorena Carmona-Moll and my daughter Camila I. Bonilla-Carmona, for bearing with me through the good and bad times of this journey.

A mi esposa e hija, gracias por su amplia tolerancia y apoyo…

TABLE OF CONTENTS

Chapter 1 - Introduction

The major emphasis of this dissertation is to better constrain the age ranges of the Antillean rudist biozones, in particular the middle Cretaceous *Coalcomana-Caprinuloidea* rudist assemblage, and to improve our understanding of the prevailing paleoceanographic conditions during deposition of these Cretaceous limestones (e.g. Johnson, 1996; Rojas et al., 1996; Skelton, 2003). Although the stratigraphic range of key rudist bivalves is commonly used to constrain the depositional age of Cretaceous fossiliferous successions in the Greater Antilles (Brown and Mitchell, 2010; Iturralde-Vinent, 1997; Rojas et al., 1996), the scarcity of age diagnostic fossils, e.g. ammonites and foraminifera, has limited the delineation of the stratigraphic ranges of the Antillean rudist assemblages. The age range of rudist assemblages is key to understanding of the major faunal collapses among the Caribbean rudist taxa believed to have been caused by changes in paleoceanographic conditions (Johnson, 1996 and 1999). Although high temperature and elevated salinity conditions are thought to have dominated the environments where rudist bivalves thrived (Fassell and Bralower, 1999; Johnson, 1996; Skelton, 2004; Zachos et al., 1994), there is little to no empirical data to support these inferences nor data on paleoceanographic conditions that would lead to interpreting increased salinity and temperatures.

In Chapters 2 and 3 biostratigraphic and chemostratigraphic techniques, such as carbon isotopes ($\delta^{13}C$) and strontium isotopes ($^{87}Sr/^{86}Sr$), are integrated to identify the stratigraphic positions of middle Cretaceous limestones in the Greater Antilles. These

include the fossiliferous limestones exposed in (1) south-central Puerto Rico (the Río Matón Limestone and Barrancas Limestone), (2) the Seibo tectonic terrane in the Dominican Republic (the Hatillo Limestone), and (3) Benbow Inlier in Jamaica (the Seafield Formation). The biostratigraphic records discussed in these chapters include caprinid rudist bivalves (e.g. Kaczor and Rogers, 1990; Skelton, 1996) and orbitolinid foraminifers (e.g. Douglass, 1961; Jiang and Robinson, 1987). In these limestones, the fossil content is characteristic of the *Coalcomana-Caprinuloidea* rudist assemblage (Brown and Mitchell, 2010; Myczyński and Iturralde-Vinent, 2005). In Chapter 2, strontium isotope (Sr^{87}/Sr^{86}) stratigraphy is used to derive numerical ages from requienid rudists collected in the Río Matón Limestone, the Hatillo Limestone, and the Seafield Formation. Derived ages (~112.5 Ma) close to the Aptian/Albian boundary obtained from the analyzed specimens compare well with the latest Aptian to Early Albian depositional age (114.03-111.55 Ma) of the *Coalcomana* interval zone reported in central Texas (Scott and Filkorn, 2007). In Chapter 3, the biostratigraphic record (rudist bivalves and orbitolinid foraminifers) and $\delta^{13}C$ chemostratigraphy from the Hatillo Limestone exposed in the Oriental and Central cordilleras of the Dominican Republic are used to improve the correlations established in Chapter 2. Published chronostratigraphic controls within the Hatillo Limestone (Kesler et al., 2005a and 2005b; Myczyński and Iturralde-Vinent, 2005) support our chemostratigraphic correlations with $\delta^{13}C$ profiles from the Vocontian Basin in France (Herrle et al., 2004), the Sierra Madre in Mexico (Bralower et al., 1999; Scholle and Arthur, 1980) and the Comanche Shelf in Texas (Phelps, 2010). The Late Aptian through Early Albian $\delta^{13}C$ record in the Greater Antilles is best correlated to the

European $\delta^{13}C$ profiles from the Vocontian Basin (Gale et al., 2011; Herrle et al., 2004), and seems to be associated with the dominance of western currents in the Tethys Ocean. The Albian $\delta^{13}C$ chemostratigraphic record of the Greater Antilles, however, is best correlated to the Gulf of Mexico records (Bralower et al., 1999; Phelps, 2010; Scholle and Arthur, 1980), and seems to be associated with the dominance of the Albian northward split surface current that flowed along the Greater Antilles volcanic arc through the Gulf of Mexico as modeled by Johnson (1999).

In Chapter 4, oxygen ($\delta^{18}O$) isotopes and fluid inclusions are used to investigate the Late Cretaceous paleoceanographic conditions (sea surface temperatures and salinities) from the Cotui Limestone exposed in southwestern Puerto Rico. This chapter also reports numerical ages based upon strontium isotope (Sr^{87}/Sr^{86}) analyses on preserved rudist shells. The Sr^{87}/Sr^{86} derived ages suggest a Late Santonian depositional age (84.45 Ma) for the Cotui Limestone. This depositional age supports the correlations of the rudist *Barrettia coatesi* (Chubb) and *Torreites tschoppi* (MacGillavey) in the Cotui Limestone with the same taxa from the Peter's Hill Limestone in Jamaica (Skelton, 1996). In this chapter, fluid inclusion analyses from marine cements found in the inner cavities of hippuritid rudists are used to derive sea surface salinities (35.3 to 41.2 ppt). The effect of these salinities on the calcite $\delta^{18}O$ values is evaluated using temperature and salinity reconstructions based on the Railsback et al. (1989) model. The three different scenarios used to calculate sea surface temperatures (SST) include: (1) equatorial western Atlantic conditions with constant 37 ppt salinities (SST: 28°C to 34°C), (2) the Red Sea and Mediterranean conditions at constant 37 ppt salinity (SST: 30°C to 37°C), and (3)

Red Sea and Mediterranean with salinity seasonal changes from 35.3 to 41.2 ppt (SST: 34°C to 38°C). These results suggest that enhanced evaporative conditions dominated the paleotropics, and agree with global circulation and mass balance models that predict warmer and more saline conditions for tropical and sub-tropical regions during the middle to Late Cretaceous.

Chapter 5 examines the socioeconomic impact of the degradation of Caribbean reefs. This chapter discusses (1) the anthropogenic stressed and natural disturbances that are thought to be influencing Caribbean reef degradation, (2) how climate change might increase the frequency and magnitude of these natural distances, (3) the historical path from 1960s healthy reefs to 2000s algal blooms and coral bleaching, (4) the current management policy focusing on establishment of marine protected areas (MPA) and no-take MPA, (5) the use of mariculture, and (6) a bold approach proposal to mitigate the socioeconomic impact of the Caribbean reefs degradation. The proposed bold approach focuses on mitigation and adaptation, rather than preservation. This approach uses the knowledge from the Cretaceous interval, where a major ecological shift occurred in reef ecosystems during the Early Cretaceous (rudist bivalves and scleractinian corals dominated reefs) and middle to Late Cretaceous (only rudist bivalve dominated reefs), to propose a new way for coral reef management. This includes the introduction into the reef ecosystems of coral and mollusk species resilient to enhanced temperature and salinities. Because the timing for normal genetic adaptation is most likely to take longer than the rate of change of climate, the genes of these organisms (specially of the mollusk) should be studied in greater detail and the mapping of their genome should be a priority.

Instead of reef ecosystems dominated by fleshy algae, the Caribbean reef ecosystems could be sustainable gardens of heat tolerant corals and mollusks. This could result in a viable addition or replacement for fisheries in the Caribbean region.

REFERENCES

Bralower, T. J., CoBabe, E., Clement, B., Sliter, W. V., Osburn, C. L., and Longoria, J., 1999. The record of global change in Mid-Cretaceous (Barremian-Albian) sections from the Sierra Madre, northeastern Mexico. Journal of Foraminiferal Research 29, 418-437.

Brown, I., and Mitchell, S. F., 2010. Lithostratigraphy of the Cretaceous succession in the Benbow Inlier, Jamaica. Caribbean Journal of Earth Science 41, 25-37.

Douglass, R. C., 1961. Orbitolinas from Caribbean islands. Journal of Paleontology 35, 475-479.

Fassell, M. L., Bralower, T. J., 1999. Warm, equable mid-Cretaceous: Stable isotope evidence. In: Barrera, E., Johnson, C. C. (Eds.), Evolution of the Cretaceous Ocean-Climate System. Geological Society of America Special Publication 332, 121-142.

Gale, A. S., Bown, P., Caron, M., Crampton, J., Crowhurst, S. J., Kennedy, W. J., Petrizzo, M. R., and Wray, D. S., 2011. The uppermost Middle and Upper Albian succession at the Col de Palluel, Hautes-Alpes, France: An integrated study (ammonites, inoceramid bivalves, planktonic foraminifera, nannofossils,

geochemistry, stable oxygen and carbon isotopes, cyclostratigraphy). Cretaceous Research 32, 59-130.

Herrle, J. O., Kössler, P., Friedrich, O., Erlenkeuser, H., and Hemleben, C., 2004. High-resolution carbon isotope records of the Aptian to Lower Albian from SE France and the Mazagan Plateau (DSDP Site 545): a stratigraphic tool for paleoceanographic and paleobiologic reconstruction. Earth and Planetary Science Letters 218, 149-161.

Iturralde-Vinent, M. A., 1997. Meeting Reports 1: Field Workshop, Dominican Republic July, 1997. Journal of Petroleum Geology 20, 489-491.

Jiang, M. J., and Robinson, E., 1987. Calcareous nannofossils and larger foraminifera in Jamaican rocks of Cretaceous to early Eocene age. In: Ahmad, R. (Eds.), Proceedings of a workshop on the status of Jamaican geology. Geological Society of Jamaica, Special Issue, 24-51.

Johnson, C. C., Barron, E. J., Kauffman, E. G., Arthur, M. A., Fawcett, P. J., Yasuda, M. K., 1996. Middle Cretaceous reef collapse linked to ocean heat transport. Geology 24, 376-380.

Johnson, C. C., and Kauffman, E. G., 2001. Cretaceous evolution of reef ecosystems: a regional synthesis of the Caribbean tropics, In: Stanley, G. D., Jr., (Ed.), The History and Sedimentology of Ancient Reef Ecosystems: Topics in Geobiology 17, 311-349.

Kaczor, L., and Rogers, J. J. W., 1990. The Cretaceous Aguas Buenas and Rio Matón limestones of southern Puerto Rico. Journal of South American Earth Sciences 3, 1-8.

Kesler, S. E., Campbell, I. H., Allen, C. M., 2005a. Age of the Los Ranchos Formation, Dominican Republic: Timing and tectonic setting of primitive island arc volcanism in the Caribbean region. Geological Society of America Bulletin 117, 987-995.

Kesler, S. E., Campbell, I. H., Smith, C. N., Hall, C. M., and Allen, C. M., 2005b. Age of the Pueblo Viejo gold-silver deposit and its significance to models for high-sulfidation epithermal mineralization. Society of Economic Geologists 100, 253–272.

Phelps, R. M., 2011. Middle-Hauterivian to lower-Campanian sequence stratigraphy and stable isotope geochemistry of the Comanche Platform, south Texas; unpublished Ph.D. thesis, The University of Texas, Austin, Texas, 198 p.

Myczyński, R., and Iturralde-Vinent, M., 2005. The late lower Albian invertebrate fauna of the Río Hatillo Formation of Pueblo Viejo, Dominican Republic. Caribbean Journal of Science 41, 782-796.

Railsback, L. B., Anderson, T. F., Ackerly, S. C., Cisne, J. L., 1989. Paleoceanographic modeling of temperature-salinity profiles from stable isotopic data. Paleoceanography 4, 585–591,

Rojas, R., Iturralde-Vinent, M., and Skelton, P. W., 1996. Stratigraphy, composition and age of Cuban rudist-bearing deposits. Revista Mexicana de la Ciencias Geológicas 12, 272-291.

Scott, R. W., 2002b. Upper Albian benthic foraminifers new in west Texas. The Journal of Foraminiferal Research 32, 43-50.

Scholle, P. A., and Arthur, M. A., 1980. Carbon isotope fluctuations in Cretaceous pelagic limestones: potential stratigraphic and petroleum exploration tool. AAPG Bulletin 64, 67-87.

Skelton, P. W., 1996. IGCP Project 364: Correlation of Caribbean ophiolites and volcanic arcs – field meeting. Episodes 19, 27-28.

Skelton, P.W.. 2003. The Cretaceous World. Cambridge University Press and The Open University, Cambridge, 350 p.

Zachos, J. C., Stott, L. D., Lohmann, K. C., 1994. Evolution of early Cenozoic marine temperatures. Paleoceanography 9, 353-387.

Chapter 2 - Strontium isotope ($^{87}Sr/^{86}Sr$) stratigraphy from the *Coalcomana-Caprinuloidea* rudist assemblage in the Greater Antilles (Puerto Rico, Dominican Republic and Jamaica)

ABSTRACT

The stratigraphic range of the *Coalcomana-Caprinuloidea* rudist assemblage from Puerto Rico, the Dominican Republic and Jamaica has been revised based on numerical ages derived from strontium isotope ($^{87}Sr/^{86}Sr$) analyses of the calcitic outer shell of requieniid rudists. The extent of diagenetic alteration was assessed by cathodoluminescence microscopy and trace element concentration analyses (Sr, Mg, Fe and Mn), and only the least altered shells were selected for the $^{87}Sr/^{86}Sr$ analyses. The $^{87}Sr/^{86}Sr$ analyses from all the analyzed Antillean rudists resulted in average ages close to the Aptian/Albian boundary (112.56 Ma). These results show that the Antillean *Coalcomana-Caprinuloidea* rudist assemblage is correlative to the latest Aptian to Early Albian *Coalcomana* interval zone from Texas and Mexico. There are, however, subtle differences in the orbitolinid foraminifer and rudist bivalve records of the Antillean *Coalcomana-Caprinuloidea* rudist assemblage that still need further revisions. In the Dominican Republic, for example, the orbitolinid fauna in the Central Cordillera include *Coskinolinoides texanus* (Keijzer), which is reported from middle Albian successions in Texas and Mexico. Moreover, the presence of primitive and advanced morphotypes of *Caprinuloidea* also suggests a possible bipartite division of the *Coalcomana-Caprinuloidea* rudist assemblage. Although the collected material from the localities with

the foraminifer *C. texanus* and the advanced form of *Caprinuloidea* failed the preservation screening for $^{87}Sr/^{86}Sr$ analyses, we speculate about the possible extension of the *Coalcomana-Caprinuloidea* rudist assemblage from the Aptian/Albian boundary through the middle Albian.

INTRODUCTION

During the latest Aptian to Albian interval, carbonate platforms extended from the Bahamas to the margins of the Gulf of Mexico across the Yucatán Peninsula and the Greater Antilles volcanic arc (Fig. 2.1) (Scott, 1990). On these carbonate platforms rudist bivalves proliferated and formed thick banks and reef deposits (Coogan, 1973 and 1977; Scott and Filkorn, 2007). In Texas and Mexico, the latest Aptian to Albian rudist biostratigraphy is based on correlations of rudist interval zones and ammonite zonations (Scott, 2002a). There are at least four latest Aptian to Albian rudist interval zones in Central Texas; (1) the latest Aptian to early Albian *Coalcomana* interval zone, (2) the middle Albian *Caprinuloidea* interval zone, (3) the early late Albian *Kimbleia* interval zones, and (4) the late Albian *Mexicaprina* interval zone (Scott, 2002a; Scott and Filkorn, 2007). Although the stratigraphic position of rudist assemblages, based on ammonite zonations, is now well understood in the Gulf Coast of North America and Mexico, the stratigraphic positions of related Antillean rudist taxa are less clear owing to structural complexity, limited outcrop and most importantly the lack of good biostratigraphic controls.

There are two identifiable Albian rudist interval zones in the Greater Antilles: (1) the lower to possibly middle Albian *Coalcomana-Caprinuloidea* rudist assemblage (Skelton, 1996), and (2) the upper Albian '*Tepeyacia* fauna' (Rojas et al., 1996). Of these rudist assemblages, the *Coalcomana-Caprinuloidea* is the one that is more widespread across the Greater Antilles, being found in Cuba (Rojas et al., 1996; Thiadens, 1936), the Dominican Republic (Iturralde-Vinent, 1997; Myczyński and Iturralde-Vinent, 2005), Jamaica (Brown and Mitchell, 2010), and Puerto Rico (Kaczor and Rogers, 1990; Skelton, 1996). *Coalcomana ramosa* (Boehm), the most dominant rudist in this assemblage, is endemic to the Caribbean province and is also found in the *Coalcomana* interval zone of Texas and Mexico (Alencáster and Pantoja-Alor, 1986; Scott, 2002a; Scott et al., 2007). In the Greater Antilles, the *Tepeyacia* fauna is restricted to the Camagüey Province in Cuba (Rojas et al., 1996). However, *Tepeyacia* is also known from the Colima and Baja California, Mexico, as well as its type locality in Puebla (Masse et al., 2007). Although the Baja California fauna is apparently lower Albian (Masse et al., 2007), the Colima fauna include the rudist genus *Immanitas*, which is certainly upper Albian based on correlations with ammonite zonations (Sano et al., 2013). In Cuba, the *Tepeyacia* fauna also contains key faunal equivalencies from the late Albian *Kimbleia* interval zone in the Gulf of Mexico, e.g. *Kimbleia albrittoni* (Perkins).

Seawater strontium isotope ($^{87}Sr/^{86}Sr$) variations correspond to competing contributions of strontium from continental weathering ($^{87}Sr/^{86}Sr \cong 0.710$), and hydrothermal release from the oceanic crust ($^{87}Sr/^{86}Sr \cong 0.703$) (Frijia and Parente, 2008; Palmer and Edmond, 1989; Spooner, 1976). As Phanerozoic variations of seawater

$^{87}Sr/^{86}Sr$ are now known in enough detail to derive numerical ages (McArthur et al., 2001), strontium isotope stratigraphy has become an important tool to establish global correlations. This technique has been successfully applied in rudist assemblages from the Mediterranean and Caribbean Tethys (Steuber, 2001; Steuber et al., 2002; Masse and Steuber, 2007; Steuber et al., 2007; Steuber and Schlüter, 2012). Strontium isotope stratigraphy offers an opportunity to correlate the Antillean rudist assemblages with the Texan rudist biostratigraphy. This study reports $^{87}Sr/^{86}Sr$ numerical ages from preserved calcitic outer shells of requieniid rudists collected from the Río Matón Limestone in Puerto Rico, the Hatillo Limestone in the Dominican Republic, and the Seafield Formation in Jamaica, in areas where *Coalcomana ramosa* (Boehm) was the dominant rudist species (Fig. 2.2). The aim of this paper is thus to elucidate the stratigraphic relevance of the Antillean *Coalcomana-Caprinuloidea* rudist assemblage.

GEOLOGIC SETTINGS

During the middle Cretaceous, the Greater Antilles region was part of an active volcanic island arc located between North and South America (Fig. 2.3; Pindell, 1991; Pindell and Kennan, 2009). In the Greater Antilles, the Cretaceous exposure is characterized by volcano-sedimentary successions in deformed igneous provinces (Puerto Rico; Schellekens, 1998) and/or tectonic terranes (Dominican Republic; Mann et al., 1991). In Jamaica, these volcano-sedimentary successions are exposed in a series of inliers surrounded by younger rocks (Brown and Mitchell, 2010). In these Cretaceous successions, the limestones are intercalated with volcanic and volcaniclastic rocks. Jolly

et al. (1998) attributed the limestones in these successions to shallow-water deposition during quiescent volcano-tectonic intervals. The units of interest for this study are exposed in the Central Igneous Province of Puerto Rico, the Seibo Tectonic Terrane in the Dominican Republic, and the Benbow Inlier of Jamaica (Fig. 2.4 – 2.6).

Puerto Rico

In Puerto Rico, there are three lenticular limestone units that contain fauna characteristic of the *Coalcomana-Caprinuloidea* rudist assemblage. These units are: (1) the Aguas Buenas Limestone member of the Torrecilla Formation, (2) the Río Matón Limestone member of Los Robles Formation and (3) the Barrancas Limestone member of the Magueyes Formation (Fig. 2.4). The most prominent of these units, the Río Matón Limestone, is exposed in south-central Puerto Rico. This unit is the basal member of Los Robles Formation, which occurs above the volcaniclastic Torrecilla Formation (Berryhill and Glover, 1960; Jolly et al., 1998). The Los Robles Formation above the Río Matón Limestone is composed of turbiditic sandstone and siltstone indicating deep marine deposition (Berryhill et al., 1960; Briggs, 1971). Although the rudist fauna in this unit indicates lower to possible middle Albian sub-stage, based upon the presence of *Coalcomana ramosa* and *Caprinuloidea perfecta* (Palmer) (Skelton, 1996), the current stratigraphic nomenclature of the Central Igneous Province of Puerto Rico denotes upper Albian to lowermost Cenomanian deposition for the Río Matón Limestone (Jolly et al., 1998; Kaczor and Roger, 1990; Pease and Briggs, 1960). Briggs (1969), and Kaczor and Roger (1990) suggested that the Torrecilla Breccia separated the Río Matón Limestone from the Aguas Buenas Limestone, hence the attribution of the Aguas Buenas Limestone

to the middle Albian and the Río Matón Limestone to the upper Albian to lowermost Cenomanian (Jolly et al., 1998; Pease and Briggs, 1960). The contrasting ages assigned to these limestones by previous regional studies and the omissions in these studies of the presence of the *Coalcomana-Caprinuloidea* rudist assemblages demonstrate the necessity to reevaluate the current stratigraphic nomenclature in the Central Igneous Province of Puerto Rico.

Dominican Republic

In the Dominican Republic, Albian carbonate deposition is reported in the Seibo Tectonic Terrane exposed in the Central and Oriental cordilleras (Fig. 2.5). These units are: (1) the Hatillo Limestone, and (2) Las Canas Limestone. Fossils from the *Coalcomana-Caprinuloidea* rudist assemblage are reported within the exposure of the Hatillo Limestone (Myczyński and Iturralde-Vinent, 2005). The Hatillo Limestone unconformably overlies the volcaniclastic Los Ranchos Formation. Toward the Central Cordillera the Las Canas Limestone covers the Hatillo Limestone, while in the Oriental Cordillera it is covered by the volcaniclastic Las Lagunas and Guayabas formations. Reliable stratigraphic controls are described from the Pueblo Viejo Gold District in the Central Cordillera, and include reports of fossils from the upper lower Albian *Douvilleiceras mammillatum* ammonite subzone in the basal units of the Hatillo Limestone (Myczyński and Iturralde-Vinent, 2005) and lower Albian zircon dates (110.9±0.8 Ma) from the underlying rocks of the upper Los Ranchos Formation (Kesler et al. 2005a, 2005b). Iturralde-Vinent (1997) reported preliminary stratigraphic ranges of

lower to possible middle Albian for the Hatillo Limestone, and upper Albian for the Las Canas Limestone.

Jamaica

The Seafield Formation is the uppermost limestone unit exposed in the Benbow Inlier in Central Jamaica (Fig. 2.6) (Brown and Mitchell, 2010). This limestone contains abundant rudists that are characteristic of the *Coalcomana-Caprinuloidea* rudist assemblage. The Seafield Formation overlies the volcaniclastic Airy Mountain Formation and is covered by the shales of the Río Nuevo Formation (upper Cenomanian to middle Turonian). The Seafield Formation consists of limestone units interbedded with mudstones, shales and conglomerates. The stratigraphic range of the Seafield Formation is based on the presence of the rudist *Coalcomana ramosa* (Brown and Mitchell, 2010) and the orbitolinid foraminifer *Orbitolina texana* (Roemer) (Jiang and Robinson, 1987), both restricted to the lower Albian in Central Texas (Scott, 2002b). Reports of the rudist *Texicaprina* in loose limestone blocks of the Seafield Formation, however, suggest that the stratigraphic range of the Seafield Formation extended up into the middle Albian (Brown and Mitchell, 2010).

MATERIALS AND METHODS

The calcitic outer shells of requieniid rudist bivalves from the Río Matón Limestone, Hatillo Limestone, and Seafield Formation were analyzed for strontium isotopes ($^{87}Sr/^{86}Sr$). The shells of caprinid rudists were originally composed mostly of aragonite with a very thin outer shell layer of low-Mg calcite (Skelton, 2013), which

makes them poor candidates for the $^{87}Sr/^{86}Sr$ analyses. Conversely, requeniid rudists contain thick outer shells originally composed of low-Mg calcite that are ideal for $^{87}Sr/^{86}Sr$ analyses. Caprinoid rudists, however, are useful for biostratigraphic correlations in Mexico and Texas, and can be used to explore the Antillean rudist biostratigraphy. The studied specimens were collected throughout four field seasons (Puerto Rico, Summer 2008 and 2009; the Dominican Republic, Fall 2010; Jamaica, Summer 2011), and are stored at the University of Kansas KECK Paleoenvironmental and Environmental Stable Isotope Laboratory (KPESIL).

In order to derive numerical ages from $^{87}Sr/^{86}Sr$ analyses, primary marine signatures and minor diagenetic effects need to be established. Our preservation filters consisted of cathodoluminescence (CL) microscopy and trace element concentration analyses (76 analyses). CL microscopy was conducted using a Reliotron III CL cathodoluminoscope attached to an Olympus BX41 research microscope with Diagnostic Instrument SPOT RT camera at the Kansas Geological Survey (KGS). In CL microscopy, luminescence is a function of the Fe^{2+} (inhibitor) and Mn^{2+} (activator) contents in the examined material (Dickson, 1990). Because calcite minerals that preserve the original marine geochemistry are generally non-luminescent (absence of Mn^{2+}), the trace elemental concentration analyses were restricted to non-luminescent areas of the collected rudist shells (Fig. 2.7).

The trace element concentration evaluation relied on the Sr, Mn and Fe concentrations. High Mn and Fe concentrations in skeletal components composed of low-Mg calcite are indicative of diagenetic alteration (Al-Aasm and Veizer, 1986). Because

diagenetic carbonates with low concentration of these trace elements are common in deposits with scarce Mn and Fe bearing minerals (Steuber et al., 2005), strontium concentrations were also used to evaluate degree of diagenetic alteration of our samples, as low Sr concentrations in low-Mg calcitic shells are indicative of diagenetic alteration (Veizer, 1983). For the trace element concentration analyses, about 100-350 μg of powdered sample was dissolved in 12 mL of 2% HNO3 and then analyzed by ICP-OES (Perkin Elmer Optima 5300DV) at the University of Kansas KECK Paleoenvironmental and Environmental Stable Isotope Laboratory (K-PESIL). The samples were extracted from polished surfaces of the rudist specimens using tungsten-carbide drill bits. ICP-OES measurements were calibrated using 4-point curves for Sr, Mn and Fe. Detection limits for the prepared solutions were 0.0002 mg/L Sr, 0.0004 mg/L Mn and 0.0038 mg/L Fe. For $^{87}Sr/^{86}Sr$ analyses only samples that contained high Sr (>900 ppm) concentrations, and low Mn (<60 ppm) and Fe (<250 ppm) concentrations were utilized (modified from: Steuber, 2001, and Masse and Steuber, 2007). From the 76 IPC-OES analyses only 20 samples passed the preservation filters.

For the $^{87}Sr/^{86}Sr$ analyses, about 1 mg of powdered sample was obtained from the same general area of the trace element concentration analyses and then dissolved in 3.5 N HNO_3. Strontium was separated from samples through ion-exchange columns filled with strontium-spec resin at the University of Kansas Isotope Geochemistry Laboratories. All samples were analyzed for high precision $^{87}Sr/^{86}Sr$ ratios on the Sector 54 Thermal Ionization Mass Spectrometer (TIMS) in the same laboratory. The applied isotope fractionation correction was $^{86}Sr/^{88}Sr = 0.1194$ using exponential correction. Isotope

ratios were adjusted to correspond to a value of 0.71248 on NBS987 for $^{87}Sr/^{86}Sr$ (external precision was 3ppm on ratio on standards during the duration of analyses) to be consistent with the McArthur et al. (2001) normalization. The precision of the derived numerical ages was calculated by combining the 2-sigma internal error of individual $^{87}Sr/^{86}Sr$ measurements (±0.000015), based upon replicate determinations of the NBS987, and the inferred errors from the McArthur et al. (2001) "look-up" table and $^{87}Sr/^{86}Sr$ seawater curve (Version 4: 08 / 04).

RESULTS

Preservation of $^{87}Sr/^{86}Sr$

The 14 analyzed rudist shells included: six from the Río Matón Limestone (Puerto Rico), one from the Barrancas Limestone (Puerto Rico), six from the Hatillo Limestone (Dominican Republic) and one from the Seafield Formation (Jamaica). Only seven of these rudist specimens met the criteria for low diagenetic alteration and were analyzed for strontium isotopes ($^{87}Sr/^{86}Sr$). These shells are listed on table 1 and are shown in figures 2.8 and 2.9. The Mn and Sr concentrations from all the studied rudist shells are shown in figure 2.8A. The diagenetic alteration of the collected shells decreased the Sr concentration and increased Mn concentrations. The use of 900 ppm Sr as the threshold for acceptable concentrations is supported by the fact that samples with Sr concentrations above 900 ppm resulted in constant $^{87}Sr/^{86}Sr$ values and samples with Sr concentration below 900 ppm contained lower $^{87}Sr/^{86}Sr$ values (Fig. 2.8B). The decreasing of $^{87}Sr/^{86}Sr$ values with diagenetic alteration is also reported from late Cretaceous rudist shells from

Jamaica (Steuber and Schlüter, 2012; Steuber et al. 2002). Steuber and Schlüter (2012) associated this pattern with island-arc setting where diagenetic fluids interact with mantle derived Sr. $^{87}Sr/^{86}Sr$ derived numerical ages are considered valid for six shells: three from Puerto Rico, two from the Dominican Republic and one from Jamaica (Table 2.1).

Stratigraphic ranges

Compared to the $^{87}Sr/^{86}Sr$ "look-up" table and reference curve for the Lower Cretaceous (McArthur et al., 2001), the analyzed specimens from Puerto Rico, the Dominican Republic and Jamaica resulted in ages close to the Aptian/Albian boundary (2012 geologic time scale). These results include $^{87}Sr/^{86}Sr$ derived ages of 112.56 Ma for the rudists from the Río Matón Limestone (Puerto Rico), 112.79 Ma for the rudists from Hatillo Limestone (Hato Mayor area – Dominican Republic), and 112.68 Ma for the rudist from the Seafield Formation (Jamaica) (Table 2.1; Fig. 2.9). Although the analyzed rudists yielded consistent average ages (mean = 112.67 Ma) close to the Aptian/Albian boundary (113Ma ±0.4), our analytical error (0.000015 $^{87}Sr/^{86}Sr$) and the inherent age uncertainty from the McArthur et al. (2001) "look-up" table resulted in age uncertainties as high as 0.93 Ma.

DISCUSSION

The latest Aptian to earliest Albian age for the Antillean *Coalcomana-Caprinuloidea* rudist assemblage compares well with that given for the *Coalcomana* interval zone in central Texas (Scott et al., 2007; Scott and Filkorn, 2007). This supports the observation of at least two middle Cretaceous rudist intervals in the Greater Antilles,

the *Coalcomana-Caprinuloidea* rudist assemblage and the *Tepeyacia* Fauna (Rojas et al., 1996; Skelton, 1996). Although precise independent biostratigraphic controls are rare in the Antillean successions, good biostratigraphic controls are reported at the base of the Hatillo Limestone in the Pueblo Viejo area of the Dominican Republic. In this area, Myczyński and Iturralde-Vinent (2005) reported fossils from the upper lower Albian *Douvilleiceras mammillatum* ammonite subzone, and Kesler et al. (2005a, 2005b) reported early Albian zircon dates from the upper Los Ranchos Formation (110.9±0.8 Ma). These ages, however, are in disagreement with the latest Aptian to earliest Albian $^{87}Sr/^{86}Sr$ derived ages for the Hatillo Limestone in the Hato Mayor area. This disparity can be explained with subtle but important orbitolinid foraminifer differences between the Hatillo Limestone in the Hato Mayor and Pueblo Viejo areas.

Orbitolinid foraminifers, like caprinoid rudists, have proven useful in the stratigraphic identification of middle Cretaceous strata in Mexico and Texas (Coogan, 1977; Scott, 2002a). The principal upper Aptian to Albian orbitolinid foraminifers used for dating fossiliferous successions are: upper Aptian to lower Albian, (1) *Orbitolina texana* (Roemer) and (2) *Paracoskinolina sunnilandensis* (Maync); middle to upper Albian (3) *Dictyoconus walnutensis* (Carsey), (4) *Coskinolinoides texanus* (Keijzer) and (5) *Barkerina barkerensis* (Frizzell and Schwartz); and the upper Albian (6) *Paracoskinolina coogani* (Scott) and (7) *Streptalveolina mexicana* (Scott). In the Hato Mayor area, Woodring (1954) reported the presence of *O. texana*. Thin sections generated from these localities revealed the presence of orbitolinid foraminifers identified as *P. sunnilandensis* and *Orbitolina subconcava* (Fig. 2.10B-C). These orbitolinid

foraminifers, and particularly the *O. texana* and *P. sunnilandensis,* support our $^{87}Sr/^{86}Sr$ derived ages close to the Aptian/Albian boundary for the Hatillo Limestone in the Hato Mayor area (Table 2.1). In the Pueblo Viejo area, however, Bowin (1966) reported the presence of *C. texanus* (Keijzer) in the same general area where Myczyński and Iturralde-Vinent (2005) reported fossils from the *Douvilleiceras mammillatum* ammonite subzone. The generated thin sections from the locality in the Pueblo Viejo area also contained orbitolinid foraminifers identified as *C. texanus* (Fig. 2.10A-B). This foraminifer suggests that the depositional range of the Hatillo Limestone in the Pueblo Viejo area extended up into the middle Albian.

A similar biostratigraphic pattern can be observed within the reported rudist taxa from the *Coalcomana-Caprinuloidea* rudist assemblage in the Greater Antilles, where the presence of primitive and advanced morphotypes of *Caprinuloidea* are reported (Fig. 2.11). The primitive form of *Caprinuloidea*, probably *C. septata* (Palmer) or *C. perfecta* (Palmer), was observed in the Río Matón Limestone (central Puerto Rico) and the Hatillo Limestone (Hato Mayor area, the Dominican Republic). Both of these localities yielded consistent $^{87}Sr/^{86}Sr$ derived ages close to the Aptian/Albian boundary (Table 2.1). The advanced form *Caprinuloidea*, probably *C. multitubifera* (Palmer) or *C. romeri*, was observed in the Barrancas Limestone (central Puerto Rico). Mitchell (2013) proposed lower Albian stratigraphic range for *C. ramosa*, *C. septata* and *C. multitubifera*, and middle Albian range for *C. romeri*. As with the reports of *Texicaprina* from the Seafield Formation (Brown and Mitchell, 2010), we suggest that the presence of the advanced

Caprinuloidea morphotypes indicates a possible extension of the deposition of the Barrancas Limestone into the middle Albian.

The $^{87}Sr/^{86}Sr$-derived ages coupled with the fossil assemblages of the Aptian/Albian units of the northeastern Caribbean indicate that the *Coalcomana-Caprinuloidea* rudist assemblage in the Greater Antilles has a stratigraphic range that extends from the Aptian/Albian transition to the middle Albian. An uppermost Aptian to lowermost Albian interval is characterized by the primitive *Caprinuloidea* rudist form and the orbitolinid foraminifers *O. texana, O. subconcava* and *P. sunnilandensis*, and a lower to middle Albian interval that is characterized by the presence of the advanced morphotypes of *Caprinuloidea* and the orbitolinid foraminifer *C. texanus.*

CONCLUSIONS

Strontium isotope stratigraphy from the *Coalcomana-Caprinuloidea* rudist assemblage in Puerto Rico, the Dominican Republic and Jamaica confirmed the practical use of rudist biostratigraphy, even though key biostratigraphic markers are scarce in the Greater Antilles. Although diagenetic alteration of original isotopic ratios limited the number of analyses for strontium isotope stratigraphy, the reported derived $^{87}Sr/^{86}Sr$ numerical ages resulted in average ages close to the Aptian/Albian boundary for the *Coalcomana-Caprinuloidea* rudist assemblage in Puerto Rico (112.56 Ma), the Dominican Republic (112.79 Ma) and Jamaica (112.68 Ma).

The biostratigraphic pattern, however, suggests that the stratigraphic levels within the *Coalcomana-Caprinuloidea* rudist assemblage extended from the Aptian/Albian

boundary to the middle Albian. This includes the uppermost Aptian to lower Albian *Coalcomana-Caprinuloidea* interval characterized by the presence of the primitive morphotypes of *Caprinuloidea*, and the orbitolinid foraminifers *O. texana* and *P. sunnilandensis.* Strontium isotope ($^{87}Sr/^{86}Sr$) derived dates from localities with this fossil assemblage resulted in ages close to the Aptian/Albian boundary. By contrast the lower to middle Albian fossil assemblage includes the advanced form of *Caprinuloidea* and the orbitolinid foraminifer *C. texanus.* In the Pueblo Viejo Area (the Dominican Republic), the lower to middle Albian stratigraphic range for this younger level of the *Coalcomana-Caprinuloidea* interval zone is supported by the early Albian zircon dates (110.9±0.8 Ma) from the upper Los Ranchos Formation (Kesler et al., 2005a; 2005b), the reports of fossils from the upper lower Albian *Douvilleiceras mammillatum* ammonite subzone at the base of the Hatillo Limestone (Myczyński and Iturralde-Vinent, 2005), and the presence of *C. texanus* in the Hatillo Limestone (Woodring, 1954).

REFERENCES

Al-Aasm, I. S., Veizer, J., 1986. Diagenetic stabilization of aragonite and low-Mg calcite; I. Trace elements in rudists. Journal of Sedimentary Petrology 56, 138-152.

Alencáster, G., Pantoja-Alor, J., 1986. Coalcomana ramosa (Boehm)(Bivalva-Hippuritacea) del Albiano Temprano del Cerro de Tuxpan, Jalisco. Boletín Sociedad Geológica Mexicana 47, 33-46.

Berryhill, H. L., Glover, L., 1960. Geology of the Cayey quadrangle, Puerto Rico: U.S. Geological Survey Miscellaneous Investigations Map I-319, scale 1:20000.

Berryhill, H. L., Briggs, R. P., Glover, L., 1960. Stratigraphy, sedimentation, and structure of Late Cretaceous rocks in eastern Puerto Rico-Preliminary report. American Association of Petroleum Geologists Bulletin 44, 137-155.

Bowin, C. O., 1966. Geology of central Dominican Republic; a case history of part of an island arc. Memoir - Geological Society of America, pp. 11-84.

Briggs, R. P., Gelabert, P. A., 1962. Preliminary report of the geology of the Barranquitas quadrangle, Puerto Rico: U.S. Geological Survey Miscellaneous Investigations Map I-336, scale 1:20000.

Briggs, R. P., 1967. The Malo and Cotorra Tuff in the Cretaceous of central Puerto Rico. In: Cohee, G. V. (Ed.), Changes in stratigraphic nomenclature by the U.S. Geological Survey, 1966. U.S. Geological Survey Bulletin I254-A, pp. A23-A29.

Briggs, R. P., 1971. Geologic map of the Orocovis quadrangle, Puerto Rico: U.S. Geological Survey Miscellaneous Investigations Map I-615, scale 1:20000.

Briggs, R. P., 1969. Change in stratigraphic nomenclature in the Cretaceous System, east-central Puerto Rico: U.S. Geological Survey Bulletin 1274-O, 31p.

Brown, I., Mitchell, S. F., 2010. Lithostratigraphy of the Cretaceous succession in the Benbow Inlier, Jamaica. Caribbean Journal of Earth Science 41, 25-37.

Coogan, A. H., 1973. New rudist from the Albian and Cenomanian of Mexico and adjacent South Texas. Revista del Instituto Mexicano del Petróleo 5, 51-83.

Coogan, A. H., 1977. Early and middle Cretaceous Hippuritacea (rudists) of the Gulf Coast. In: Bebout, D. G. and Loucks, R. G. (Eds.), Cretaceous carbonates of

Texas and Mexico. Bureau of Economic Geology Report of Investigations 89, pp. 32–70.

Dickson, T., 1990. Carbonate mineralogy and chemistry. In: Tucker, M., and Wright, P. (Eds.), Carbonate Sedimentology. Blackwell Science Publication, Oxford, United Kingdom, pp. 284-313.

Douglass, R. C., 1961. Orbitolinas from Caribbean islands. Journal of Paleontology 35, 475-479.

Draper, G., Mann, P., Lewis, J. F., 1994. Hispaniola. In: Donovan, S. K., and Jackson, T. A. (Eds.), Caribbean geology: an introduction. University of the West Indies Publisher's Association, Kingston, Jamaica, pp. 29-150.

Escuder Viruete, J., Díaz de Neira, A., Hernaiz Huerta, P.P., Monthel, J., J., G.S., Joubert, M., Lopera, E., Ullrich, T., Friedman, R., Mortensen, J., Pérez-Estaún, A., 2006. Magmatic relationships and ages of Caribbean Island arc tholeiites, boninites and related felsic rocks, Dominican Republic. Lithos 90, 161-186.

Frijia, G., Parente, M., 2008. Strontium isotope stratigraphy in the upper Cenomanian shallow-water carbonates of the southern Apennines: Short-term perturbations of marine $^{87}Sr/^{86}Sr$ during the oceanic anoxic event 2. Paleogeography, Paleoclimatology, Paleoecology 261, 15-29.

Glover, L., 1961. Preliminary report on the geology of the Coamo quadrangle, Puerto Rico: U.S. Geological Survey Miscellaneous Geologic Investigations Map I-335, scale 1:20000.

Iturralde-Vinent, M. A., 1997. Meeting Reports 1: Field Workshop, Dominican Republic July, 1997. Journal of Petroleum Geology 20, 489-491.

Jiang, M. J., Robinson, E., 1987. Calcareous nannofossils and larger foraminifera in Jamaican rocks of Cretaceous to early Eocene age. In: Ahmad, R. (Ed.), Proceedings of a workshop on the status of Jamaican geology. Geological Society of Jamaica, Special Issue, pp. 24-51.

Jolly, J. T., Lidiak, E. G., Schellekens, J. H., Santos, H., 1998. Volcanism, tectonics and stratigraphic correlations in Puerto Rico. In Lidiak, E. G. (Ed.), Tectonics and Geochemistry of the Northeastern Caribbean: Geological Society of America Special Paper 322, pp. 1-34.

Kaczor, L., Rogers, J. J. W., 1990. The Cretaceous Aguas Buenas and Rio Matón limestones of southern Puerto Rico. Journal of South American Earth Sciences 3, 1-8.

Kesler, S. E., Campbell, I. H., Allen, C. M., 2005a. Age of the Los Ranchos Formation, Dominican Republic: Timing and tectonic setting of primitive island arc volcanism in the Caribbean region. Geological Society of America Bulletin 117, 987-995.

Kesler, S. E., Campbell, I. H., Smith, C. N., Hall, C. M., Allen, C. M., 2005b. Age of the Pueblo Viejo gold-silver deposit and its significance to models for high-sulfidation epithermal mineralization. Society of Economic Geologists 100, 253–272.

Mann, P., Draper, G., Lewis, J. F., 1991. An overview of the geologic and tectonic development of Hispaniola. In: Mann, P., Draper, G., and Lewis, J. F. (Eds.), Geologic and tectonic development of the North America-Caribbean Plate boundary in Hispaniola. Geological Society of American Special Paper 262, pp. 1-28.

Masse, J.P., Beltramo, J., Martinez-Reyes, J., Arnaud-Vanneau, A., 2007. Revision of Albian Polyconitid and Monopleurid rudist bivalves from the New World. In: Scott, R. W. (Ed.), Cretaceous rudists and carbonate platforms: Environmental feedback. Society for Sedimentary Geology Special Publication 87, pp 167-180.

Masse, J.P., Steuber, T., 2007. Strontium isotope stratigraphy of Early Cretaceous rudist bivalves. In: Scott, R. W. (Ed.), Cretaceous rudists and carbonate platforms. Environmental feedback: Society for Sedimentary Geology Special Publication 87, pp.159-166.

McArthur, J. M., Howarth, R. J., Bailey, T. R., 2001. Strontium isotope stratigraphy: LOWESS version 3: Best fit to the marine Sr-isotope curve for 0-509 Ma and accompanying look-up table for deriving numerical age. The Journal of Geology 109, 155-170.

Mitchell, S.F., 2013. A revision of selected Lower Cretaceous American caprinoid rudists: implications for phylogeny and biostratigraphy. Caribbean Journal of Earth Science 45, 47-75.

Myczyński, R., Iturralde-Vinent, M., 2005. The late lower Albian invertebrate fauna of the Río Hatillo Formation of Pueblo Viejo, Dominican Republic. Caribbean Journal of Science 41, 782-796.

Palmer, M. R., Edmond, J. M., 1989. Cesium and rubidium in submarine hydrothermal fluids; evidence for recycling of alkali elements. Earth and Planetary Science Letter 95, 8-14.

Pease, M. H., Briggs, R. P., 1960. Geology of the Comerío quadrangle, Puerto Rico: U.S. Geological Survey Miscellaneous Geologic Investigations Map I-320, scale 1:20000.

Pindell, J. L., 1991. Geologic rationale for hydrocarbon exploration in the Caribbean and adjacent regions. Journal of Petroleum Geology 14, 237-257.

Pindell, J. L., Kennan, L., 2009. Tectonic evolution of the Gulf of Mexico, Caribbean and northern South America in the mantle reference frame: an update. Geological Society, London, Special Publications 328, 1-55.

Rogers, C. L., 1979. Geologic map of the Caguas quadrangle, Puerto Rico: U.S. Geological Survey Miscellaneous Geologic Investigations Map I-1152, scale 1:20000.

Rojas, R., Iturralde-Vinent, M., Skelton, P. W., 1996. Stratigraphy, composition and age of Cuban rudist-bearing deposits. Revista Mexicana de la Ciencias Geológicas 12, 272-291.

Sano, S., Iba, Y., Skelton, P.W., Aguilar-Pérez, J. and Tanabe, K., 2013. First record of *Immanitas* (Bivalvia, Hippuritida) from northern California,U.S.A. Caribbean Journal of Earth Science 45, 77-84.

Schellekens, J. H., 1998. Geochemical evolution and tectonic history of Puerto Rico. In: Lidiak, E. G. (Ed.), Tectonics and Geochemistry of the Northeastern Caribbean. Geological Society of America Special Paper 322, pp. 35-66.

Scott, R. W., 1990. Models and stratigraphy of mid-Cretaceous reef communities, Gulf of Mexico. SEPM (Society for Sedimentary Geology) Concepts in Sedimentology and Paleontology 2, 1-102.

Scott, R. W., 2002a. Albian Caprinid rudist from Texas re-evaluated. Journal of Paleontology 76, 408-423.

Scott, R. W., 2002b. Upper Albian benthic foraminifers new in west Texas. The Journal of Foraminiferal Research 32, 43-50.

Scott, R. W., Filkorn, H. F., 2007. Barremian-Albian rudist zones, U.S. Gulf of Mexico. In: Scott, R. W. (Ed.), Cretaceous rudists and carbonate platforms: Environmental feedback. Society for Sedimentary Geology Special Publication 87, pp. 167-180.

Scott, R. W., Molineux, A. N., Löser, H., and Mancini, E. A., 2007. Lower Albian sequence stratigraphy and coral buildups: Glen Rose Formation, Texas, U.S.A. In: Scott, R. W. (Ed.), Cretaceous rudists and carbonate platforms: Environmental feedback. Society for Sedimentary Geology Special Publication 87, pp 167-180.

Skelton, P. W., 1996, IGCP Project 364: Correlation of Caribbean ophiolites and volcanic arcs – field meeting. Episodes 19, 27-28.

Skelton, P.W., 2013. Rudist classification for the revised Bivalvia volumes of the 'Treatise on Invertebrate Paleontology.' Caribbean Journal of Earth Science 45, 9-33.

Spooner, E. T. C., 1976. The strontium isotopic composition of seawater, and seawater-oceanic crust interaction. Earth and Planetary Science Letter 31, 167-174.

Steuber, T., 2001. Strontium isotope stratigraphy of Turonian-Campanian Gosau-type rudist formations in the Northern Calcareous and Central Alps (Austria and Germany). Cretaceous Research 22, 429-441.

Steuber, T., Mitchell, S. F., Buhl, D., Gunter, G., Kasper, H. U., 2002. Catastrophic extinction of Caribbean rudist bivalves at the Cretaceous-Tertiary boundary. Geology 30, 999-1002.

Steuber, T., Korbar, T., Jelaska, V., Gušić, I., 2005. Strontium isotope stratigraphy of Upper Cretaceous platform carbonates of the island of Brač (Adriatic Sea, Croatia) – Implications for global correlation of platform evolution and biostratigraphy. Cretaceous Research 26, 741-756.

Steuber, T., Parente, M., Hagmaier, M., Immenhauser, A., Van Der Kooij, B., Frijia, G., 2007. Latest Maastrichtian species-rich rudist associations of the Apulian Margin of Salento (S Italy). In Scott, R. W. (Ed.), Cretaceous rudists and carbonate platforms: Environmental feedback. Society for Sedimentary Geology Special Publication 87, pp. 151-158.

Steuber, T., Schlüter, M., 2012. Strontium-isotope stratigraphy of Upper Cretaceous rudist bivalves: Biozones, evolutionary patterns and sea-level change calibrated to numerical ages. Earth-Science Review 114, 42-60.

Thiadens, A. A., 1936. On some caprinids and a monopleurid from southern Santa Clara. Proceedings of the Section of Sciences 39, 1132-1141.

Veizer, J. 1983. Trace elements and isotopes in sedimentary carbonates. In: Reeder, R. J. (Ed.), Carbonates: mineralogy and chemistry. Reviews in Mineralogy 11, pp. 265–299.

Woodring, W. P., 1954. Caribbean land and sea through the ages: Geological Society of America Bulletin 65, 719-732.

FIGURES AND TABLES

Table 2.1
Analytical results of calcitic shells from Puerto Rico, the Dominican Republic and Jamaica

Locality Sample ID	$^{87}Sr/^{86}Sr$	±2 s.e. $\times 10^6$	Sr	Mg	Fe	Mn		Age (Ma)	
Río Matón Limestone									
RM01-3	0.707254	15	1124	630	bdl	34	<113.90	112.98	>112.28
RM02-3	0.707262	15	1097	387	bdl	32	<113.66	112.73	>112.07
RM-04	0.707298	15	1106	1437	bdl	35			
RM-07	0.707277	15	1213	2014	bdl	31			
RM (mean)	0.707287	21					<112.93	112.05	>111.30
Puerto Rico (mean)	**0.707278**	**30**					**<113.93**	**112.56**	**>111.55**
Hatillo Limestone									
DA-03	0.707285	15	1267	1029	bdl	28			
DA-04	0.707285	15	1075	2120	bdl	31			
DA-05	0.707262	15	1296	1532	234	32			
DA-06	0.707262	15	1362	930	220	33			
DA (mean)	0.707273	15					<113.20	112.43	>111.80
DA01-1	0.707258	15	1154	2436	bdl	38	<113.78	112.85	>112.17
DA02-1	0.707244	15	1030	1143	bdl	27			
DA02-3	0.707250	15	1032	1270	bdl	20			
DA02-4	0.707254	15	1198	912	bdl	19			
DA02 (mean)	0.707249	17					<114.03	113.15	>112.36
Dominican Republic (mean)	**0.707260**	**27**					**<114.03**	**112.79**	**>111.82**
Seafield Formation									
JAM-06	0.707264	15	1321	3020	205	58			
Jamaica	**0.707264**	**15**					**<113.57**	**112.68**	**>112.01**

Numerical ages are derived from McArthur et al. (2001); bdl – below detection limit (average 190 ppm Fe); ±2 s.e. – 2 standard error.

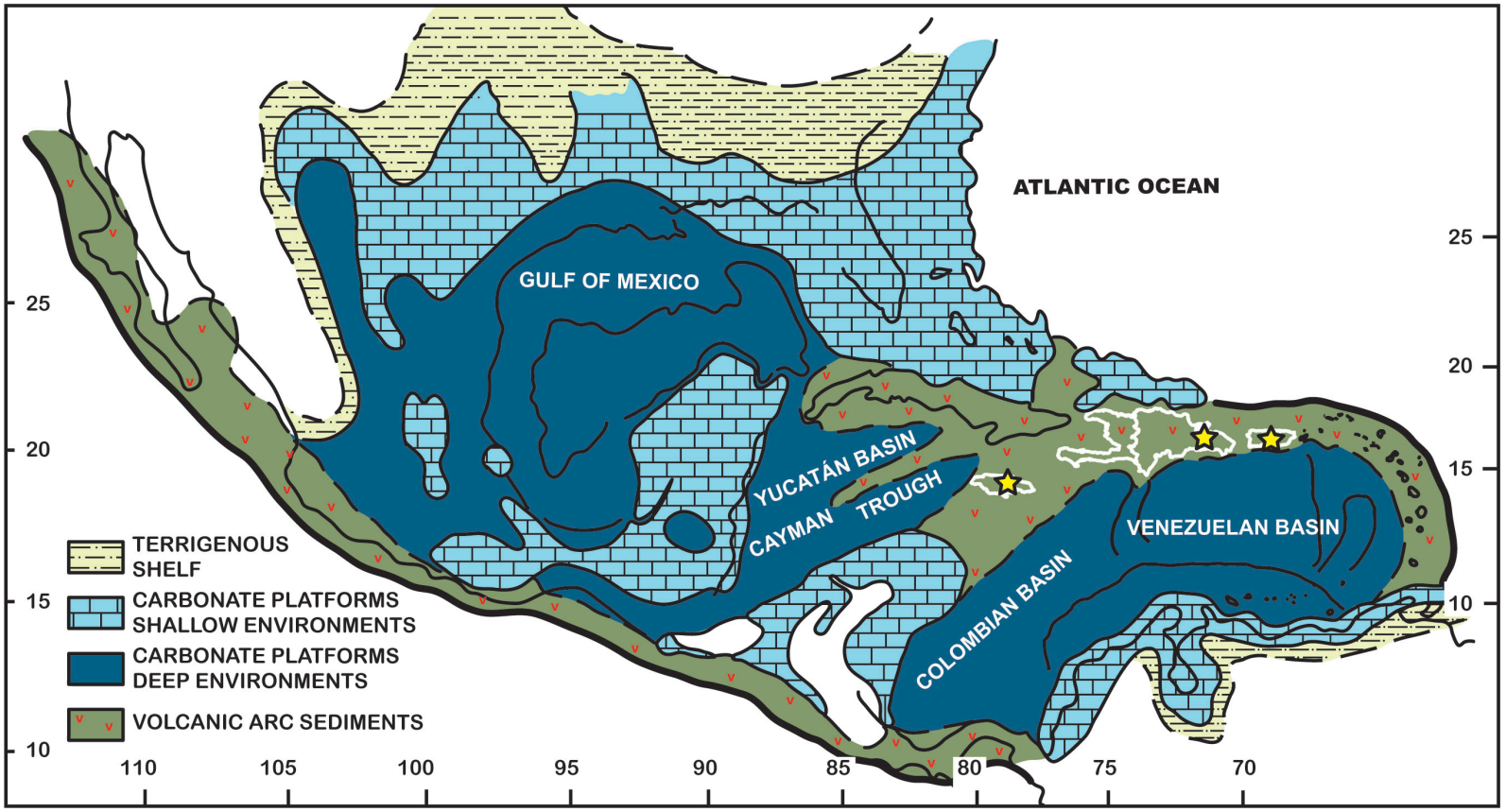

Figure 2.1. Distribution of Aptian-Albian Cretaceous sedimentary rocks in the Caribbean and circum-Caribbean regions (after: Scott and Filkorn, 2007; Pindell et al., 2009). Yellow stars show the general location of the study areas in Puerto Rico, the Dominican Republic and Jamaica (white outlines).

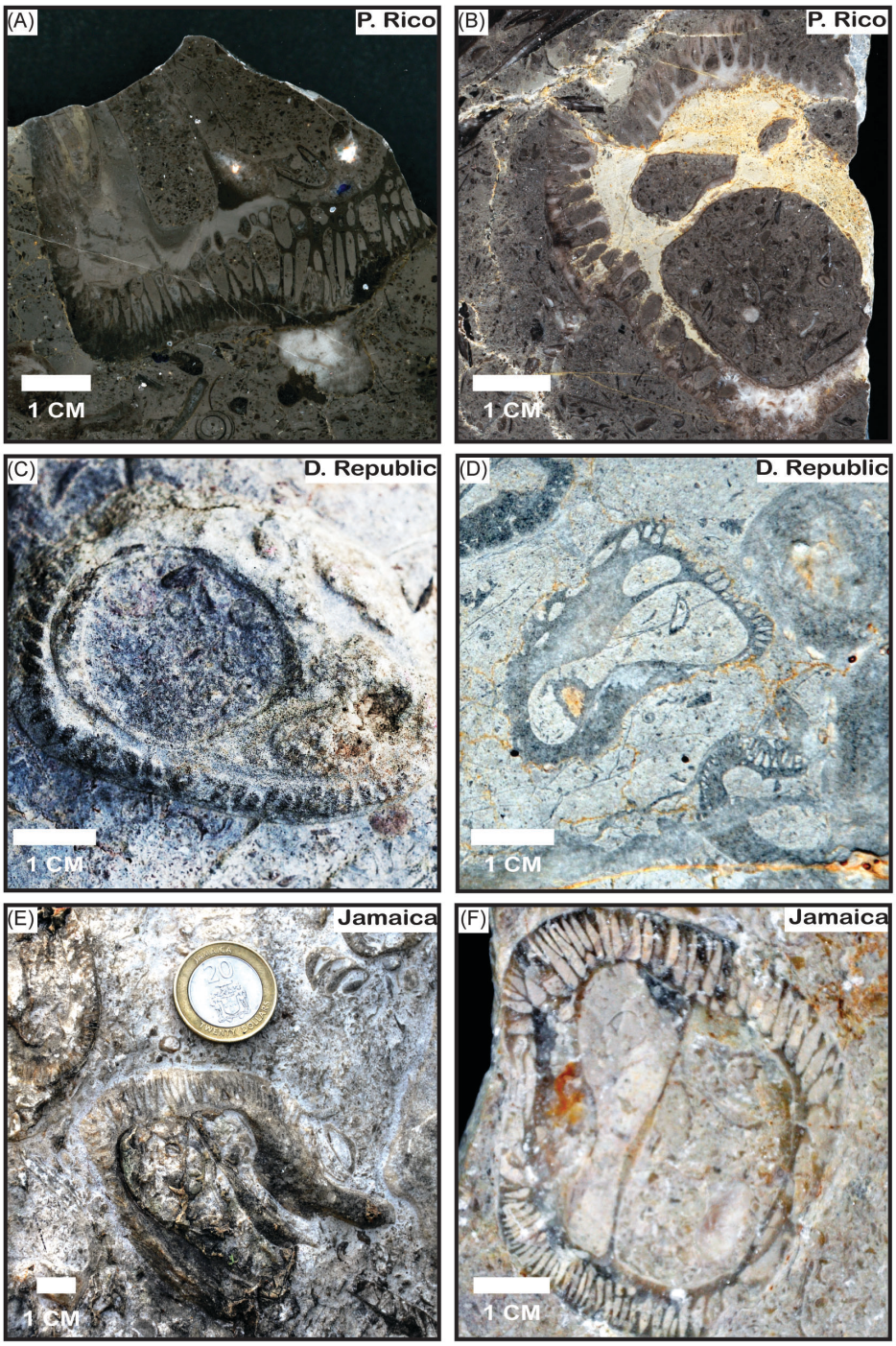

Figure 2.2. Rudist *C. ramosa* from Puerto Rico in the Barrancas Limestone (A) and Río Matón Limestone (B), from the Dominican Republic in the Hatillo Limestone (C and D), and Jamaica from the Seafield Formation (E and F).

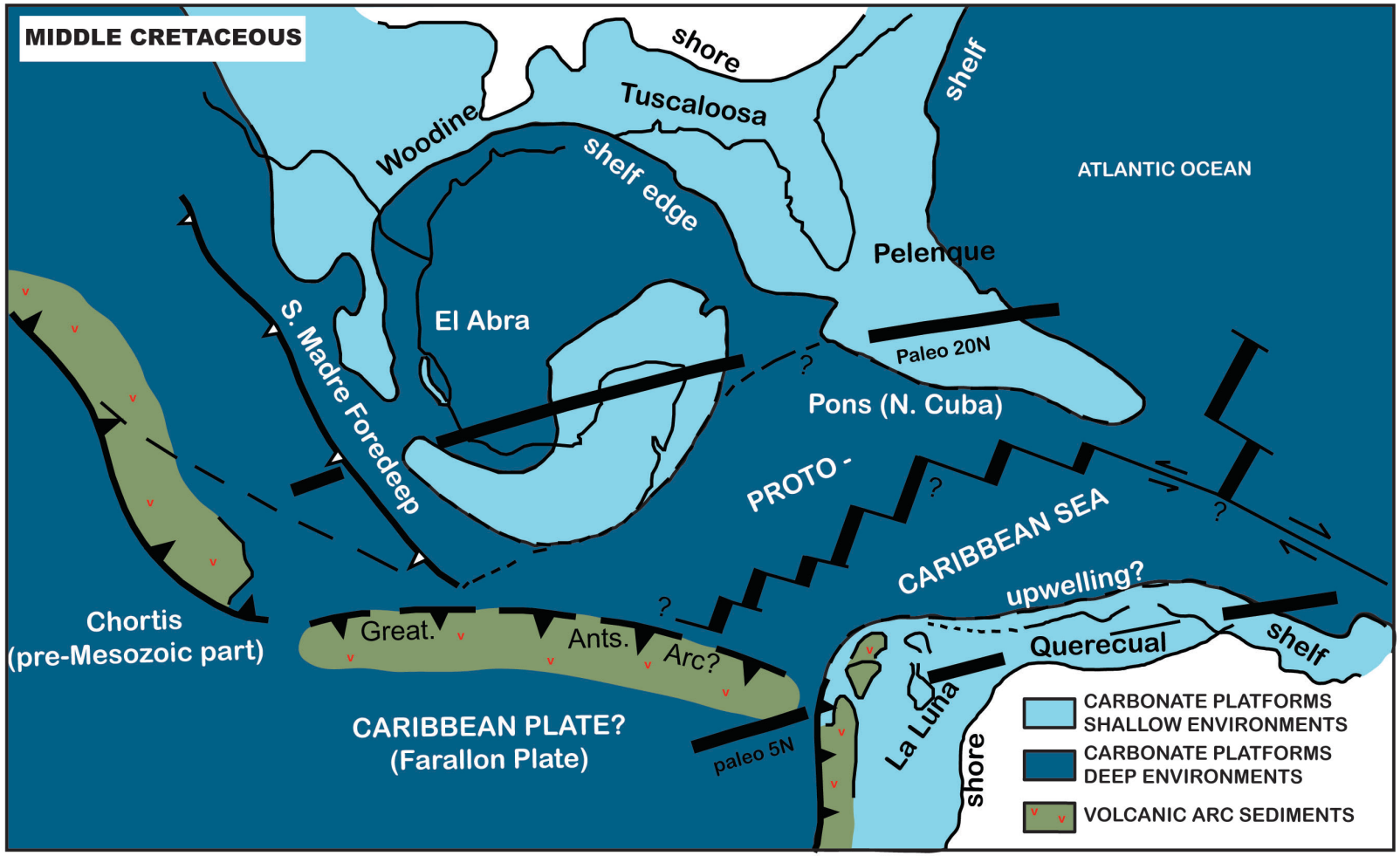

Figure 2.3. Mid-Cretaceous paleogeographic reconstruction of the Caribbean Basin showing the position of the Greater Antilles volcanic island arc between North America and South America (after: Pindell, 1991).

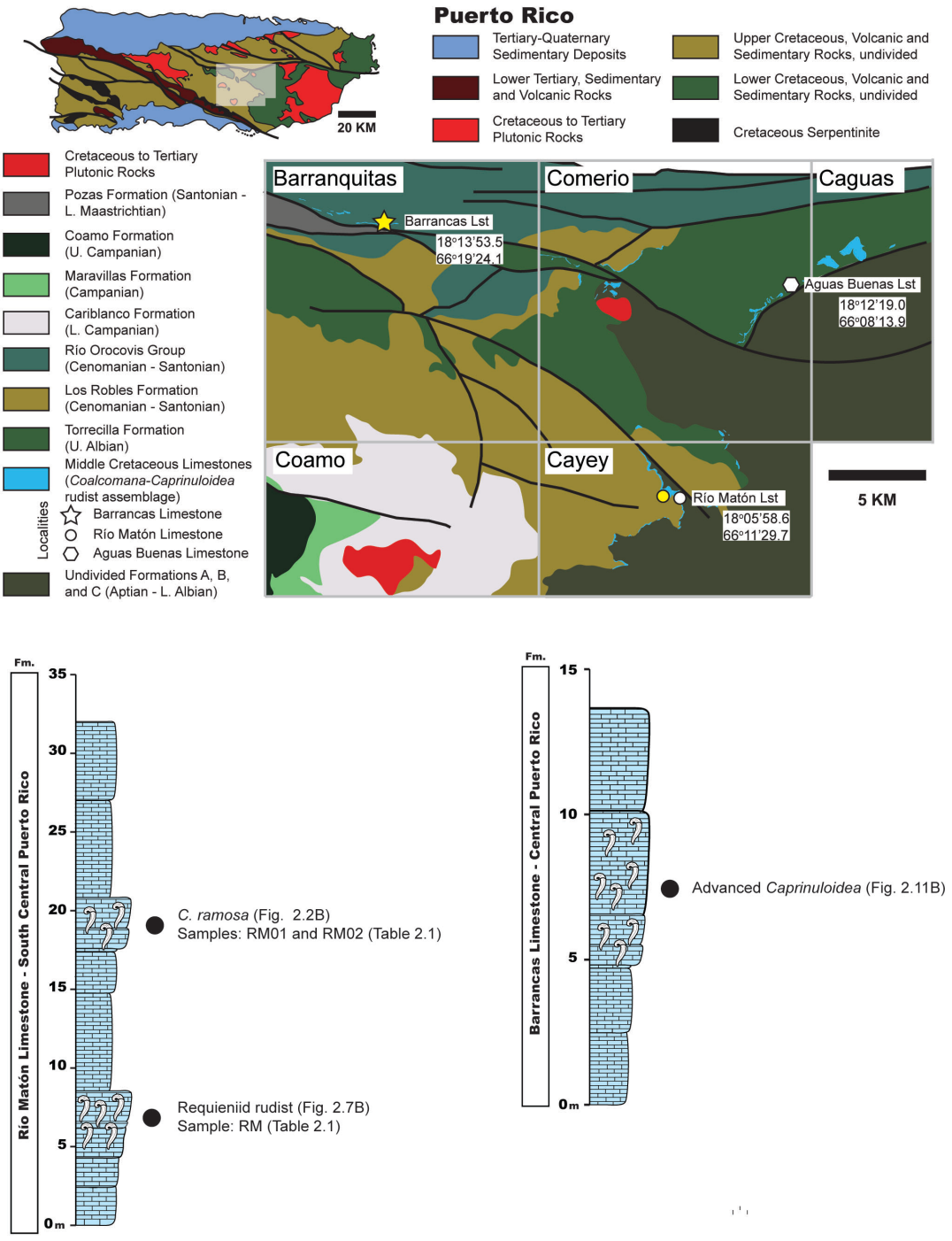

Figure 2.4. Geologic map of Puerto Rico showing the distribution of the general geology and a close-up of the Barranquitas, Coamo, Comerío, Cayey and Caguas USGS quadrangles (after: Berryhill and Glover, 1960; Briggs and Gelabert, 1962; Briggs, 1967; Glover, 1961; Jolly et al., 1998; Pease and Briggs, 1960; Roger, 1979). The stratigraphic profiles from the Río Matón and Barrancas limestones mark the position of the studied materials.

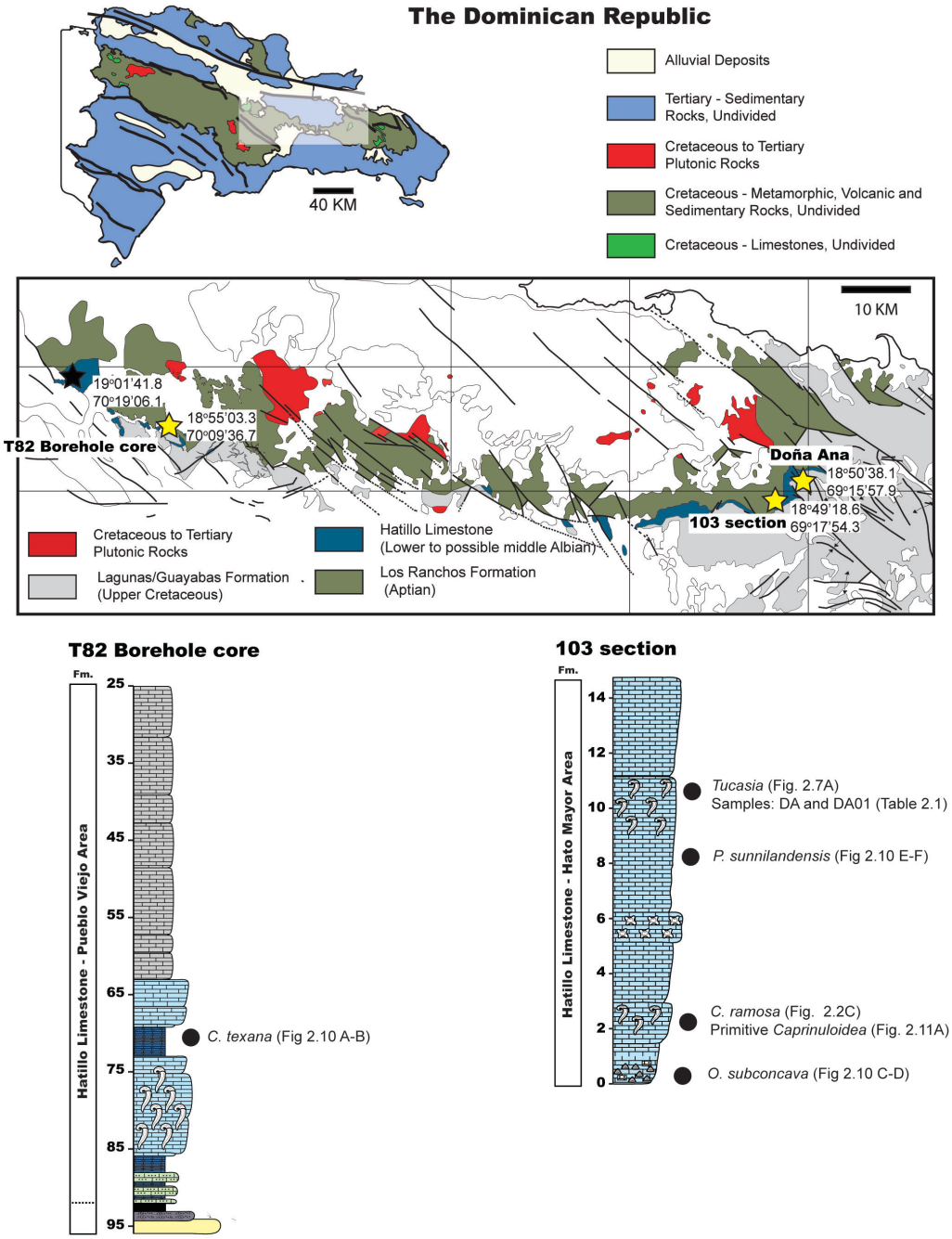

Figure 2.5. Geologic map of the Dominican Republic showing the distribution of the general geology and a close-up of the Seibo Tectonic Terrane (after: Escuder-Viruete et al. 2006; Draper et al., 1994). The stratigraphic profiles from the Hatillo Limestone from the borehole core T82 (Pueblo Viejo area) and 103 section (Hato Mayor area) mark the position of the studied materials. No stratigraphic profiles were measured from the Doña Ana outcrop.

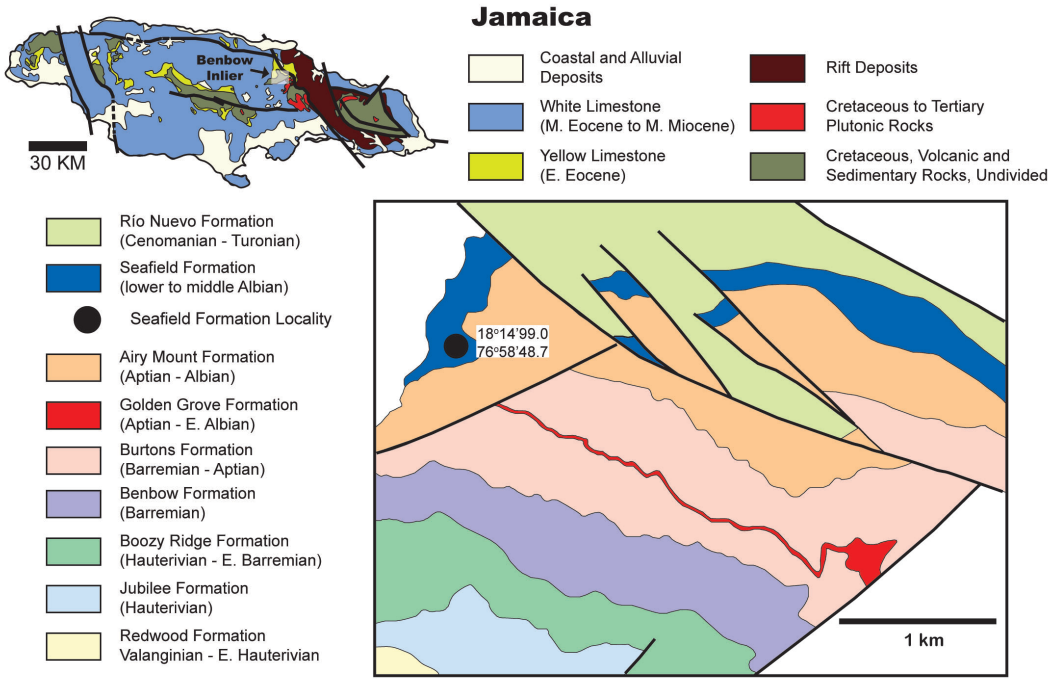

Figure 2.6. Geologic map of Jamaica showing the distribution of the general geology and a close-up of the Benbow Inlier (after: Brown and Mitchell, 2010). No stratigraphic profiles were measured from the Seafield Formation.

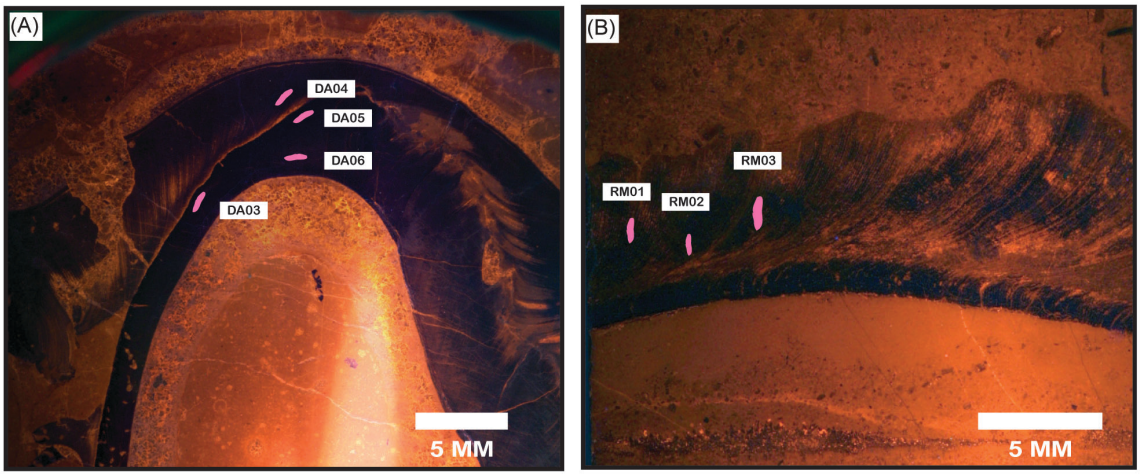

(C) Location	Sample ID	Sr	Mg	Fe	Mn
Puerto Rico					
Río Matón Limestone	RM01	673	2667	360	75
	RM02	687	2264	400	54
	RM03	916	2677	349	55
Dominican Republic					
Hatillo Limestone	DA03	1267	1029	bdl	28
	DA04	1075	2120	bdl	31
	DA05	1296	1532	bdl	32
	DA06	1361	930	bdl	33

Figure 2.7. (A) Cathodoluminescence image of the calcitic outer shell of the rudist *Toucasia* from the Hatillo Limestone in the Oriental Cordillera of the Dominican Republic showing the sampled areas for trace element concentrations (pink areas). (B) Cathodoluminescence image of the calcitic outer shell of a requieniid rudist from the Río Matón Limestone in central Puerto Rico showing the sampled areas (pink areas). (C) Table showing the analytical results of trace element concentrations (underlined sample ID – passed preservation criteria; red labels indicate results outside the preservation ranges.

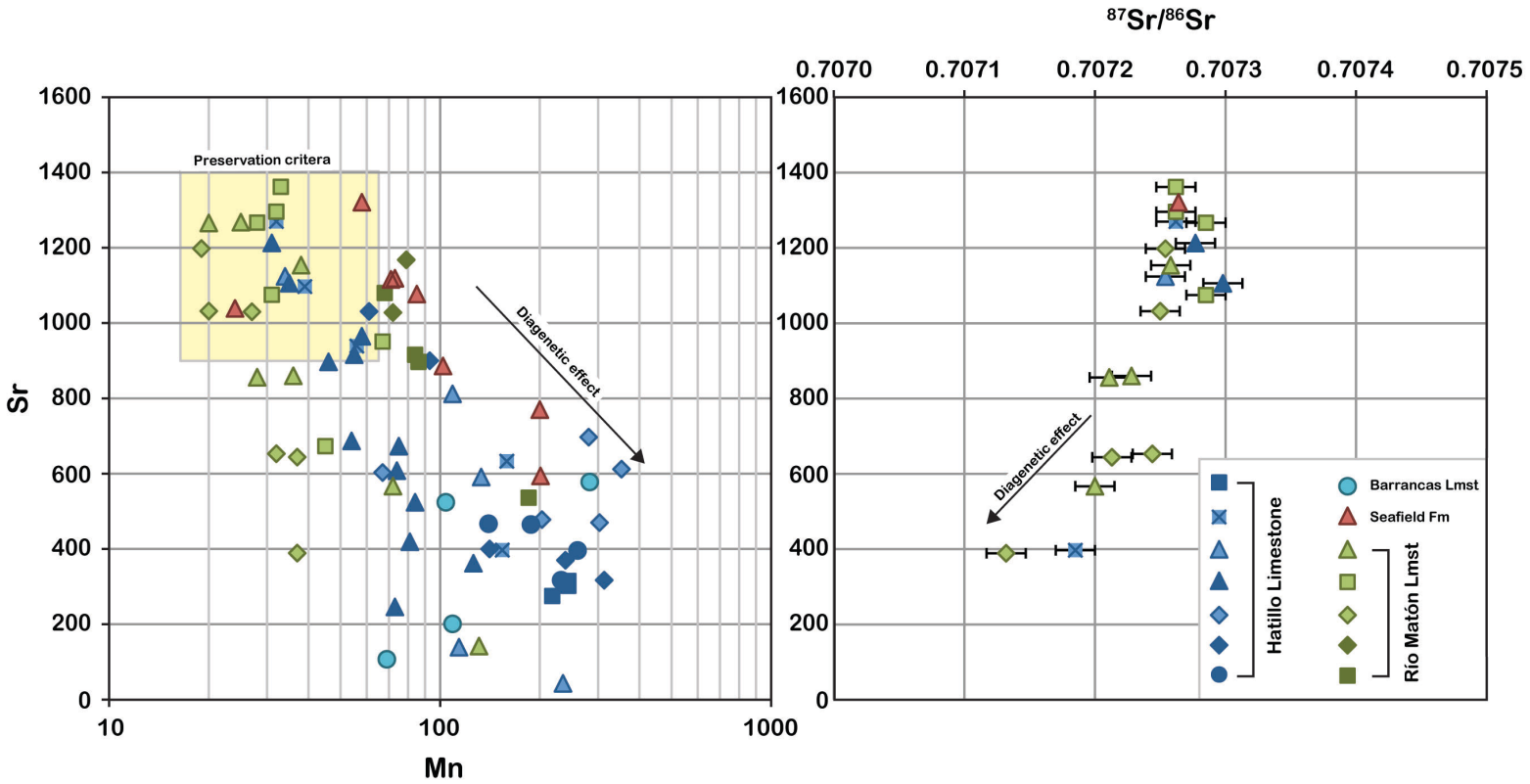

Figure 2.8. (A) Mn vs. Sr cross plot from the analyzed requieniid rudists showing the diagenetic alteration pattern of our low-Mg calcitic shells (B) $^{87}Sr/^{86}Sr$ vs. Sr concentrations cross plot showing lower $^{87}Sr/^{86}Sr$ values in sample with Sr concentrations <900 ppm. (Puerto Rico – blue; the Dominican Republic – green; Jamaica – red).

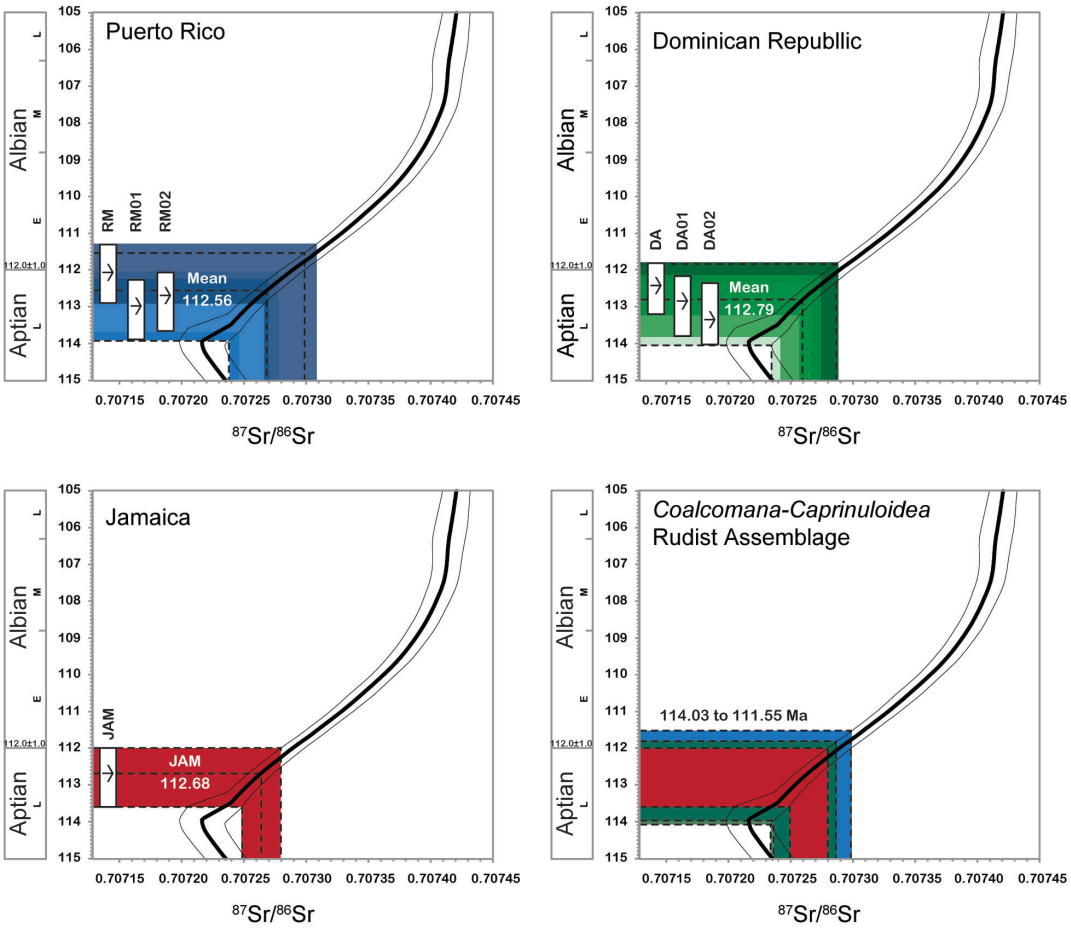

Figure 2.7. Numerical ages derived from strontium isotope stratigraphy of requieniid rudists collected in Río Matón Limestone (Puerto Rico), the Hatillo Limestone (Hato Mayor area, the Dominican Republic) and Seafield Formation (Jamaica). The vertical bars indicate the maximum and minimum ages associated with the analytical precision of samples and from uncertainties of the seawater strontium isotope curve of McArthur et al. (2001).

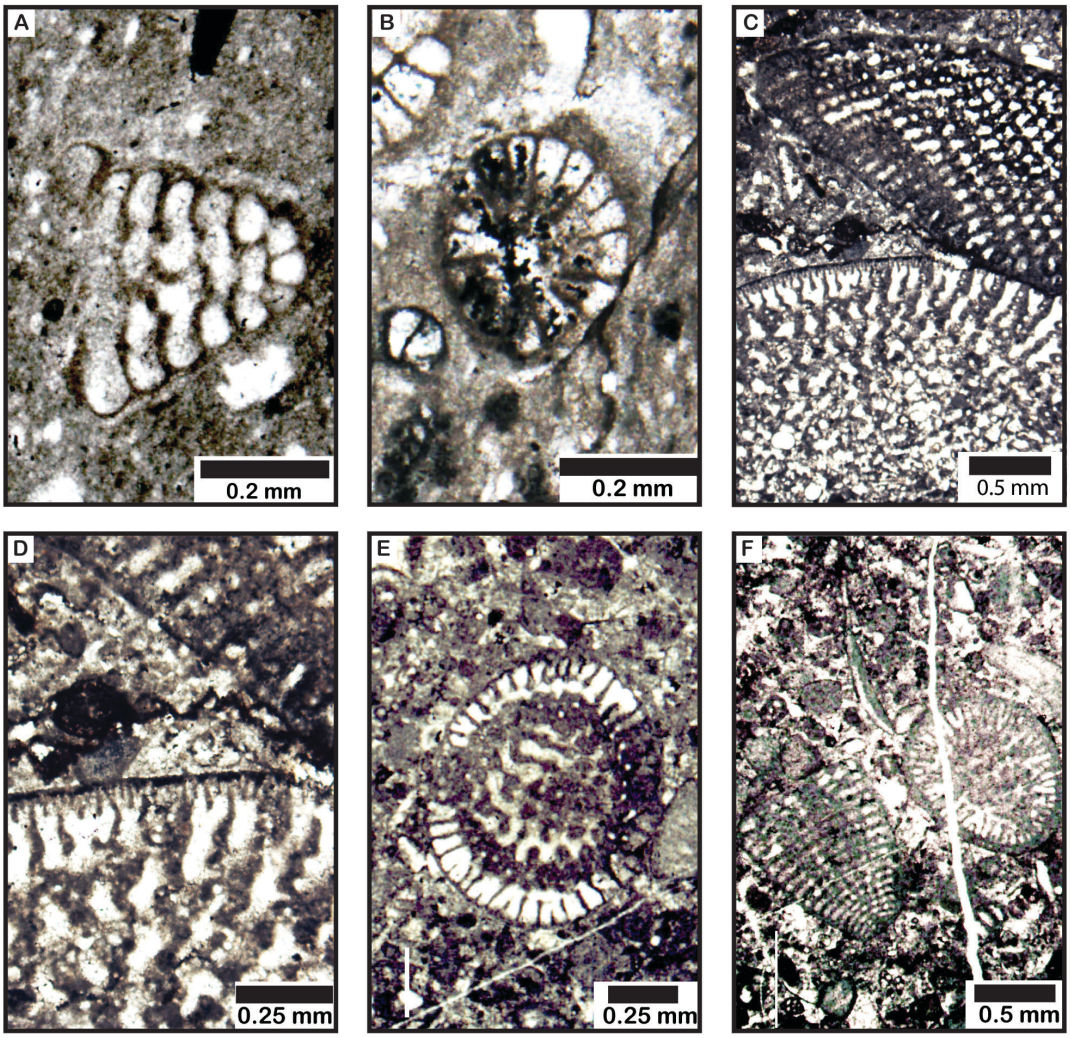

Figure 2.10. A: Axial section of the *Coskinolinoides texanus* in the Hatillo Limestone Central Cordillera. B: Basal section of the *Coskinolinoides texanus* in Hatillo Limestone Central Cordillera. C: Portion of axial sections of the *Orbitolina subconcava* in the Hatillo Limestone Oriental Cordillera. D: Close-up of axial sections of the *Orbitolina subconcava* in the Hatillo Limestone Oriental Cordillera. E: Basal and axial sections of the *Paracoskinolina sunnilandensis* in the Hatillo Limestone Oriental Cordillera. F: Basal section of the *Paracoskinolina sunnilandensis* in the Hatillo Limestone Oriental Cordillera.

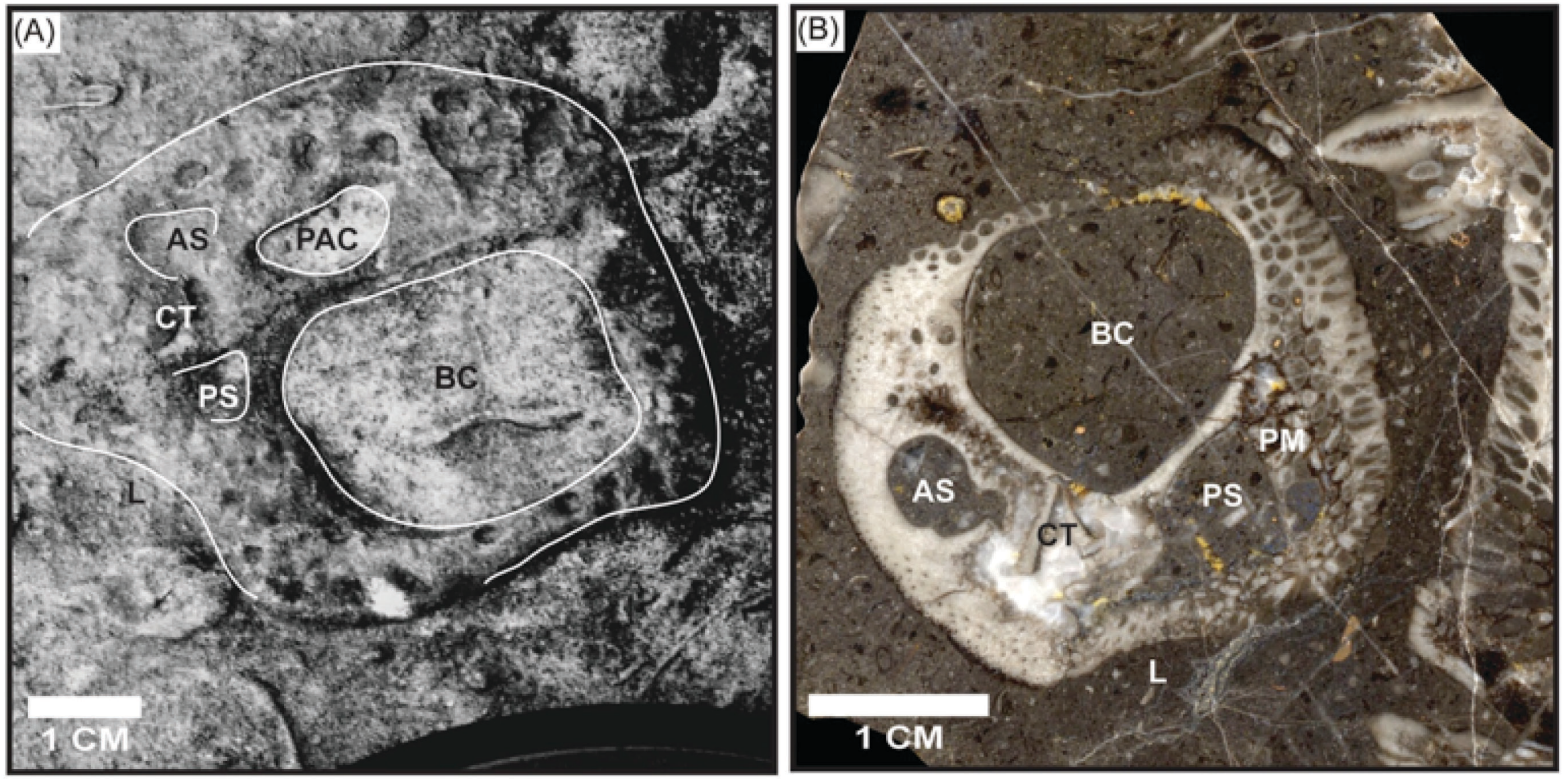

Figure 4.11. (A) Right valve of the primitive form of the rudist *Caprinuloidea* from the Hatillo Limestone exposed in the Hato Mayor area (DR). (B) Right valve of the advance form of the rudist *Caprinuloidea* from the Barrancas Limestone (PR).

Chapter 3 - Carbon isotope ($\delta^{13}C$) stratigraphy of the middle Cretaceous Hatillo Limestone in the Seibo tectonic terrane of the Dominican Republic

ABSTRACT

The Hatillo Limestone in the Dominican Republic was evaluated for its biostratigraphic and chemostratigraphic ($\delta^{13}C$) records. This lithostratigraphic unit is exposed in the Seibo Tectonic Terrane in the Central Cordillera (Pueblo Viejo area) and Oriental Cordillera (Hato Mayor area) of the Dominican Republic, and consists of: (1) basal calcarenites and marly limestones, (2) skeletal rudist packstones to grainstones, (3) upper marly limestones, and (4) lime-mud lithofacies. The biostratigraphic record in the Hato Mayor area shows strong affinities with the latest Aptian to Early Albian Glen Rose Limestone in Central Texas, consisting of rudist taxa characteristic of the *Coalcomana-Caprinuloidea* rudist assemblage, and the orbitolinid foraminifers *Orbitulina subconcava* (Leymerie) and *Paracoskinolina sunnilandensis* (Maync) in the rudist skeletal packstone to grainstone lithofacies. In Chapter 2, $^{87}Sr/^{86}Sr$ analyses for the Hatillo Limestone in the Hato Mayor area indicated depositional ages close to the Aptian/Albian boundary. The early Albian age for the Hatillo Limestone in the Pueblo Viejo area is supported by published zircon ages from the underlying upper Los Ranchos Formation and reports of the *Douvilleiceras mammillatum* ammonite subzone in the basal units of the Hatillo. In this area, the presence of the *Coskinolinoides texanus* (Keijzer) in the upper marly limestone lithofacies, however, suggests that the Hatillo Limestone extended up into the middle Albian.

Our key $\delta^{13}C$ chemostratigraphic events from the Hatillo Limestone consist of: (1) a positive $\delta^{13}C_{org}$ excursion of +5 ‰ occurring in the carbonaceous sediments of the upper Los Ranchos Formation, and (2) a short-lived negative excursion of -5.0 ‰ $\delta^{13}C_{org}$ and -3.0 ‰ $\delta^{13}C_{carb}$ occurring in the skeletal-rudist packstone to grainstone lithofacies in the Central Cordillera. The short-lived negative $\delta^{13}C$ excursion shows strong affinities with the negative $\delta^{13}C$ shift associated with the Mediterranean OAE1b Niveau Léehardt (Urbino) event. The middle Albian *Coskinolinoides texanus* (Keijzer) in the units following this event supports our correlation with the final short-lived negative $\delta^{13}C$ excursion from the Mediterranean record. The similarities and differences between the $\delta^{13}C$ chemostratigraphic records from the Greater Antilles, the Gulf of Mexico and Mediterranean Tethys are herein used to study the middle Cretaceous paleoceanographic conditions. The Aptian through lower Albian chemostratigraphic interval is best correlated to the Mediterranean $\delta^{13}C$ profiles from the Vocontian Basin, France. This better correlation suggests stronger connection between the Mediterranean and Caribbean Tethys, probably associated with the dominance of western Tethys oceanic current. The stronger Albian correlation with the Gulf of Mexico, however, suggests a better connection of oceanic currents between these regions than those during the Aptian. This paleoceanographic change could be associated with the location of the Greater Antillean volcanic arc and/or the origination of the Costa Rica-Panama volcanic arc between the Americas acting as barriers for the Caribbean-Pacific ocean circulations resulting in the intensification of surface oceanic currents between Greater Antilles and the Gulf of Mexico.

INTRODUCTION

Enhanced volcano-tectonic activity has led to extensive deformation and undifferentiated stratigraphic successions in the Greater Antilles (Berryhill et al., 1960; Iturralde-Vinent and Lidiak, 2006). Index fossils are scarce and/or poorly preserved within this Antillean Cretaceous successions, and only few studies have focused on the recognition of depositional periods with known biostratigraphic groups, e.g. foraminifers and ammonites (Barragán et al., 2011; Douglass, 1961; Myczyński and Iturralde-Vinent, 2005). Rudist bivalves, on the other hand, are one of the most common and locally abundant Cretaceous fossil groups in the Caribbean and circum-Caribbean regions (Johnson and Kauffman, 2001; Scott, 2002a). The great utility of rudist biostratigraphy is due to their rapid diversification with several extinction crises (Scott and Filkorn, 2007). In Texas, middle Cretaceous rudist biostratigraphy is based upon stratigraphic associations of caprinid rudists with known ammonite zones (Kennedy et al., 1999; Scott, 2002a; Young, 1974). Orbitolinids are large benthic foraminifers that occur in similar environments as rudist bivalves (Coogan, 1977). The utility of orbitolinid biostratigraphy is based upon their integration with the stratigraphic ranges of rudist bivalves and ammonite zonations in Texas and Mexico (Scott and Gonzalez-León, 1991; Scott and Kerans, 2004). Although the stratigraphic range of key rudist bivalves is commonly used to constrain the depositional age of Cretaceous fossiliferous successions in the Greater Antilles (Brown and Mitchell, 2010; Iturralde-Vinent, 1997; Rojas et al., 1996), limited reports of other age-diagnostic fossils and other chronostratigraphic controls have created problems identifying the stratigraphic ranges of rudist-bearing formations.

In the Greater Antilles, middle Cretaceous successions are characterized by the presence of the *Coalcomana-Caprinuloidea* rudist assemblage (Skelton, 1996). *Coalcomana ramosa* (Boehm), the key species of this assemblage, is the diagnostic rudist for the identification of this assemblage (Alencáster and Pantoja-Alor, 1986). In the Glen Rose Limestone of Central Texas, the presence of *Coalcomana ramosa* and the orbitolinid foraminifer *Orbitolina texana* (Roemer) with fossils from the *Douvilleiceras mammillatum* ammonite subzone are used to constrain the depositional age of the *Coalcomana* interval zone to the Early Albian (Scott, 2002a; Scott and Filkorn, 2007). Equivalencies of the *Coalcomana* interval zone are found in the Encino and Vallecitos formations of Mexico (Boehm, 1898; Alencáster and Pantoja-Alor, 1986), Glen Rose Limestone of Texas (Scott, 2002a; Scott and Filkorn, 2007), the Hatillo Limestone of the Dominican Republic (Myczyński and Iturralde-Vinent, 2005), the Río Matón Limestone of Puerto Rico (Kaczor and Rogers, 1990; Skelton, 1996), the Seafield Formation of Jamaica (Chubb, 1971; Brown and Mitchell, 2010), and the Provincial Formation of Cuba (Rojas et al., 1996).

The middle Cretaceous volcano-sedimentary succession in the Dominican Republic has been extensively studied because of its economic importance in the Pueblo Viejo Gold District. This has resulted in good stratigraphic controls at the base of the Hatillo Limestone, where the *Coalcomana-Caprinuloidea* rudist assemblage is reported (Myczyński and Iturralde-Vinent, 2005). This chapter presents the first carbon isotope ($\delta^{13}C$) chemostratigraphic record from the upper Los Ranchos Formation and Hatillo Limestone successions in the Seibo tectonic terrane of the Dominican Republic (Fig. 3.1).

The $\delta^{13}C$ profiles are integrated with rudist bivalve and orbitolinid foraminifer biostratigraphy, and compared to published zircon U-Pb ages (Early Albian) from the upper Los Ranchos Formation (Kesler et al., 2005a,b), reports of fossils from the *Douvilleiceras mammillatum* ammonite subzone (upper lower Albian) at the base of the Hatillo Limestone in the Pueblo Viejo area (Myczyński and Iturralde-Vinent, 2005) and the $^{87}Sr/^{86}Sr$ derived ages from the Hatillo Limestone in the Hato Mayor area (Chapter 2). Our chemostratigraphic record from the Hatillo Limestone also provides a new perspective on the oceanic circulation regime that influenced the expansion of the middle to Late Cretaceous carbonate platforms in the Caribbean and Circum-Caribbean regions, and the deposition of organic-rich marine units on the northern boundary of South America (e.g. Bralower and Lorente, 2003).

GEOLOGIC SETTINGS

During the middle Cretaceous, the Antillean region (Fig. 3.2) was part of an active island arc located between North and South America (Pindell, 1991; Pindell and Kennan, 2009). The Antillean active island arc can be divided into: (1) Jurassic basement, (2) Early Cretaceous Primitive Island Arc (PIA), and (3) Late Cretaceous to Eocene/Oligocene Calc-alkaline Arc (CA) (Lebrón and Perfit, 1993). The boundary between the PIA and CA rocks from Puerto Rico and the Dominican Republic are described as a disconformity locally capped by shallow-water limestone deposits (Draper et al., 1994). In the Dominican Republic, the best exposure of this stratigraphic succession occurs in the Seibo tectonic terrane, and includes the PIA rocks from the Los

Ranchos Formation unconformably overlain by the Hatillo Limestone, and the post-Albian CA Las Lagunas and Guayabas formations (Fig. 3.1).

Los Ranchos Formation

The Los Ranchos Formation, in the Pueblo Viejo area hosts one of the world's largest gold-silver reserves and one of the largest open pit mines in the Western Hemisphere (Kesler et al., 1981; Sillitoe, 2008). This formation is largely composed by volcano-sedimentary successions deposited in marine settings (Kesler et al., 2005a,b). In the Pueblo Viejo area, the Los Ranchos Formation is divided into four lithostratigraphic units: (1) Quita Sueño, (2) Platanal, (3) Zambrana, and (4) Pueblo Viejo members (Kesler et al., 1991). Whereas the first three members are largely composed of volcanic and volcaniclastic rocks, the Pueblo Viejo Member consists of laminated carbonaceous siltstones and sandstones with local conglomerate layers. The contact between the Pueblo Viejo Member and the overlying Hatillo Limestone has been described as a locally faulted disconformity (Bowin, 1966; Kesler et al., 1991; Nelson, 2000).

The presence of land-plant fossil material in the carbonaceous sediments of the Pueblo Viejo Member suggests terrestrial depositional environments of part of the Los Ranchos Formation (Smiley, 2002). The terrestrial flora includes the genus *Brachyphyllum*, which was originally used to constrain the depositional age of Los Ranchos Formation to Neocomian. This age has been revised using U-Pb ages from zircons in the Quita Sueño and the Pueblo Viejo members (Kesler et al., 2005a,b). In the Quita Sueño Member, two zircon populations were described in massive quartz-feldspar porphyry; the age of the younger population was 113.9±0.8 Ma (Aptian) and, the older

population 118.6±0.5 Ma (Aptian). The date of the Pueblo Viejo Member was generated from a single zircon population in a quartz porphyry fragmental rock, and yielded ages of 110.9±0.8 Ma (Early Albian).

Hatillo Limestone

The Hatillo Limestone has been described as a light to dark-gray massive, biogenic limestone (Bowin, 1966; Iturralde-Vinent, 1997; Myczyński and Iturralde-Vinent, 2005). The three distinctive depositional units described from this formation are: (1) a basal transgressive surface (Russel and Kesler, 1991), (2) massive biogenic limestone unit with reef constituents (Myczyński and Iturralde-Vinent, 2005), and (3) distinctly bedded deep-water carbonates (García-Senz, 2004). Bowin (1966) suggested Aptian to Albian deposition for the Hatillo Limestone based upon the foraminiferal fauna of *Orbitolina texana*, *Cuneolina* sp., *Coskinolinoides texanus* and unidentified *Globigerinida*. In the basal units of the Hatillo Limestone, Russel and Kesler (1991) described a transgressive succession and reported the late Albian to Cenomanian echinoid genera: *Holectypus*, *Conulus*, *Holaster*, *Salenia*, *Cardiaster*, *Pygopyrina* and *Hemiaster*. The best biostratigraphic controls of the Hatillo Limestone, however, are the reports of fossils of the upper lower Albian *Douvilleiceras mammillatum* ammonite subzone at the base of the limestone in the Pueblo Viejo area (Myczyński and Iturralde-Vinent, 2005). In the Hato Mayor area, $^{87}Sr/^{86}Sr$ analyses from the calcitic outer shell of requeniid rudists resulted in derived ages close to the Aptian/Albian boundary (112.56 Ma).

MATERIAL AND METHODS

Fieldwork was conducted during the Fall of 2010 in the Sanchez Ramírez and Hato Mayor del Rey provinces, with logistical assistance from the National Geological Survey of the Dominican Republic. Measured stratigraphic sections include: (1) a borehole core and (2) outcrop sections on the grounds of the Barrick Gold Corporation (former Rosario Gold Mine – 18°55'02.46" N; 70°09'38.13" W) in the Pueblo Viejo area (Sanchez Ramírez Province), and (3) an outcrop section along route 103 (18°49'17.84" N; 69°17'54.44" W) north of the Hato Mayor community (Hato Mayor del Rey Province). The borehole core T82 at the Pueblo Viejo gold district was the most continuous stratigraphic section with approximately 100m of recovered core (depths: 125 to 25m). This section was logged, measured and sampled within the core library of the Barrick Gold Corporation. The chemostratigraphic record obtained from this core was used as reference to establish our $\delta^{13}C$ chemostratigraphic correlations.

The studied sections were selected with regard to length, accessibility, stratigraphic continuity, and the presence of rudist taxa characteristic of the *Coalcomana-Caprinuloidea* rudist assemblage in the limestone units. These fossils were used to identify our strata of interest in the Seibo tectonic terrane. Samples were collected at closely spaced intervals (25 to 50 cm between samples) to facilitate the generation of the $\delta^{13}C$ chemostratigraphic profiles. The thin sections generated from this sampling led to the identification of orbitolinid foraminifers used to improve our biostratigraphic framework from the Hatillo Limestone (Fig. 3.3). Other fossils (primarily rudist bivalves)

were described, photographed and collected noting their stratigraphic position within the stratigraphic sections (Fig. 3.4).

Carbonate $\delta^{13}C$

Thin sections and polished slabs were generated to describe the depositional textures of the collected samples. This information was used to limit the carbon isotope analyses from carbonate sample ($\delta^{13}C_{carb}$) to lime mudstone and/or micritic matrix of bioclastic textures (skeletal wackestones and packstones). For these analyses, about 80-100µg of powdered carbonate sample was microdrilled with tungsten-carbide drill bits from polished slabs. The powdered samples were vacuum roasted at 200°C for one hour to remove volatile organics before the isotopic analyses. The $\delta^{13}C_{carb}$ analyses were conducted using phosphoric acid (H_3PO_4) digestion at 75 °C on a ThermoFinnigan KIEL III attached to a dual inlet system ThermoFinnigan MAT 253 isotope ratio mass spectrometer at the University of Kansas, KECK Paleoenvironmental and Environmental Stable Isotope Laboratory (KPESIL). All reported $\delta^{13}C_{carb}$ values refer to the VPDB standard with precision better than ±0.1 ‰ (VPDB) as calculated from the results of multiple analyses of NBS-18 and NBS-19.

Organic Matter $\delta^{13}C$

For the organic matter carbon isotope analyses ($\delta^{13}C_{org}$), approximately 5g of each sample was powdered, dried at 60°C for 48 hours, and decarbonated following a modified procedure from Midwood and Boutton (1998). The decarbonation method consisted in the acidification of samples in 30mL of 0.1M hydrochloric acid (HCL) for

24 hours. Multiple acidifications were necessary to assure that all the carbonate content was consumed in the reaction. The resulting organic residue was rinsed with nanopure water to neutral pH (pH = 6 to 7), and dried at 60°C to constant weight. Between 10 to 30mg from volcaniclastic samples, and 100 μg to 1 mg from carbonate samples were weighed in silver capsules and combusted at 980°C using a Costech Elemental Analyzer connected to a continuous flow system ThermoFinnigan MAT 253 isotope ratio mass spectrometer at the KU KPESIL facilities. All reported $\delta^{13}C_{org}$ refer to the VPDB standard with instrumental precision of ±0.35 ‰ (VPDB) based on multiple analyses of DROM, USGS-24, IAEA-600 (caffeine), and ANU (sucrose).

RESULTS

Borehole core T82 section

The borehole core T82 section consists of 32.7m of Los Ranchos Formation and 68m of the Hatillo Limestone (Fig. 3.5A). This is the only section where the volcaniclastic and carbonaceous sedimentary rocks of Los Ranchos Formation were studied. In this section, 7.4m of the Los Ranchos succession are missing at 10m from the base of the core. This volcaniclastic succession consists of 30.4m of interbedded sandstones and conglomerates. Above, the unit abruptly changes to 2.3m of unconsolidated carbonaceous sandstone and siltstone. The contact between the Los Ranchos Formation and the Hatillo Limestone is recorded by a sharp change from unconsolidated carbonaceous sediments of the Pueblo Viejo Member to the well-cemented calcareous sandstone at the base of the Hatillo Limestone.

In this section, the Hatillo Limestone consists of four distinctive lithofacies: (1) basal calcarenites and marly limestones, (2) rudist-skeletal packstones to grainstones, (3) upper marly limestones, and (4) lime-mudstones (Fig. 3.5A). The basal calcarenites and marly limestone lithofacies have a total thickness of 6.1m, including 3.8m of interbedded calcareous sandstones and marly limestones, and 2.3m of marly limestones. The fossil content of this lithofacies consists of fragments of corals and caprinid rudists. The rudist-skeletal packstone to grainstone lithofacies occurs directly above the basal calcarenites and marly limestone lithofacies, and includes 13m of massive, light-grey fossiliferous limestone. In this lithofacies, rudist fragment are abundant and are mostly composed of *C. ramosa* (Fig. 3.4C). In addition to the rudists, other common skeletal constituents are corals and echinoids. The upper marly limestone lithofacies has a total thickness of 9.9m, and consists of 3.8m of marly limestone and 6.1m of dark-gray limestone. This lithofacies includes the orbitolinid foraminifer *C. texanus* (Fig. 3.3E-F). Other skeletal constituents include small gastropods and sponges. The lime-mudstone lithofacies lies toward the upper 38.4m of the Hatillo Limestone succession, and consists of light-gray limestone with planktic constituents, such as the foraminifer *Globigerinida*, and scarce macrofossils (Fig. 3.3 G-H).

The carbon isotope ($\delta^{13}C_{org}$ and $\delta^{13}C_{carb}$) chemostratigraphic profiles derived from this section include the $\delta^{13}C_{org}$ curve from the upper Los Ranchos Formation, and the $\delta^{13}C_{org}$ and $\delta^{13}C_{carb}$ curves from the Hatillo Limestone (3.5A). The $\delta^{13}C$ pattern from these profiles can be divided into four distinctive segments: (1) a positive $\delta^{13}C_{org}$ excursion of +5‰ occurring in the carbonaceous sediments of the Pueblo Viejo Member,

(2) a positive $\delta^{13}C_{carb}$ excursion of +1.5‰ in the Hatillo Limestone basal calcarenites and marly limestone lithofacies, (3) a short-lived negative excursion of -5.0‰ $\delta^{13}C_{org}$ and -3.0‰ $\delta^{13}C_{carb}$ occurring in the Hatillo Limestone skeletal-rudist packstone to grainstone lithofacies, and (4) a small negative excursion of approximately -0.6‰ $\delta^{13}C_{carb}$ followed by a small positive excursion of +0.3‰ $\delta^{13}C_{carb}$ toward the lime-mud lithofacies of the Hatillo Limestone. The $\delta^{13}C_{org}$ from the lime-mud lithofacies is characterized by high isotopic variability between samples and no apparent chemostratigraphic pattern.

Barrick Gold section

The Barrick Gold section consists of 24m of the lime-mudstone lithofacies (Fig. 3.5B). This section includes similar lithology and fossil content as the lime-mudstone lithofacies in the T82 borehole core section. The section consists of 7.5m of light-gray mudstone with no macrofossils, overlain by 16.5m of light to medium-gray mudstone to wackestone with some skeletal fragments. At 16.3m from the base, there is 4.5m of section covered by soil and rock debris. The carbon isotope ($\delta^{13}C_{org}$ and $\delta^{13}C_{carb}$) chemostratigraphic record derived from the Barrick Gold section includes a negative excursion of -1.0‰ ($\delta^{13}C_{carb}$) starting at approximately 6m from the base of the section, followed by a small positive excursion of +0.5‰ ($\delta^{13}C_{carb}$) at 10m from the base of the section. The $\delta^{13}C_{org}$ record from this section is characterized by high isotopic variability between samples and no apparent chemostratigraphic pattern.

103 section

The 103 section (Fig. 3.5C) in the Hato Mayor area contained the best exposure of the rudist-skeletal packstone to grainstone lithofacies. This section consists of 14m of dark to medium-gray limestone occurring directly above weathered units of Los Ranchos Formation. The section initiates with the deposition of reddish limestone units with abundant orbitolinid foraminifers, *Orbitolina subconcava* (Fig. 3.3A-B). These units transitionally change to limestone with abundant chondrodontid and rudist bivalves (Fig. 3.4A-B and D-F). At this point in the stratigraphic section, the orbitolinid foraminifer *Paracoskinolina sunnilandensis* becomes common (Fig. 3.3C-D). The succeeding units contain oncoids nucleated around shell fragments (Fig. 3.3G). Toward the upper part of this section rudist bivalves become abundant once again. The principal rudist, *C. ramosa,* is also the main rudist constituent within the rudist-skeletal packstone to grainstone lithofacies from the Pueblo Viejo area. Other common skeletal fragments are corals and gastropods (Fig. 3.4G-H). The carbon isotope ($\delta^{13}C_{org}$ and $\delta^{13}C_{carb}$) chemostratigraphic record derived from the Hato Mayor area (103 section) include negative excursions of -1.6 ‰ $\delta^{13}C_{org}$ and -1.2 ‰ $\delta^{13}C_{carb}$ occurring in the middle of the section (~5 m from the limestone base) followed by small positive excursion of 0.7 ‰ $\delta^{13}C_{org}$ and 0.5 ‰ $\delta^{13}C_{carb}$ in the upper part of the section (~10m from the base of the limestone).

DISCUSSION

Stratigraphic range

The potential of rudist biostratigraphy has been established in the Barremian to Albian rudist-bearing successions of the Gulf of Mexico (Coogan, 1977; Scott, 2002a; Scott and Filkorn, 2007). There are four rudist assemblages characterizing the Albian carbonate platforms in Texas (Scott, 2002a; Scott and Filkorn, 2007). These are: (1) the late Aptian to early Albian *Coalcomana* interval zone, (2) the late early to early late Albian *Caprinuloidea* interval zone, (3) the early late Albian *Kimbleia* interval zones and (4) the late Albian *Mexicaprina* interval zone (Fig. 3.6). The late Aptian to early Albian *Coalcomana* interval zone is best known from the Glen Rose Formation in Central Texas, where *C. ramosa* occurs next to fossils from the upper lower Albian *Douvilleiceras mammillatum* ammonite subzone (Scott and Filkorn, 2007). Based upon the presence of the rudist *C. ramosa* and the reports of the *Douvilleiceras mammillatum* ammonite subzone in the Hatillo Limestone (Myczyński and Iturralde-Vinent, 2005), the *Coalcomana* interval zone best describes the Antillean *Coalcomana-Caprinuloidea* rudist assemblage.

There are, however, differences between the orbitolinid foraminifer records in the Pueblo Viejo and Hato Mayor areas. These benthic foraminifers, like caprinid rudists, are useful for dating Early to middle Cretaceous strata in Mexico and Texas (Coogan, 1977; Scott, 2002a). Important orbitolinid foraminifers include: the upper Aptian to lower Albian (1) *Orbitulina texana* (Roemer) and (2) *Paracoskinolina sunnilandensis* (Maync), the middle to upper Albian (3) *Dictyoconus walnutensis* (Carsey), (4) *Coskinolinoides*

texanus (Keijzer) and (5) *Barkerina barkerensis* (Frizzell and Schwartz), and the upper Albian (6) *Paracoskinolina coogani* (Scott) and (7) *Streptalveolina mexicana* (Scott) (Fig. 3.6). The presence of *P. sunnilandensis* and reports of *O. texana* (Woodring, 1954) support similar stratigraphic ranges between the *Coalcomana* interval zone in Central Texas and the *Coalcomana-Caprinuloidea* rudist assemblage in the Hato Mayor area. In the Pueblo Viejo area, however, Bowin (1966) reported the foraminifer *C. texanus*, which suggests that the deposition of the Hatillo Limestone extended up into the middle Albian. $^{87}Sr/^{86}Sr$ numerical ages from the Hato Mayor resulted in ages close to the Aptian/Albian boundary for the Hatillo Limestone (Chapter 2). Although none of the collected samples from the Pueblo Viejo area yielded $^{87}Sr/^{86}Sr$ numerical ages, the stratigraphic controls at the base of the limestone and the presence of *C. texanus* in this area suggest an upper lower Albian to middle Albian depositional range.

Isotopic signatures

In order to establish any correlations for the Antillean $\delta^{13}C$ chemostratigraphic data, primary marine signatures and diagenetic effects need to be established. For carbonate samples, the intensity of diagenetic alteration can be estimated by the degree of $\delta^{13}C_{carb}$ and $\delta^{18}O_{carb}$ covariance (Jenkyns et al., 1994; Luciani et al., 2004; Wendler et al., 2009). High degree of covariance suggests strong enough diagenetic alteration to affect $\delta^{13}C_{carb}$ and low preservation of primary marine signatures. Cross-plot relationships from $\delta^{13}C_{carb}$ and $\delta^{18}O_{carb}$ were used to identify areas with the most intense diagenetic alteration (Fig. 3.5 and 3.7). Additionally, the $\delta^{13}C_{org}$ chemostratigraphic profiles were

used as independent criteria to assess preservation, where the reproduction of carbon isotope excursions in both the $\delta^{13}C_{carb}$ and $\delta^{13}C_{org}$ profiles were interpreted as original signatures.

The $\delta^{13}C_{carb}$ and $\delta^{18}O_{carb}$ cross-plot from all data suggests some diagenetic alteration in the Hatillo Limestone record, but not likely enough to have altered the $\delta^{13}C_{carb}$ signatures. The only exception occurs at the base of the Hatillo Limestone in the T82 borehole core section (Fig. 3.7), where depleted $\delta^{13}C_{carb}$ and $\delta^{18}O_{carb}$ covariation suggest strong diagenetic overprinting of the original marine $\delta^{13}C_{carb}$ signature. The diagenetic origin of this depleted $\delta^{13}C_{carb}$ is supported by the absence of this excursion in the $\delta^{13}C_{org}$ record. Depleted $\delta^{13}C_{carb}$ and $\delta^{18}O_{carb}$ are consistent with alteration of ^{12}C-enriched fluids from degraded organic carbon. This diagenetic alteration is often associated with the subaerial exposure of shallow-water carbonates and the addition of isotopically negative CO_2 derived from soils through meteoric diagenesis. In the Hatillo Limestone, however, the depleted $\delta^{13}C_{carb}$ and $\delta^{18}O_{carb}$ values occur at the base of the limestone succession. The nature of the Pueblo Viejo Gold District mineralization is being used to explain this diagenetic overprinting. In this area, Sillitoe et al. (2006) identified hydrothermal alteration within the basal units of the Hatillo Limestone. The Sillitoe et al. (2006) study established that the Hatillo Limestone acted as a barrier to migrating upward fluid, which enhanced the deposition of ore bodies in the Pueblo Viejo Member (Los Ranchos Formation). The hydrothermal fluids moving upward through the carbonaceous units of the upper Los Ranchos Formation are inferred to be the driving mechanism for resetting the $\delta^{13}C$ signature at the base of the Hatillo Limestone.

The $\delta^{13}C_{org}$ records generated from the lime-mudstone lithofacies in the borehole core T82 and Barrick Gold sections yielded an unclear chemostratigraphic pattern. This $\delta^{13}C_{org}$ variability could be related to the small amount of recovered organic residue, which was less than 100µg for most of the samples in this lithofacies. The other possibility could be different sources of organic matter throughout these stratigraphic successions. However, the reproduction of the $\delta^{13}C_{carb}$ chemostratigraphic patterns from the two lime-mudstone sections at the Pueblo Viejo Gold District suggests good preservation of the $\delta^{13}C_{carb}$ marine signatures.

Correlations

There are a few detailed carbon isotope profiles that show the global $\delta^{13}C$ signature within the Aptian/Albian transition. Some of the most complete records include those from the Resolution Guyot in the Pacific (Jenkyns and Wilson, 1999), the Sierra Madre in northern Mexico (Scholle and Arthur, 1980; Bralower et al., 1999), the Comanche Shelf in Texas (Phelps, 2011), the Blake Nose in the Western Atlantic (Huber et al., 2011; Wilson and Norris, 2001) and the Vocontian Basin in southeastern France (Herrle et al., 2004; Gale et al., 2011) (Fig. 3.8). Carbon isotope ($\delta^{13}C$) chemostratigraphic correlations are based on pronounced shifts in the $\delta^{13}C$ signature, which are linked to changes in organic carbon burial (Kump and Arthur, 1999). The Aptian/Albian transition is characterized by pronounced carbon isotope excursions that are associated with the OAE1b Niveau Kilian (Jacob), Niveau Paquier (Paquier) and Niveau Léehardt (Urbino) events (Bralower and Thierstein, 1984; Jenkyns, 1980, 2010;

Schlanger and Jenkyns, 1976). The key chemostratigraphic events from the Los Ranchos and Hatillo Limestone succession include: (1) the positive carbon isotope excursion ($\delta^{13}C_{org}$) in the upper Los Ranchos Formation, and (2) the short-lived negative carbon isotope excursion ($\delta^{13}C_{carb}$ and $\delta^{13}C_{org}$) in the Hatillo Limestone (Fig. 3.9A).

Our first point of correlation is the positive carbon isotope excursion ($\delta^{13}C_{org}$) within the carbonaceous sediments of the Pueblo Viejo Member in the upper Los Ranchos Formation. Kesler et al. (2005a, b) described these carbonaceous sediments as marginal marine deposits, and zircon dates from this lithostratigraphic unit indicated Early Albian age (110.9±0.8 Ma; Kesler et al. 2005a, b). In their paper, the timing of deposition of the Pueblo Viejo Member was coeval with the OAE1b Paquier Event. The $\delta^{13}C$ chemostratigraphic pattern from this unit compares well with the Al2 event described in the Comanche Shelf in Texas (Phelps, 2011) and the Vocontian Basin in France (Herrle et al., 2004) (Fig. 3.9 and 3.10). Although not directly associated with the Paquier event, this chemostratigraphic event (Al2) is part of the OAE1b set. Erbacher et al. (2001) suggested that the mechanism leading to the OAE1b was poor ventilation within partially isolated basins in the Western Tethys. For Kesler et al. (2005a,b) the Pacific origin of the Caribbean Plate explained this poor oceanic ventilation. In this model, the middle Cretaceous position of the Greater Antilles volcanic arc between North and South America resulted in the blockage of Tethys-Pacific ocean circulation (Fig. 3.2, 3.8 and 3.11).

Our second point of correlation is the short-lived negative carbon isotope excursion ($\delta^{13}C_{org}$ and $\delta^{13}C_{carb}$) in the skeletal-rudist packstone to grainstone lithofacies

of the Hatillo Limestone. This abrupt negative carbon isotope excursion implies rapid introduction of isotopically light ^{12}C in the ocean-atmosphere system. Jenkyns (2003; 2010) described similar negative excursions in the Mesozoic-Palaeogene OAEs. These events were credited to rapid dissociation, release and oxidation of methane from gas hydrates, which caused short-term negative shifts in the carbon isotope record of up to several per mil (‰). There are three negative carbon isotope excursions described in association with the OAE1b; (1) Niveau Kilian (Jacob), (2) Niveau Paquier (Paquier) and (3) Niveau Léehardt (Urbino) events (Gale et al., 2011; Herrle et al., 2004). The short-lived negative carbon isotope excursion from the Hatillo Limestone is correlated to the Al4 to Al5 chemostratigraphic events from the Niveau Léehardt (Urbino) recorded in the Comanche Shelf, Texas (Phelps, 2011) and the Vocontian Basin, France (Herrle et al., 2004) (Fig. 3.9 and 3.10). This correlation is supported by the presence of fossils of the upper lower Albian *Douvilleiceras mammillatum* ammonite subzone at the base of the Hatillo Limestone (Myczyński and Iturralde-Vinent, 2005) and the Al4 to Al5 events in the chemostratigraphic record of the Vocontian Basin (Gale et al., 2011; Herrle et al., 2004). Moreover, the presence of the middle Albian *C. texanus* in the units above this chemostratigraphic event in the Hatillo Limestone supports our correlation with the final lower Albian short negative excursion in the Vocontian Basin. Luciani et al. (2004) described a similar chemostratigraphic event in the Gargano Promontory pelagic succession (Southern Italy), consisting of an abrupt negative $\delta^{13}C_{carb}$ shift in the lower Albian (described as the Urbino event) and a $\delta^{13}C_{carb}$ return during the middle Albian.

The absence of the Hato Mayor chemostratigraphic pattern in the Pueblo Viejo area is probably related to either erosion or lack of deposition during an interval of subaerial exposure of the Los Ranchos volcanic core. The $\delta^{13}C_{org}$ pattern from the volcaniclastic succession of the Los Ranchos Formation compares well with the Ap12 to Ap14 chemostratigraphic events from the Vocontian Basin (Herrle et al., 2004), and the carbonaceous sediments of the Pueblo Viejo Member to the Al2 chemostratigraphic event from the Vocontian Basin (Herrle et al., 2004) and Comanche Shelf (Phelps, 2011). This correlation suggests that the chemostratigraphic events close to the Aptian/Albian boundary (Ap15 through Al1 chemostratigraphic events) are absent in the Pueblo Viejo area. We propose that this missing interval coincides with the deposition of the Hatillo Limestone in the Hato Mayor area. Thus, the $\delta^{13}C$ chemostratigraphic record from the Hato Mayor area is correlated to the latest Aptian's Al1 chemostratigraphic event from the Vocontian Basin (Herrle et al., 2004) (Fig. 3.9).

Our correlations suggest that the Hatillo Limestone depositional succession was dominated by the gradual development of the carbonate platform on the flank of the Los Ranchos volcanic core in response to relative sea level rise. This is supported by the transgressive nature of the Hatillo Limestone at the Pueblo Viejo characterized by (1) nearshore basal calcarenites and marly limestone lithofacies, (2) nearshore to shallow-water skeletal-rudist packstone to grainstone and upper marly limestone lithofacies, and (3) deep-water lime-mudstone lithofacies.

PALEOCEANOGRAPHIC IMPLICATIONS

The differences and similarities between the Antillean chemostratigraphic profiles and the $\delta^{13}C$ records from the Gulf of Mexico and the Mediterranean Tethys suggest a major paleoceanographic change during the Aptian/Albian transition. The latest Aptian to earliest Albian records from the Hatillo Limestone are best correlated to the $\delta^{13}C$ profiles from the Mediterranean Tethys in the Vocontian Basin (Herrle et al., 2004; Gale et al., 2011) (Fig. 3.10B), whereas, the lower to middle Albian Hatillo Limestone chemostratigraphic record is best correlated to the $\delta^{13}C$ profiles from the Gulf of Mexico (Bralower et al., 1999; Scholle and Arthur, 1980; Phelps, 2011) (Fig. 3.10A). These differences are probably associated with changes in the Tethys oceanic surface currents during the middle Cretaceous.

Johnson (1999) used a paleobiologic proxy to infer the dispersal routes of rudist planktonic larvae, and surface oceanic currents in the Caribbean and Gulf of Mexico regions. In the Johnson (1999) model, the main Aptian to Albian oceanic current flowed westward along the coastal areas of northern South America and continued to the Pacific Ocean. Split currents, however, flowed along the Greater Antilles volcanic arc before turning northward through the Gulf Coast of Mexico, and finally eastward along the coast of southern North America (arrow A in Fig. 3.11) (Johnson, 1999). Villamil et al. (1999) used a similar model to explain the deposition of lower Albian to Coniacian organic-rich shales in the northern margin of South America. In the Villamil et al. (1999) model, the deposition of these organic-rich marine deposits was associated with enhanced productivity in upwelling systems influenced by northward displacement of surface

water. More recently, Suarez et al. (2011) incorporated a northward split of a westward traveling air mass to model the global hydrologic cycle during the middle Cretaceous in order to adequately simulate their empirical data. Moreover, Johnson (1999) described broader geographic distribution for the Albian branching currents than those during the Aptian (Fig. 3.11, arrows B, C and D). The better late Aptian correlation of the Greater Antilles chemostratigraphic patterns with those of France (Vocontian Basin) is probably associated with the dominance of westward flowing currents over the Tethys region. During the Albian, however, the disconnect from the eastern Tethys and dominance of the northward flowing split current resulted in the improved correlations between the Greater Antilles chemostratigraphic record and those of Mexico and Texas.

Divergence among the Caribbean and Pacific paleobiogeographic records of shallow marine biota supports this significant Aptian/Albian paleoceanographic change. During the Barremian-early Aptian period, the Caribbean and Pacific regions shared similar Tethyan tropical to sub-tropical biota in their shallow-water carbonates (Iba and Sano, 2007, 2008; Iba et al., 2009; Iba et al., 2011; Skelton et al., 2011). Iba and Sano (2008) used the pectinid bivalve *Neithea* to study the paleobiogeographic changes between the Tethys and Pacific regions during the middle Cretaceous. Although these bivalves flourished in the Tethys realm until the Late Cretaceous, in the Pacific record the onset of their demise occurred during the late Aptian-early Albian interval with complete eradication during the late Albian. Iba et al. (2011) proposed that this poor faunal connection between the Tethys and Pacific realms was related to a paleogeographic change that resulted from ocean circulation and/or temperature changes.

As suggested by Kesler et al. (2005a, 2005b), the Pacific origin for the Caribbean plate is proposed to be the driver for a major paleoceanographic change during the Aptian/Albian transition. The middle Cretaceous position of the Greater Antillean volcanic arc between the Americas, and/or the origination of the Costa Rica-Panama arc in the same general area, resulted in weaker Tethys-Pacific ocean circulation and the strengthening of the northern current split as modeled by Johnson (1999). This is supported by (1) enhanced late earlyAlbian to middle Albian chemostratigraphic correlation with the Gulf of Mexico record, (2) the modeled stronger Albian surface oceanic current connection between the Caribbean and the Gulf Coast of Mexico (Johnson, 1999), and (3) the Albian divergence of the Caribbean and Pacific *Neithea* record.

CONCLUSIONS

The biostratigraphic record from the Hatillo Limestone included orbitolinid faunal differences between the Hato Mayor and Pueblo Viejo areas. In the Hato Mayor area, the presence of *P. sunnilandensis* indicated latest Aptian to lower Albian deposition. The presence of the *C. texanus* in the Pueblo Viejo area, however, indicated that the Hatillo Limestone extended up into the middle Albian. Strontium isotope ($^{87}Sr/^{86}Sr$) derived numerical ages from the Hatillo Limestone in the Hato Mayor area indicate ages close to the Aptian/Albian boundary, whereas in the Pueblo Viejo area a lower Albian to middle Albian stratigraphic range is supported by the presence of fossils from the *Douvilleiceras*

mammillatum ammonite subzone and the orbitolinid foraminfer *C. texanu* (Myczyński and Iturralde-Vinent, 2005).

The carbon isotope record from the Hatillo Limestone was correlated to $\delta^{13}C$ profiles from the Comanche Shelf in Texas (Phelps, 2011), the Sierra Madre in Mexico (Bralower et al., 1999) and the Vocontian Basin in France (Herrle et al., 2004). The key Hatillo Limestone chemostratigraphic events were (1) the positive $\delta^{13}C_{org}$ excursion of +5 ‰ occurring in carbonaceous sediments of the Pueblo Viejo Member of Los Ranchos Formation, and (2) the short-lived negative excursion of -5.0 ‰ $\delta^{13}C_{org}$ and -3.0 ‰ $\delta^{13}C_{carb}$ occurring in the Hatillo Limestone. The positive carbon isotope excursion in the carbonaceous sediments of the Pueblo Viejo Member was correlated to the Al2 event from the Comanche Shelf (Phelps, 2011) and the Vocontian Basin (Herrle et al., 2004). This correlation is supported by reported zircon dates (110.9±0.8 Ma) from the Pueblo Viejo Member (Kesler et al., 2005a, 2005b). The short-lived negative excursion in the skeletal-rudist packstone to grainstone lithofacies was correlated to the Al4 to Al5 events OAE1b Niveau Léehardt (Urbino) event in the Vocontian Basin (Herrle et al., 2004). This correlation is supported by the presence of fossils from the upper lower Albian *Douvilleiceras mammillatum* ammonites in both sections (Gale et al., 2011; Herrle et al., 2004; Myczyński and Iturralde-Vinent, 2005), and the presence of middle Albian *C. texanus* in the units above the Hatillo Limestone chemostratigraphic event.

The documented similarities and differences between the Antillean and Gulf of Mexico chemostratigraphic records suggest a major paleoceanographic change during the Aptian/Albian transition. During the Aptian, enhanced oceanic current connection

between the Mediterranean and Caribbean Tethys is proposed to be the driving mechanism for better chemostratigraphic correlations between these areas. Similarly, the improved Albian chemostratigraphic correlations between the Caribbean and Gulf of Mexico suggest a better connection of the surface oceanic currents for this region. The dominance of a northward split surface current, as modeled by Johnson (1999), is proposed to be the driving mechanism for the better oceanic current connection and chemostratigraphic correlations between the Greater Antilles and Gulf of Mexico during the Albian interval. This paleoceanographic change also coincides with a major paleobiogeographic divergence between the Tethys and Pacific record (Iba and Sano, 2008; Iba et al., 2011). The more eastward position of the Greater Antilles volcanic arc and/or the origination of the Panama-Costa Rica arcs between the Americas, coupled with lower relative sea level (or arc emergence) acted as a barrier for the Caribbean-Pacific ocean circulation and the intensification of the northward oceanic surface current that flowed from the Greater Antilles through the Gulf of Mexico.

REFERENCES

Alencáster, G., and Pantoja-Alor, J., 1986. Coalcomana Ramosa (Boehm) (Bivalvia-Hippuritacea) del Albiano Temprano del Cerro de Tuxpan, Jalisco. Boletín Sociedad Geológica Mexicana 47, 33-46.

Barragán, R., Rojas-Consuegra, R., and Szives, O., 2011. Late Albian (Early Cretaceous) ammonites from the Provincial Formation of central Cuba. Cretaceous Research, 32, 447-455.

Berryhill, H. L., Briggs, R. P., and Glover, L., 1960. Stratigraphy, sedimentation, and structure of Late Cretaceous rocks in eastern Puerto Rico-preliminary report. Bulletin of the American Association of Petroleum Geologists 44, 137-155.

Boehm, G., 1898. Ueber Caprinidenkalke aus Mexico: Zeitschrift der deutschen geologischen Gesellschaft 50, 323-332.

Bowin, C. O., 1966. Geology of central Dominican Republic; a case history of part of an island arc. The Geological Society of America Memoir 98, 11-84.

Bralower, T.J., and Thierstein, H.R., 1984. Low productivity and slow deep-water circulation in mid-Cretaceous oceans. Geology 12, 614-618.

Bralower, T. J., CoBabe, E., Clement, B., Sliter, W. V., Osburn, C. L., and Longoria, J., 1999. The record of global change in Mid-Cretaceous (Barremian-Albian) sections from the Sierra Madre, northeastern Mexico. Journal of Foraminiferal Research 29, 418-437.

Brown, I., and Mitchell, S. F., 2010. Lithostratigraphy of the Cretaceous succession in the Benbow Inlier, Jamaica. Caribbean Journal of Earth Science 41, 25-37.

Chubb, L. J., 1971. Rudist of Jamaica. Palaeontographica Americana 7, 161-257.

Coogan, A. H., 1977. Early and middle Cretaceous Hippuritacea (rudists) of the Gulf Coast. Gulf Coast Association of Geological Societies Transactions 27, 32–70.

Douglass, R. C., 1961. Orbitolinas from Caribbean islands. Journal of Paleontology 35, 475-479.

Draper, G., Mann, P., and Lewis, J. F., 1994. Chapter 7: Hispaniola, In: Donovan, S. K., and Jackson, T. A., (Eds.), Caribbean Geology An Introduction: The University of West Indies Publishers' Association (IWIPA), Jamaica, 129-150.

Escuder-Viruete, J., Díaz de Neira, A., Hernáiz-Huerta, P.P., Monthel, J., García-Senz, J., Joubert, M., Lopera, E., Ullrich, T., Friedman, R., Mortensen, J., Pérez-Estaún, A., 2006. Magmatic relationships and ages of Caribbean Island arc tholeiites, boninites and related felsic rocks, Dominican Republic. Lithos 90, 161-186.

Erbacher, J., Huber, B. T., Norris, R. D., and Markey, M., 2001. Increased thermohaline stratification as a possible cause for an ocean anoxic event in the Cretaceous period. Nature 409, 325-327.

García-Senz, J., 2004. Mapa geológico a 1:50 000 de Hato Mayor del Rey (6372-III). Hoja y Memoria. Programa SYSMIN 7 ACP DO 024 de Cartografía Geotemática de la República Dominicana. Proyecto L-Este. Consorcio IGME-BRGM-INYPSA. Dirección General de Minería, Santo Domingo.

Gale, A. S., Bown, P., Caron, M., Crampton, J., Crowhurst, S. J., Kennedy, W. J., Petrizzo, M. R., and Wray, D. S., 2011. The uppermost Middle and Upper Albian succession at the Col de Palluel, Hautes-Alpes, France: An integrated study (ammonites, inoceramid bivalves, planktonic foraminifera, nannofossils, geochemistry, stable oxygen and carbon isotopes, cyclostratigraphy). Cretaceous Research 32, 59-130.

Grötsch, J., Billing, I., and Vahrenkamp, V., 1998. Carbon-isotope stratigraphy in shallow-water carbonates; implications for Cretaceous black-shale deposition. Sedimentology 45, 623-634.

Herrle, J. O., Kössler, P., Friedrich, O., Erlenkeuser, H., and Hemleben, C., 2004. High-resolution carbon isotope records of the Aptian to Lower Albian from SE France and the Mazagan Plateau (DSDP Site 545): a stratigraphic tool for paleoceanographic and paleobiologic reconstruction. Earth and Planetary Science Letters 218, 149-161.

Huber, B. T., MacLeod, K. G., Gröcke, D. R., and Kucera, M., 2011. Paleotemperature and paleosalinity inferences and chemostratigraphy across Aptian/Albian boundary in the subtropical North Atlantic. Paleoceanography 26, 1-20.

Iba, Y., and Sano, S., 2007. Mid-Cretaceous step-wise demise of the carbonate platform biota in the Northwest Pacific and establishment of the North Pacific biotic province. Palaeogeography, Palaeoclimatology, Palaeoecology 245, 462-482.

Iba, Y., and Sano, S., 2008. Paleobiogeography of the pectinid bivalve Neithea, and its pattern of step-wise demise in the Albian Northwest Pacific. Palaeogeography, Palaeoclimatology, Palaeoecology 267, 138-146.

Iba, Y., Sano, S., Skelton, P.W., Kagi, H., and Tanabe, K., 2009. First record of Late Albian canaliculate rudist from northern California and re-assessment of Durania? californica Anderson, 1958. Cretaceous Research 30, 540-546.

Iba, Y., Sano, S., and Tanabe, K., 2011. A Tethyan Bivalve, Neithea (Cretaceous Pectinid) from Northern California, and Its Biogeographic Implications. Paleontological Research 15, 62-67.

Iturralde-Vinent, M. A., 1997. Meeting Reports 1, Field Workshop, Dominican Republic July, 1997. Journal of Petroleum Geology 20, 489-491.

Iturralde-Vinent, M. A., and Lidiak, E. G., 2006. Caribbean tectonic, magmatic, metamorphic and stratigraphic events; implications for plate tectonics. Geologica Acta 4, 1-5.

Jenkyns, H.C., 1980. Cretaceous anoxic events: from continents to oceans. Journal of the Geological Society 137, 171-188.

Jenkyns, H. C., Gale, A. S., and Corfield, R. M., 1994. Carbon- and oxygen-isotope stratigraphy of the English Chalk and Italian Scaglia and its palaeoclimatic significance. Geological Magazine 131, 1-34.

Jenkyns, H. C., and Wilson, P. A., 1999. Stratigraphy, paleoceanography, and evolution of Cretaceous Pacific Guyots: Relics from a greenhouse earth. American Journal of Science 299, 341-392.

Jenkyns, H. C., 2003. Evidence for rapid climate change in the Mesozoic-Palaeogene greenhouse world. Philosophical Transactions, Royal Society of London, 361, 1885-1916.

Jenkyns, H. C., 2010. Geochemistry of oceanic anoxic events: Geochemistry Geophysics. Geosystems 11, 1-30.

Jolly, J. T., Lidiak, E. G., Schellekens, J. H., and Santos, H., 1998. Volcanism, tectonics and stratigraphic correlations in Puerto Rico. In Lidiak, E. G., (ed.), Tectonics and Geochemistry of the Northeastern Caribbean: Geological Society of America, Special Paper 322, 1-34.

Johnson, C. C., 1999. Evolution of Cretaceous surface current circulation patterns, Caribbean and Gulf of Mexico. In Barrera, E., and Johnson, C. C., (eds)., Evolution of the Cretaceous ocean-climate systems. Geological Society of America, Special Paper 332, 329-343.

Johnson, C. C., and Kauffman, E. G., 2001. Cretaceous evolution of reef ecosystems: a regional synthesis of the Caribbean tropics. In Stanley, G. D., Jr., (ed.), The History and Sedimentology of Ancient Reef Ecosystems: Topics in Geobiology 17, 311-349.

Kaczor, L., and Rogers, J. J. W., 1990. The Cretaceous Aguas Buenas and Rio Matón limestones of southern Puerto Rico. Journal of South American Earth Sciences 3, 1-8.

Kennedy, W. J., Gale, A. S., Hancock, J. M., Crampton, J. S., and Cobban, W. A., 1999. Ammonites and inoceramid bivalves from close to the middle-upper Albian boundary around Forth Worth, Texas. Journal of Paleontology 73, 1101-1125.

Kesler, S. E., Campbell, I. H., Allen, C. M., 2005a. Age of the Los Ranchos Formation, Dominican Republic: Timing and tectonic setting of primitive island arc volcanism in the Caribbean region. Geological Society of America Bulletin 117, 987-995.

Kesler, S. E., Campbell, I. H., Smith, C. N., Hall, C. M., Allen, C. M., 2005b. Age of the Pueblo Viejo gold-silver deposit and its significance to models for high-sulfidation epithermal mineralization. Society of Economic Geologists 100, 253–272.

Kesler, S. E., Russell, N., Polanco, J., McCurdy, K., and Cumming, G. L., 1991. Geology and geochemistry of the Early Cretaceous Los Ranchos Formation, central Dominican Republic. In Mann, P., Draper, G., and Lewis, J. F., (eds.), Geologic and tectonic development of the North America-Caribbean plate boundary in Hispaniola: Geological Society of America, Special Paper 262,187-201.

Kesler, S. E., Russell, N., Seaward, M., Rivera, J., McCurdy, K., Cumming, G. L., and Sutter, J. F., 1981. Geology and geochemistry of sulfide mineralization underlying the Pueblo Viejo gold-silver oxide deposit, Dominican Republic. Economic Geology 76, 1096-1117.

Kump, L. R., and Arthur, M. A., 1999. Interpreting carbon-isotope excursion: carbonates and organic matter. Chemical Geology 161, 181-198.

Lebrón, M. C., and Perfit, M. R., 1993. Stratigraphic and petrochemical data support subduction polarity reversal of the Cretaceous Caribbean island arc. The Journal of Geology 101, 389-396.

Luciani, V., Cobianchi, M., and Jenkyns, H. C., 2004. Albian high-resolution biostratigraphy and isotope stratigraphy: The Coppa della Nuvola pelagic succession of the Gargano Promontory (Southern Italy). Eclogae Geologicae Helvetiae 97, 77-92.

Mancini, E. A., and Scott, R. W., 2006. Sequence Stratigraphy of Comanchean Cretaceous Outcrop Strata of Northeast and South-Central Texas: Implications for Enhanced Petroleum Exploration. Gulf Coast Association of Geological Societies Transactions - Gulf Coast Association of Geological Societies 56, 539-550.

Midwood, A. J., and Boutton, T. W., 1998. Soil carbonate decomposition by acid has little effect on $\delta^{13}C$ of organic matter. Soil Biology and Biochemistry 30, 1301-1307.

Myczyński, R., Iturralde-Vinent, M., 2005. The late lower Albian invertebrate fauna of the Río Hatillo Formation of Pueblo Viejo, Dominican Republic. Caribbean Journal of Science 41, 782-796.

Nelson, C. E., 2000. Volcanic domes and gold mineralization in the Pueblo Viejo district, Dominican Republic. Mineralium Deposita 35, 511-525.

Phelps, R. M., 2011. Middle-Hauterivian to lower-Campanian sequence stratigraphy and stable isotope geochemistry of the Comanche Platform, south Texas; unpublished Ph.D. thesis, The University of Texas, Austin, Texas, 198 p.

Pindell, J. L., 1991. Geologic rationale for hydrocarbon exploration in the Caribbean and adjacent regions. Journal of Petroleum Geology 14, 237-257.

Pindell, J. L., Kennan, L., 2009. Tectonic evolution of the Gulf of Mexico, Caribbean and northern South America in the mantle reference frame: an update. Geological Society, London, Special Publications 328, 1-55.

Pindell, J. L., Kennan, L., Wright, D., Erikson, J., 2009. Clastic domains of sandstone in central/eastern Venezuela, Trinidad, and tectonic constraints on provenance and

pelaeogeography. Geological Society, London, Special Publications 328, 743-797.

Rojas, R., Iturralde-Vinent, M., and Skelton, P. W., 1996. Stratigraphy, composition and age of Cuban rudist-bearing deposits. Revista Mexicana de la Ciencias Geológicas 12, 272-291.

Russell, N., and Kesler, S.E., 1991. Geology of the maar-diatreme complex hosting precious metal mineralization at Pueblo Viejo, Dominican Republic. In Mann, P., Draper, G., and Lewis, J. F., (eds.), Geologic and tectonic development of the North America-Caribbean plate boundary in Hispaniola. Geological Society of America, Special Paper 262, 203–215.

Schlanger, S.O., and Jenkyns, H.C., 1976. Cretaceous oceanic anoxic events; causes and consequences. Netherlands Journal of Geosciences 55, 179-184.

Scholle, P. A., and Arthur, M. A., 1980. Carbon isotope fluctuations in Cretaceous pelagic limestones: potential stratigraphic and petroleum exploration tool. AAPG Bulletin 64, 67-87.

Scott, R. W., and Gonzalez-León, C., 1991. Paleontology and biostratigraphy of Cretaceous rocks, Lampazos area, Sonora, Mexico. In Pérez-Segura, E., and Jacques-Ayala, C., (Eds.), Studies of Sonoran Geology. Geological Society of America, Special Paper 254, 51-67.

Scott, R. W., 2002a. Albian Caprinid rudist from Texas re-evaluated. Journal of Paleontology 76, 408-423.

Scott, R. W., 2002b. Upper Albian benthic foraminifers new in west Texas. The Journal of Foraminiferal Research 32, 43-50.

Scott, R. W., and Kerans, C., 2004. Late Albian carbonate platform chronostratigraphy, Devil Rivers Formation cycles, west Texas. Courier Forschungsinstitut Senckenberg 247, 129-148.

Scott, R. W., and Filkorn, H. F., 2007. Barremian-Albian rudist zones, U.S. Coast. Society for Sedimentary Geology Special Publication 87, 167-180.

Sillitoe, R. H., 2008. Major gold deposits and belts of the North and South American Cordillera: Distribution, tectonomagmatic settings, and metallogenic considerations. Economic Geology 103, 663-687.

Sillitoe, R. H., Hall, D. J., Redwood, S. D., and Waddell, A. H., 2006. Pueblo Viejo high-sulfidation epithermal gold-silver deposit, Dominican Republic: A new model of formation beneath barren limestone cover. Economic Geology 101, 1421-1435.

Skelton, P. W., 1996. IGCP Project 364: Correlation of Caribbean ophiolites and volcanic arcs – field meeting. Episodes 19, 27-28.

Skelton, P.W., Sano, S.I., and Masse, J.P., 2011. Rudists and the Pacific in the Late Jurassic and Early Cretaceous. Scripta Geologica 142, 13-14.

Smiley, C., 2002. Lower cretaceous plants from the Dominican Republic Volume. In Jackson, T. A., (Ed.), Caribbean geology into the third millennium: transactions of the fifteenth Caribbean geological conference: The University of West Indies Publishers' Association (IWIPA), Jamaica, p. 119-130.

Suarez, M.B., González, L.A., and Ludvigson, G.A., 2011. Quantification of a greenhouse hydrologic cycle from equatorial to polar latitudes: The mid-Cretaceous water bearer revisited. Paleogeography, Paleoclimatology, Palaeoecology 307, 301-312.

Villamil, T., Arango, C., and Hay, W.W., 1999. Plate tectonic paleoceanographic hypothesis for Cretaceous source rock and cherts of northern South America. In Barrera, E., and Johnson, C. C., (eds.), Evolution of the Cretaceous ocean-climate systems: Geological Society of America, Special Paper 332, 191-202.

Wendler, I., Wendler, J., Gräfe, K. U., Lehmann, J., and Willems, H., 2009. Turonian to Santonian carbon isotope data from the Tethys Himalaya, southern Tibet. Cretaceous Research 30, 961-979.

Woodring, W. P., 1954. Caribbean land and sea through the ages. Geological Society of America Bulletin 65, 719-732.

Young, K., 1974. Lower Albian and Aptian (Cretaceous) ammonites of Texas. Geoscience and Man 8, 175-228.

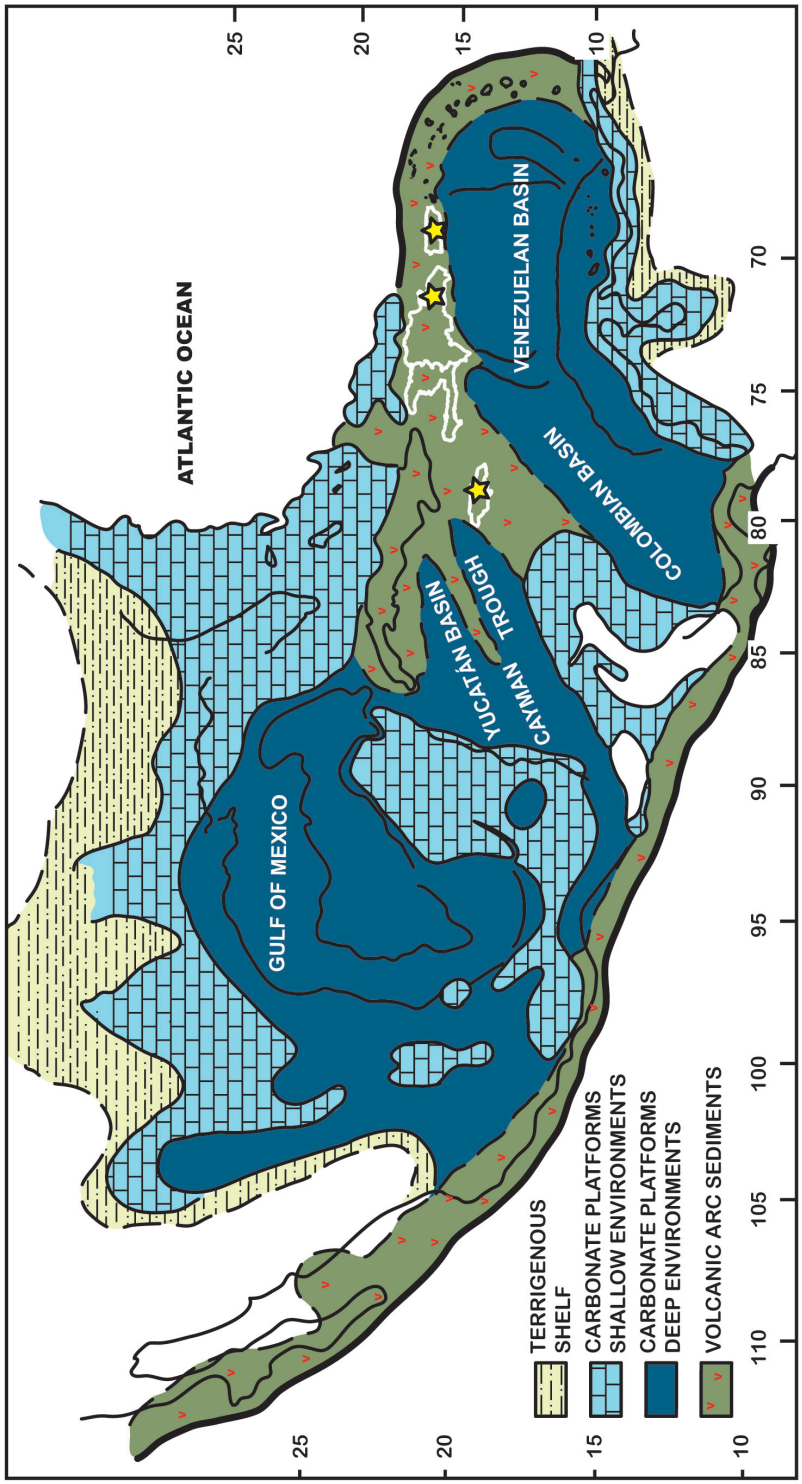

Figure 2.1. Distribution of Aptian-Albian Cretaceous sedimentary rocks in the Caribbean and circum-Caribbean regions (after: Scott, 1984; Scott and Filkorn, 2007; Pindell et al., 2009). Yellow stars show the general location of the study areas in Puerto Rico, the Hispaniola and Jamaica (white outline).

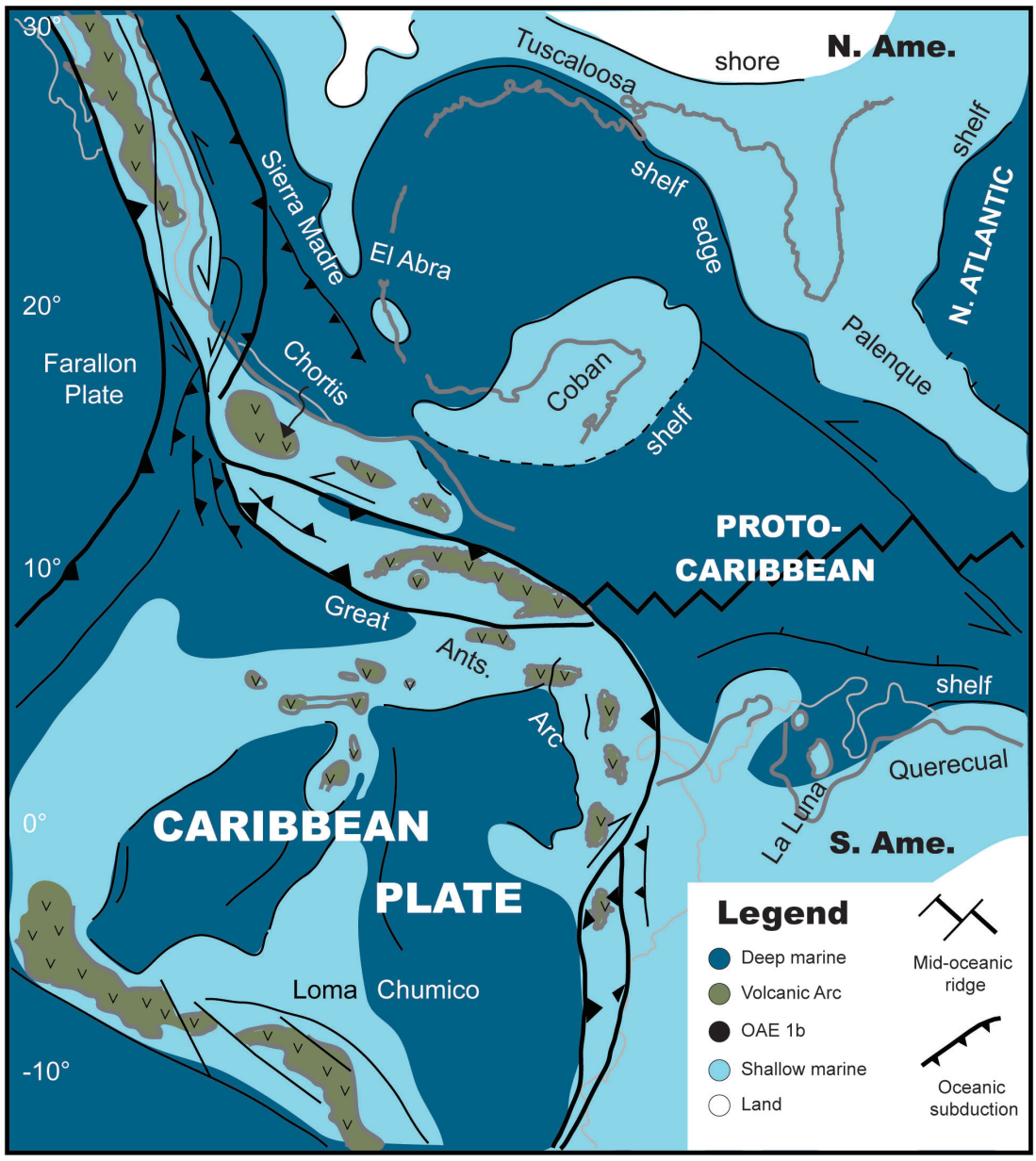

Figure 3.2 The North American, Caribbean and South American plate tectonic reconstruction during the Albian stage (modified after: Pindell and Kennan, 2009). Note that the Greater Antilles volcanic arc is located between the Americas. This paleogeographic reconstruction might account for the poor ocean circulation that resulted in the Ocean Anoxic Events OEA1b in the Western Tethys, where the position of the Greater Antilles acted as a barrier for the Tethys-Pacific ocean circulation.

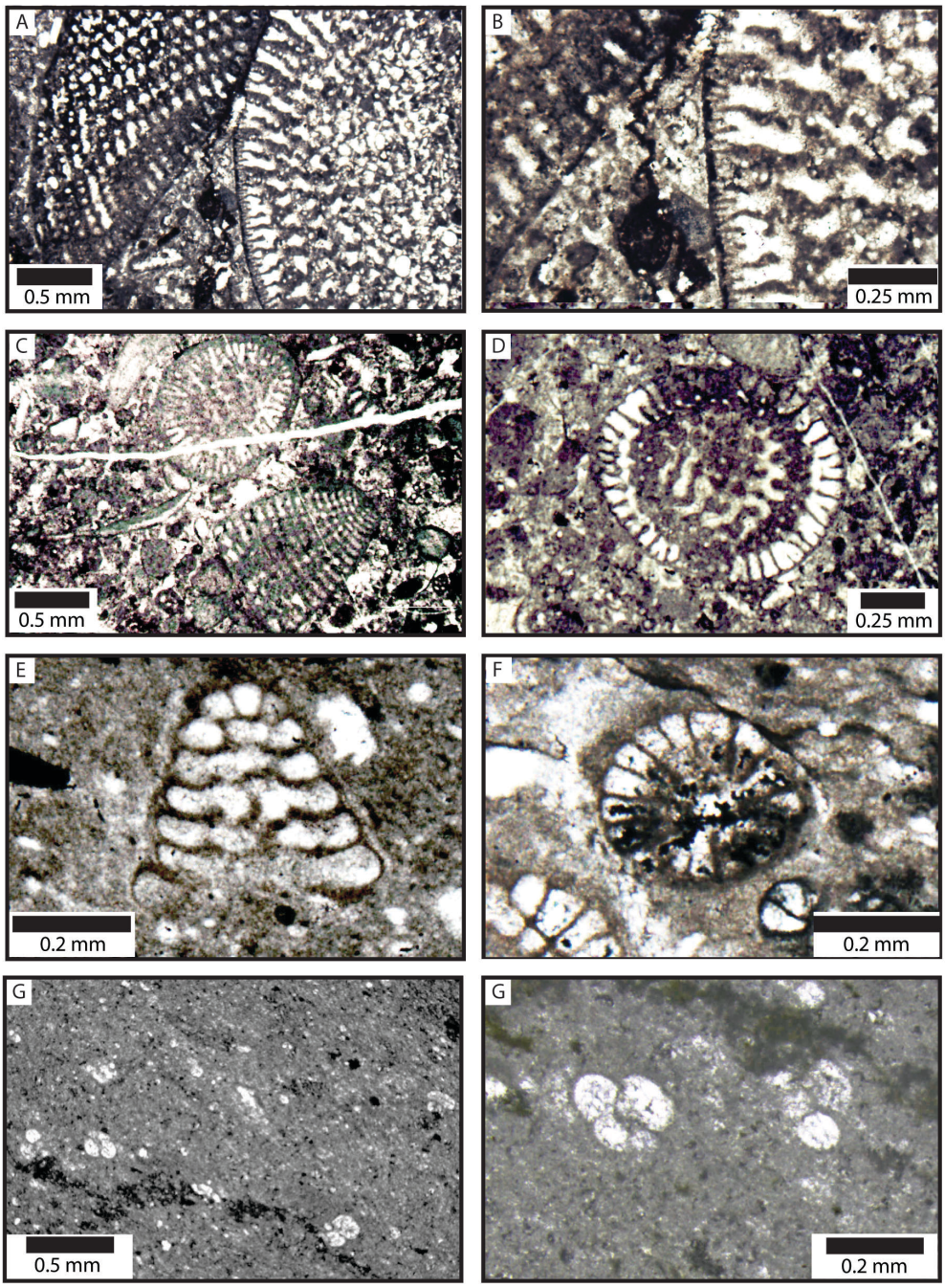

Figure 3.3 A and B: Axial sections of *Orbitulina subconcava* in the Hato Mayor area. C: Basal and axial sections of *Paracoskinolina sunnilandensis* in the Hato Mayor area. D: Basal section of *Paracoskinolina sunnilandensis* in the Hato Mayor area. E: Axial section of *Coskinolinoides texanus* in the Pueblo Viejo area. F: Basal section of *Coskinolinoides texanus* in the Pueblo Viejo area. G and H: *Globigerinida* foraminifers in the Pueblo Viejo area.

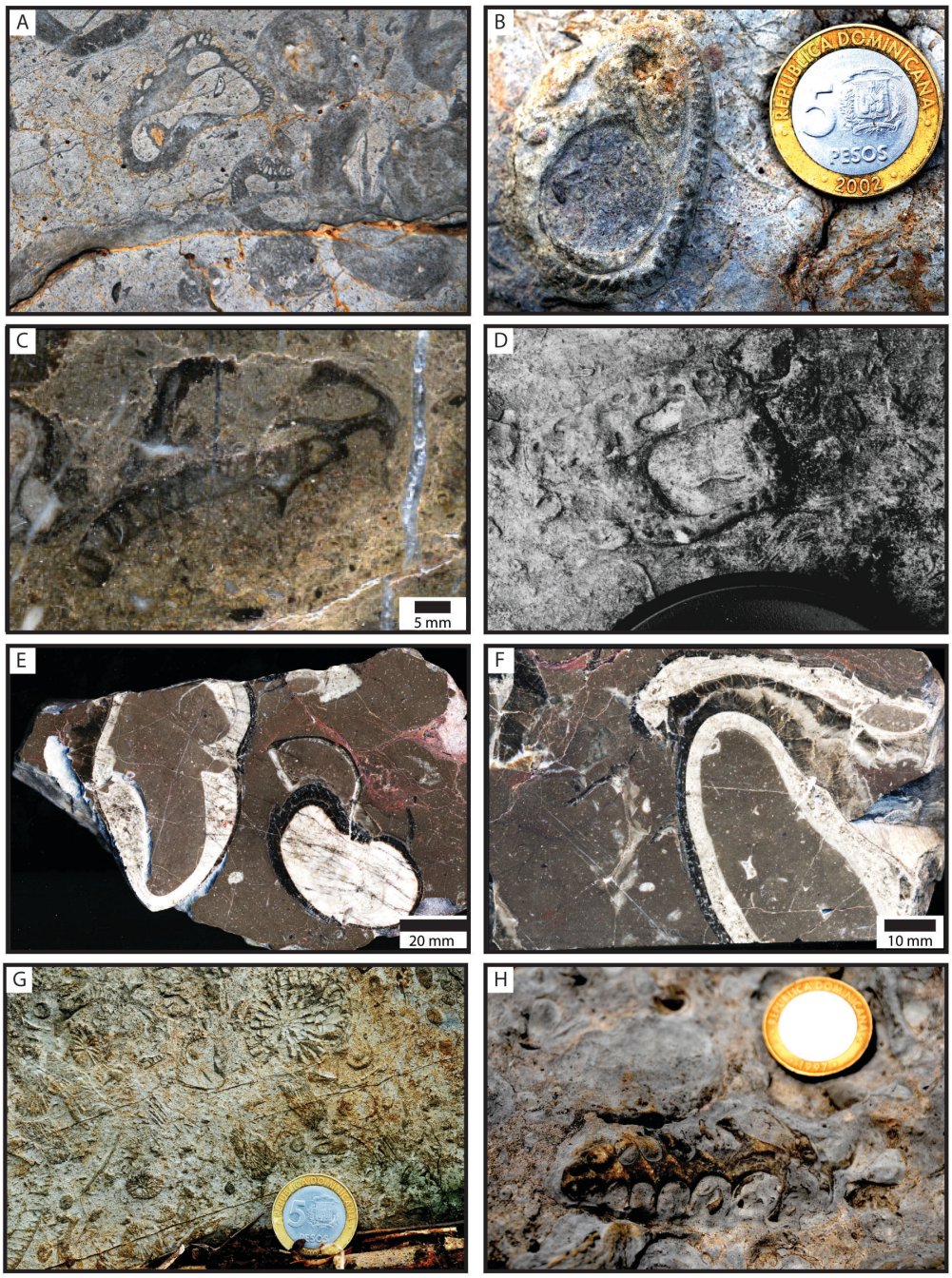

Figure 3.4 A: *Coalcomana ramosa* in the Hato Mayor area. B: *Coalcomana ramosa* in the Hato Mayor area. C: *Coalcomana ramosa* fragment in the borehole core T82 section (Pueblo Viejo area). D: Primitive-form of *Caprinuloidea* sp. in the Hato Mayor section. E and F: *Toucasia* sp. in the Hato Mayor section. G: Corals and rudist bivalves in the Hato Mayor area. H: Oncolitic limestone in the Hato Mayor area showing an oncoid formed around a *Nerineid* gastropod.

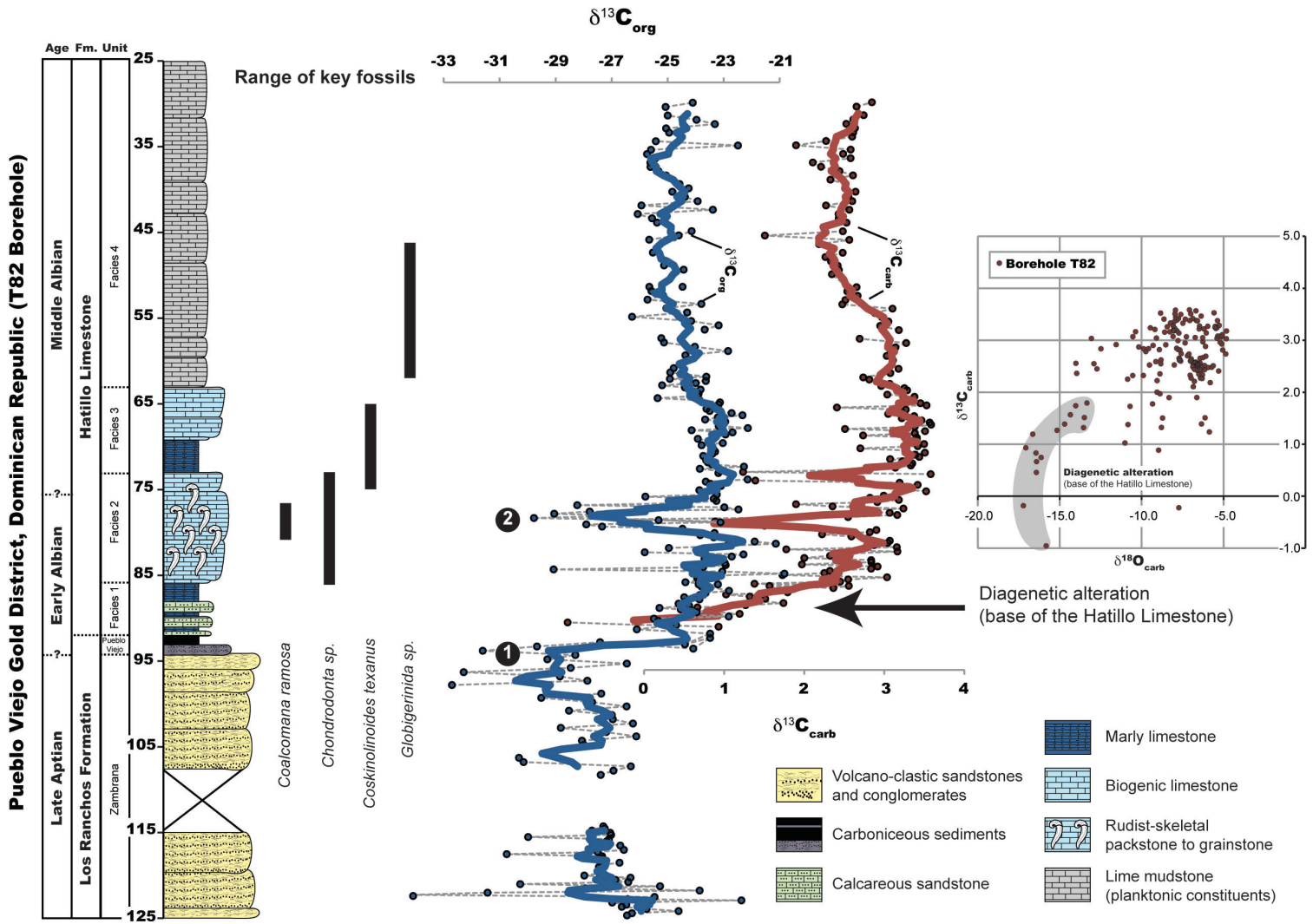

Figure 3.5A Carbon isotope ($\delta^{13}C_{carb}$ and $\delta^{13}C_{org}$) chemostratigraphy compared to lithostratigraphic succession and biostratigraphic record from borehole core T82 section in the Pueblo Viejo Area.

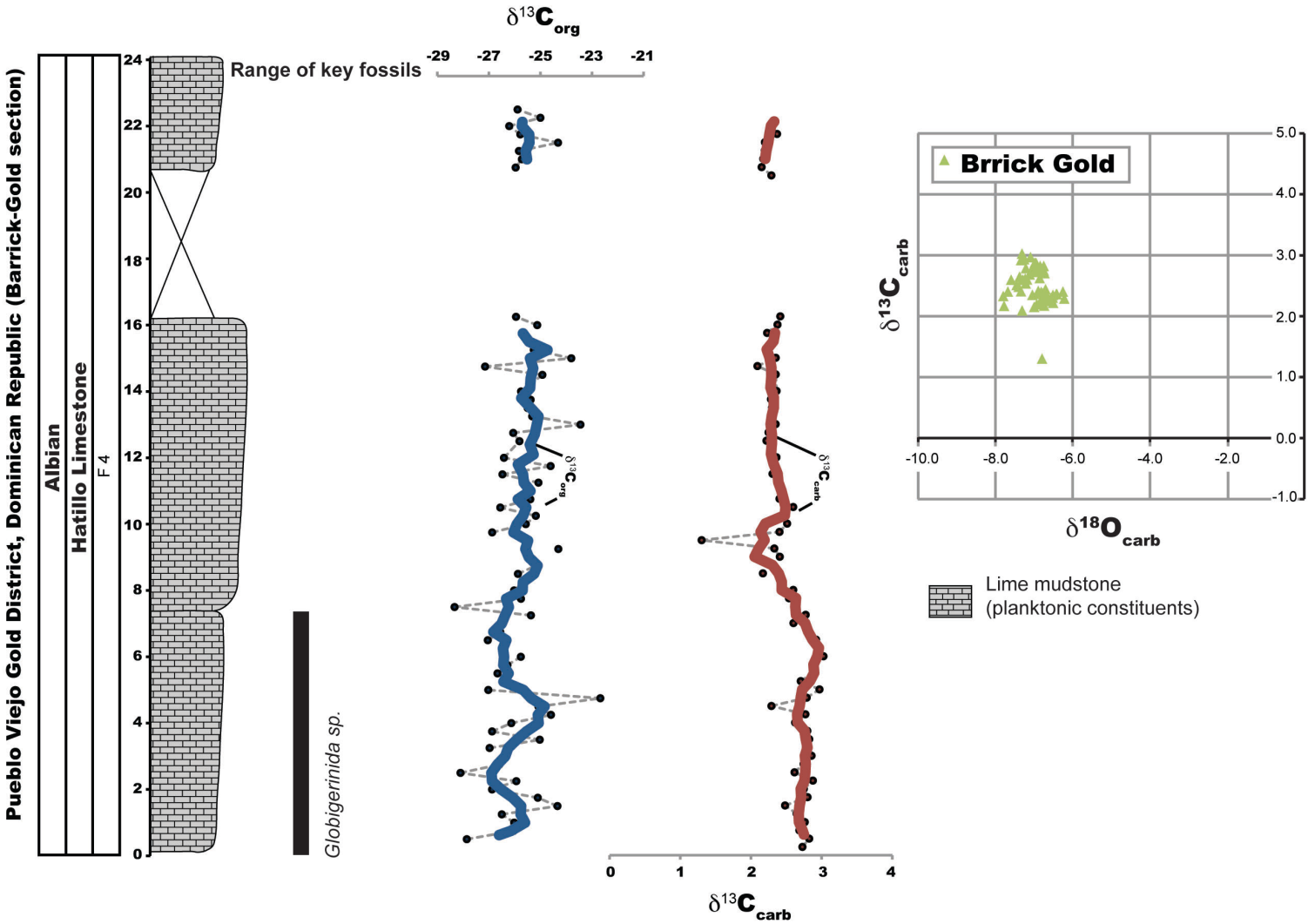

Figure 3.5B Carbon isotope ($\delta^{13}C_{carb}$ and $\delta^{13}C_{org}$) chemostratigraphy compared to lithostratigraphic succession and biostratigraphic record from Barrick-Gold section in the Pueblo Viejo Area.

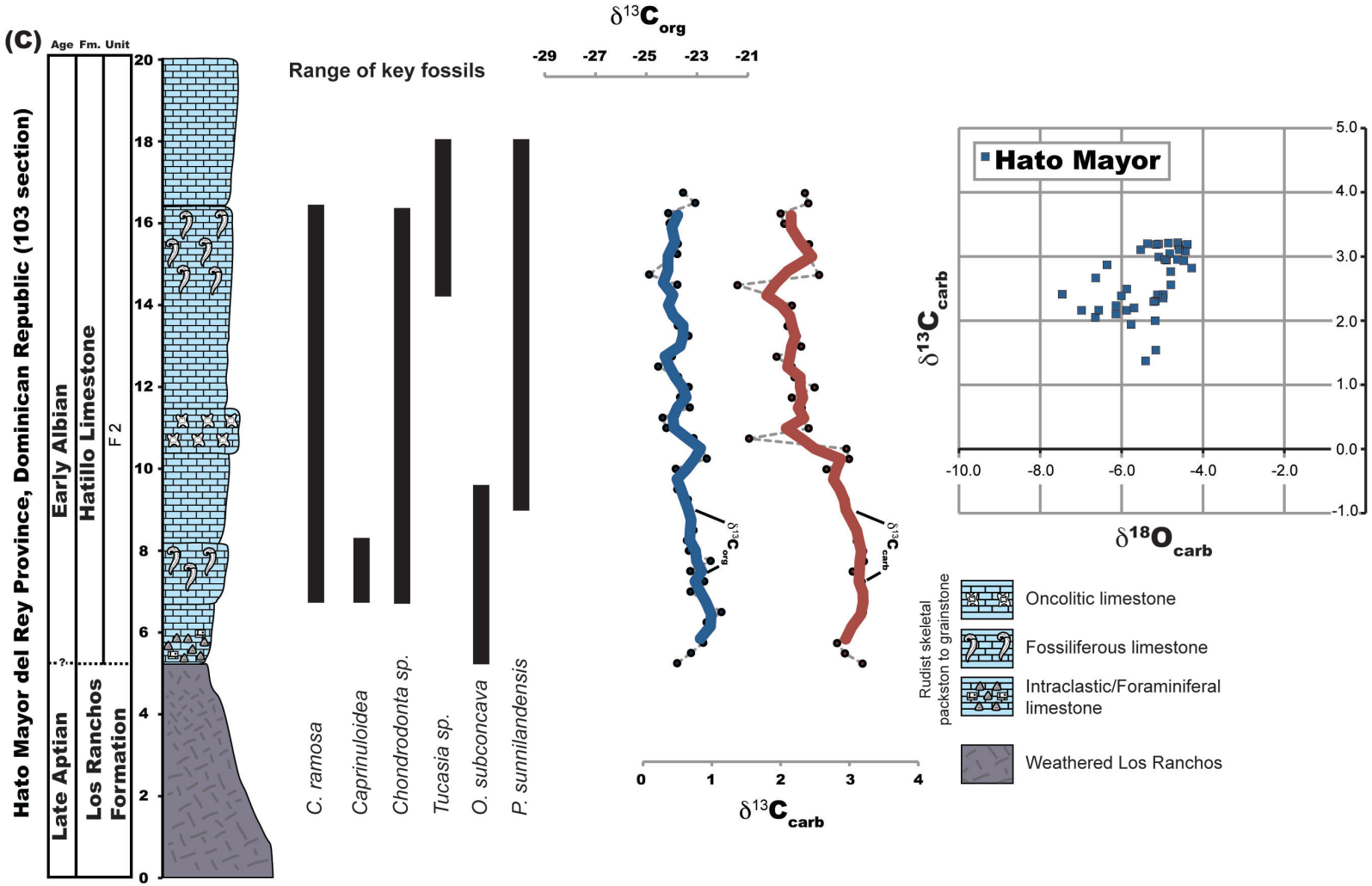

Figure 3.5C Carbon isotope ($\delta^{13}C_{carb}$ and $\delta^{13}C_{org}$) chemostratigraphy compared to lithostratigraphic succession and biostratigraphic record from 103 section in the Hato Mayor Area.

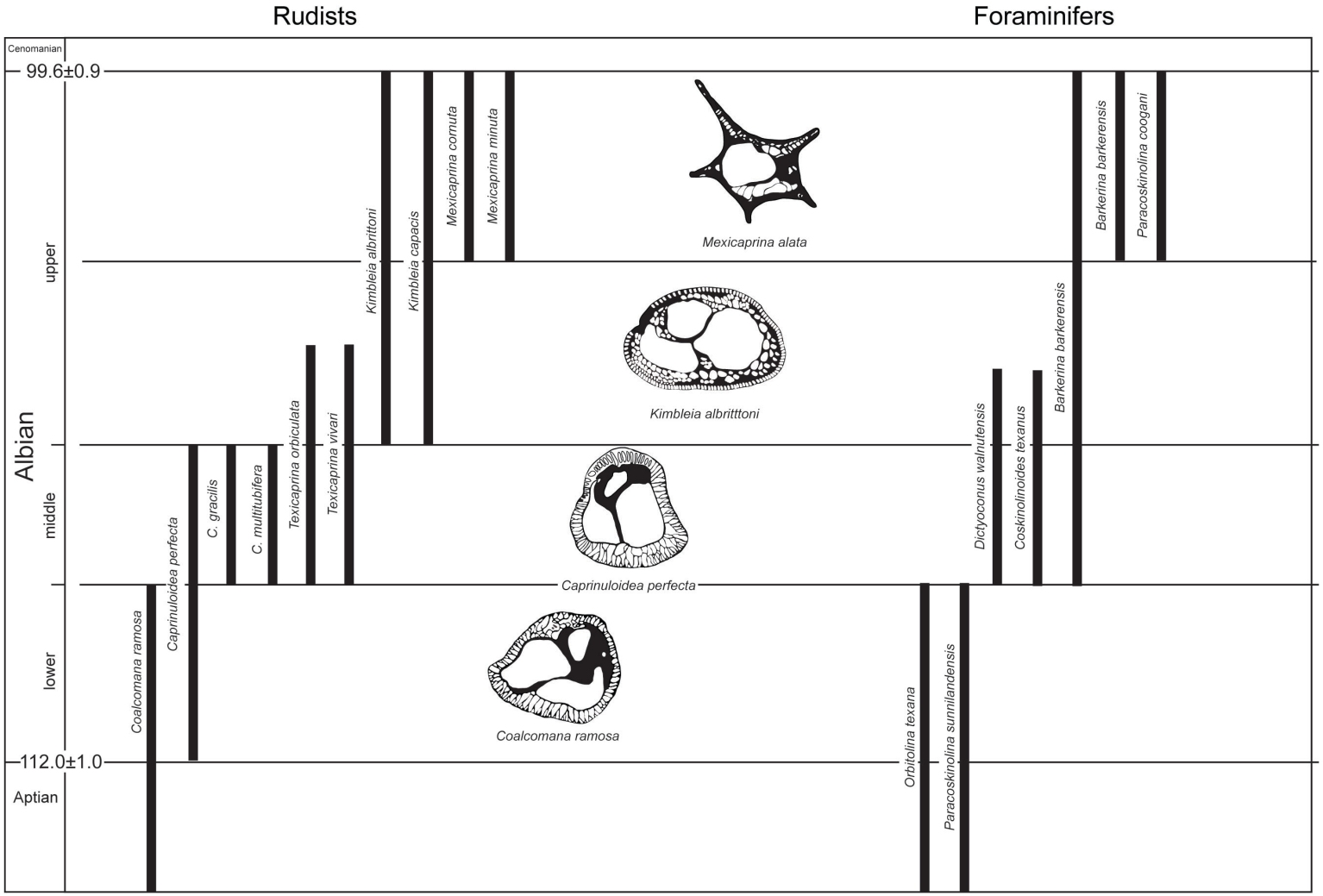

Figure 3.6 Stratigraphic ranges of selected caprinid rudist and orbitolinid foraminifers in Central Texas (modified after: Scott, 2002a,b; Scott and Filkorn, 2007).

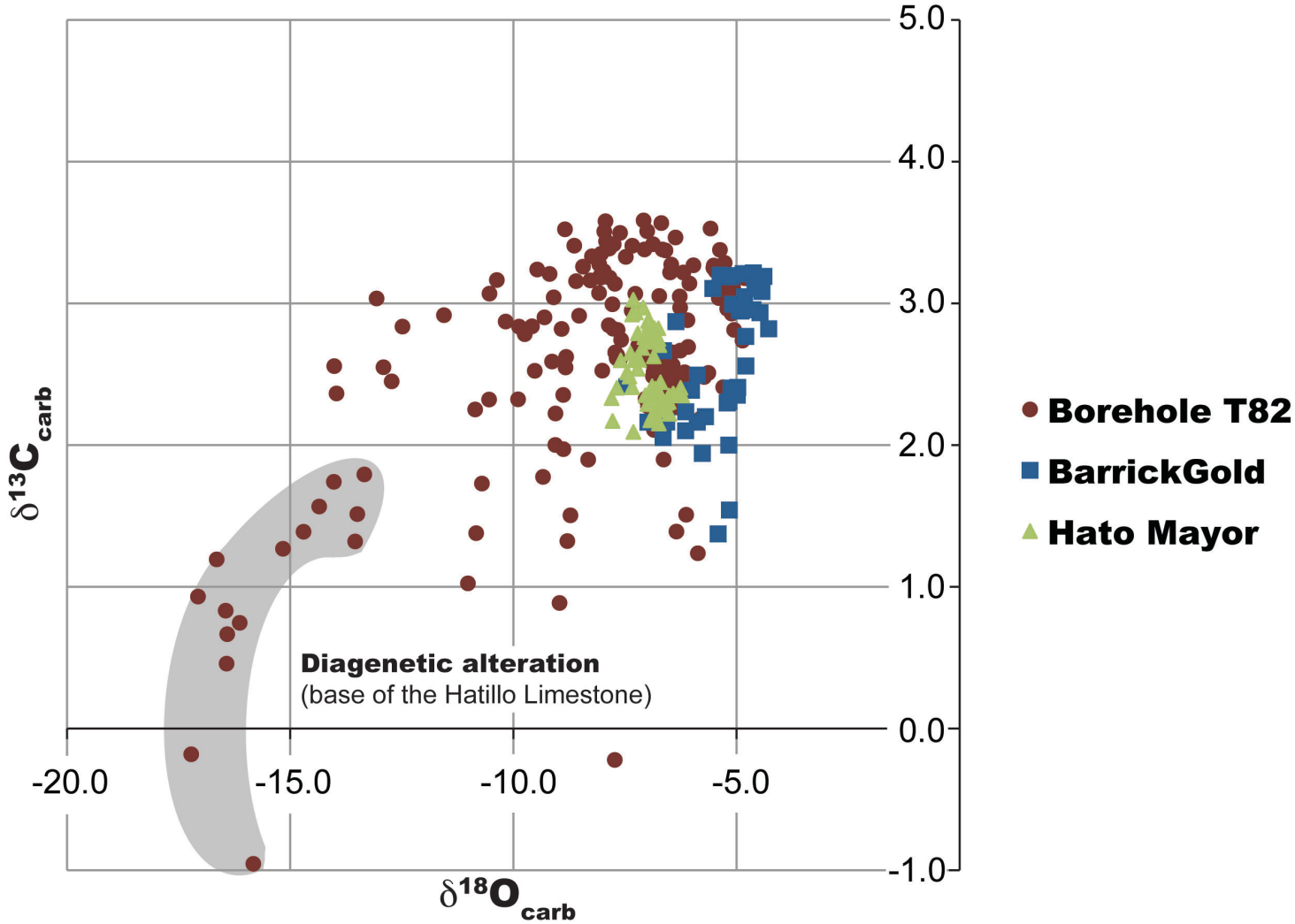

Figure 3.7 Cross-plot of $\delta^{13}C_{carb}$ and $\delta^{18}O_{carb}$ values from the borehole core T82, Barrick-Gold and Hato Mayor sections. The highlighted area shows the diagenetic alteration at the base of the Hatillo Limestone in the borehole core T82 section, Pueblo Viejo area.

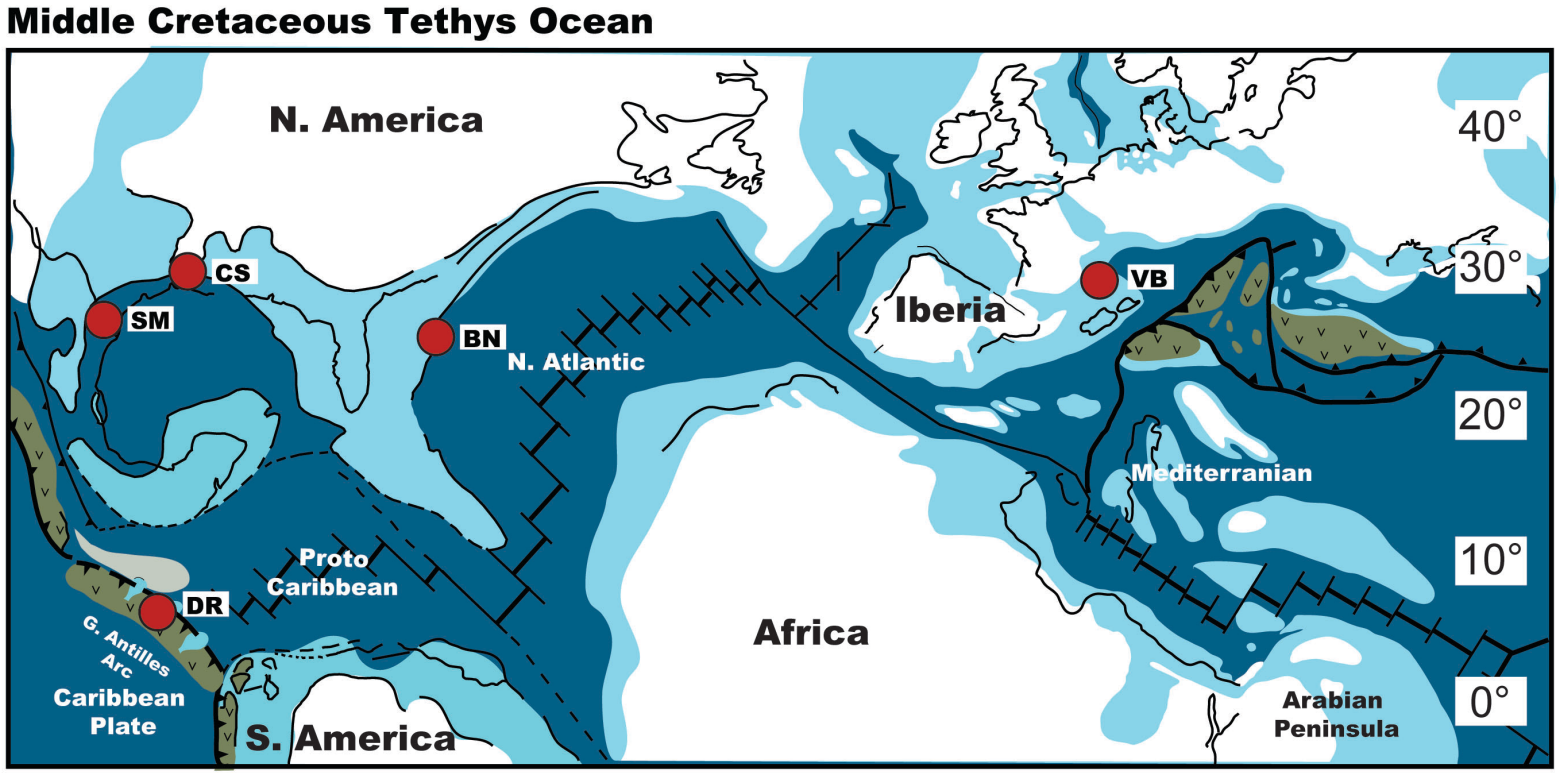

Figure 3.8 Paleographic reconstruction of the Tethys Ocean during the middle Cretaceous. The red dots illustrate the location of the Aptian-Albian $\delta^{13}C$ profiles used to correlate the Hatillo Limestone chemostratigraphic record in the Dominican Republic. SM – Sierra Madre, Mexico (Scholle and Arthur, 1980; Bralower et al., 1999); CS – Comanche Shelf, Texas (Phelps, 2011); DR – Hatillo Limestone, the Dominican Republic (this study); BN – Blake Nose, western Atlantic (Huber et al., 2011; Wilson and Norris, 2001); VB – Vocontian Basin, France (Herrle et al., 2004; Gale et al., 2011).

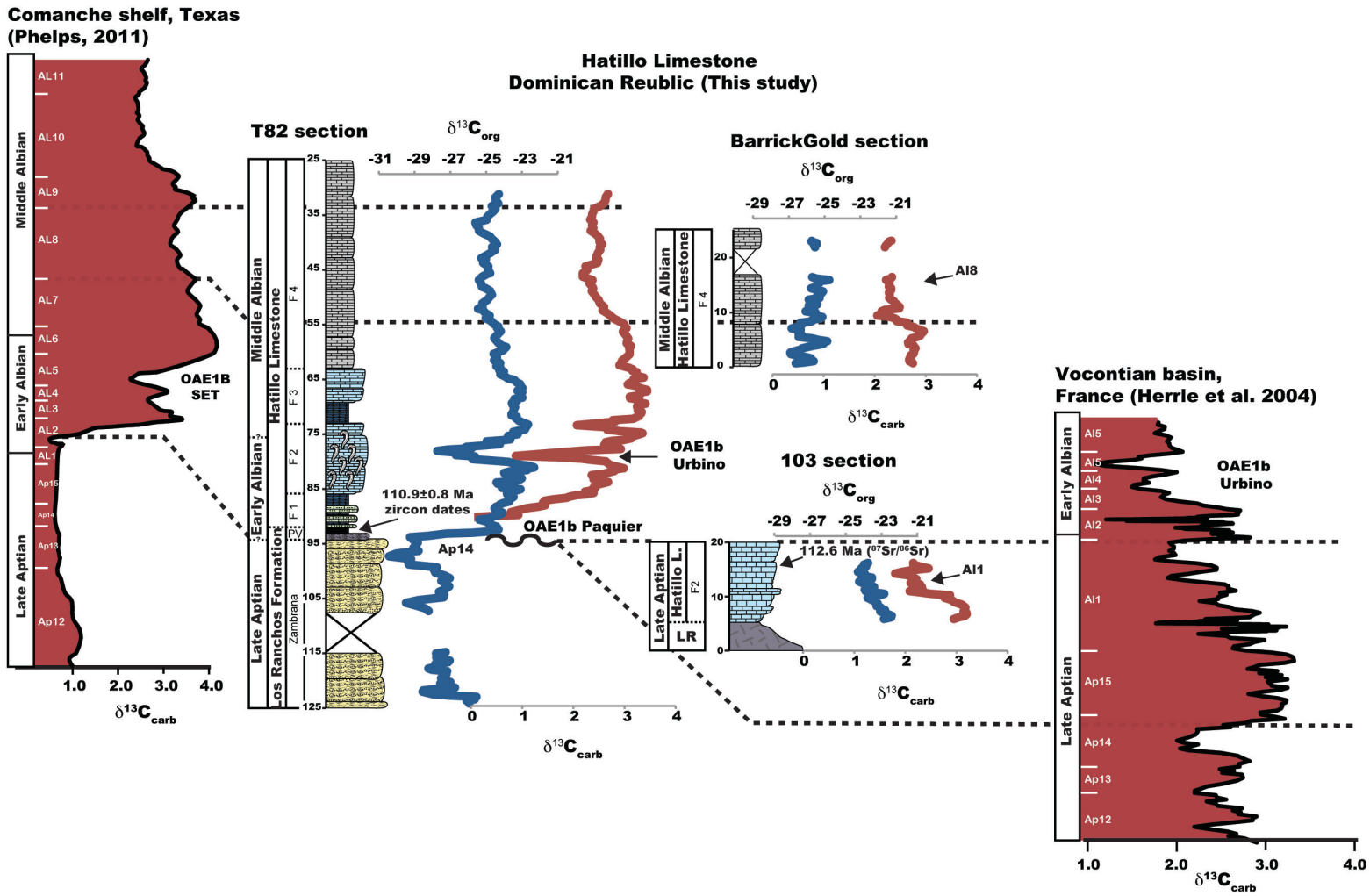

Figure 3.9 Local correlations of the Hatillo Limestone in the Pueblo Viejo Area (Borehole core T82 section and Barrick Gold section in the Pueblo Viejo Gold District), and the Hato Mayor Area (103 section), compared to the $\delta^{13}C$ chemostratigraphic profiles from the Comanche Shelf in Texas (Phelps, 2011) and Vocontian Basin (Herrle et al., 2004).

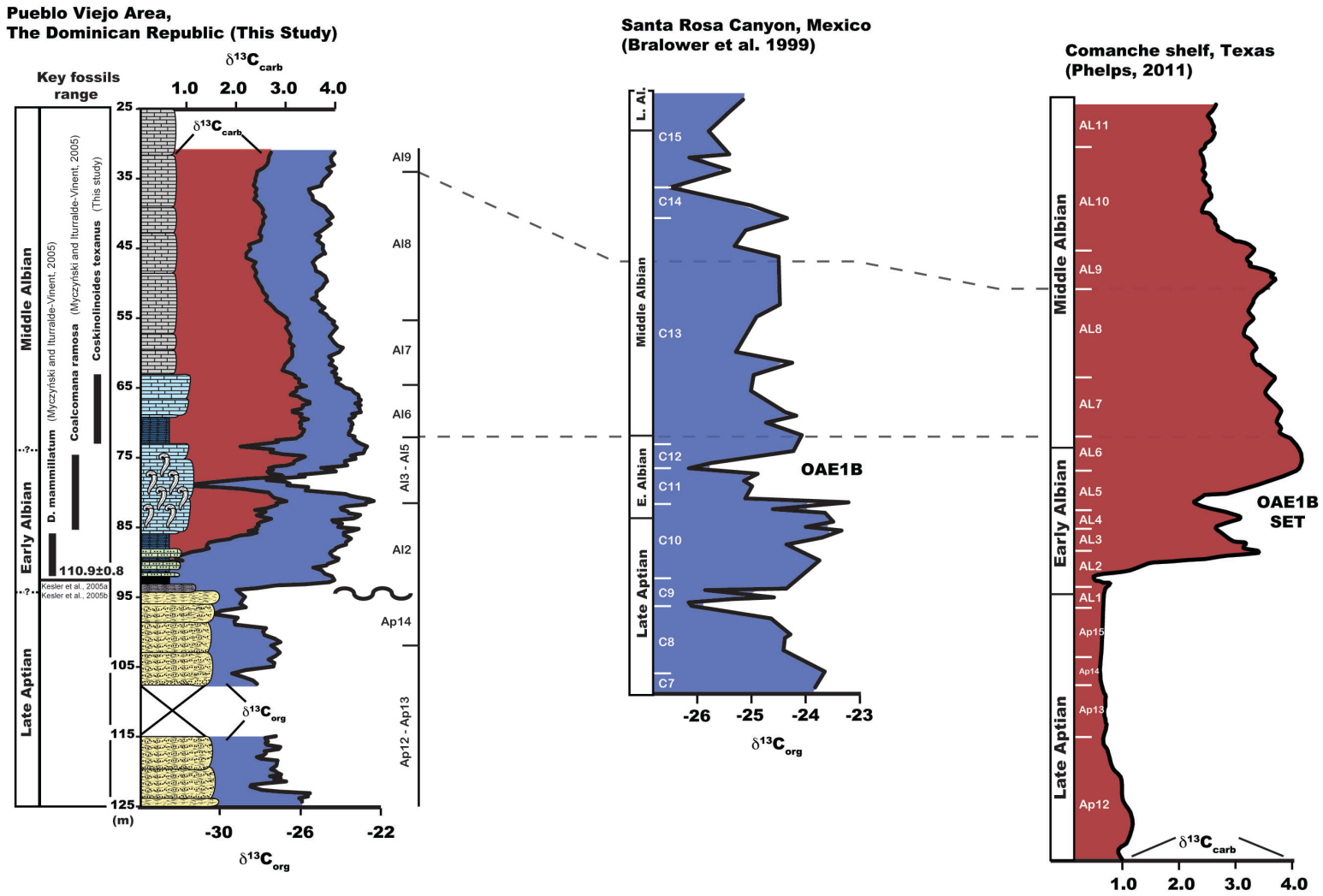

Figure 3.10A Correlation of the Hatillo Limestone chemostratigraphy with the $\delta^{13}C$ records from the Gulf of Mexico (Bralower et al., 1999; Phelps, 2011).

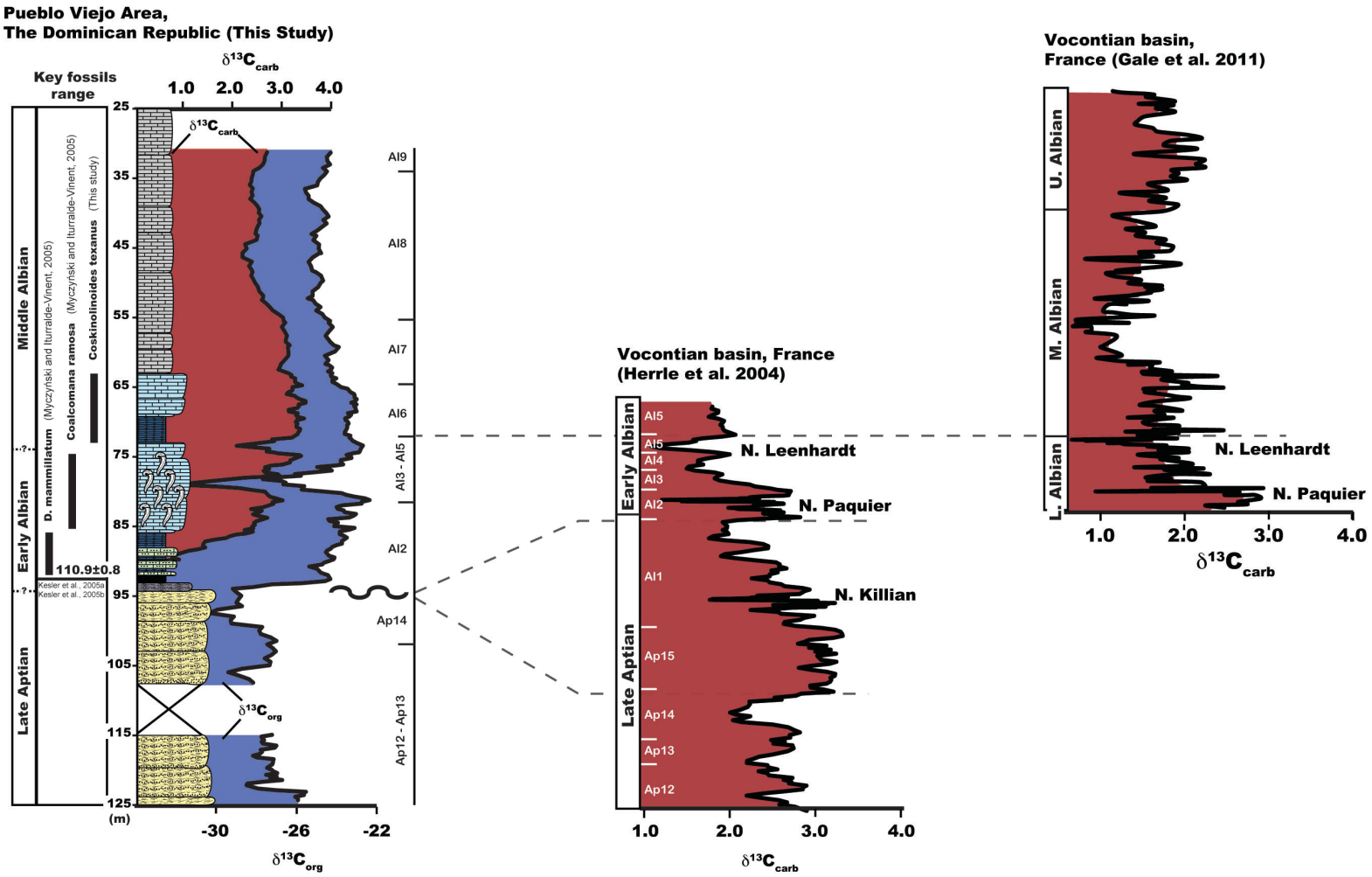

Figure 3.10B Correlation of the Hatillo Limestone chemostratigraphy with the $\delta^{13}C$ records from the Mediterranean Tethys (Herrle et al., 2004; Gale et al., 2011).

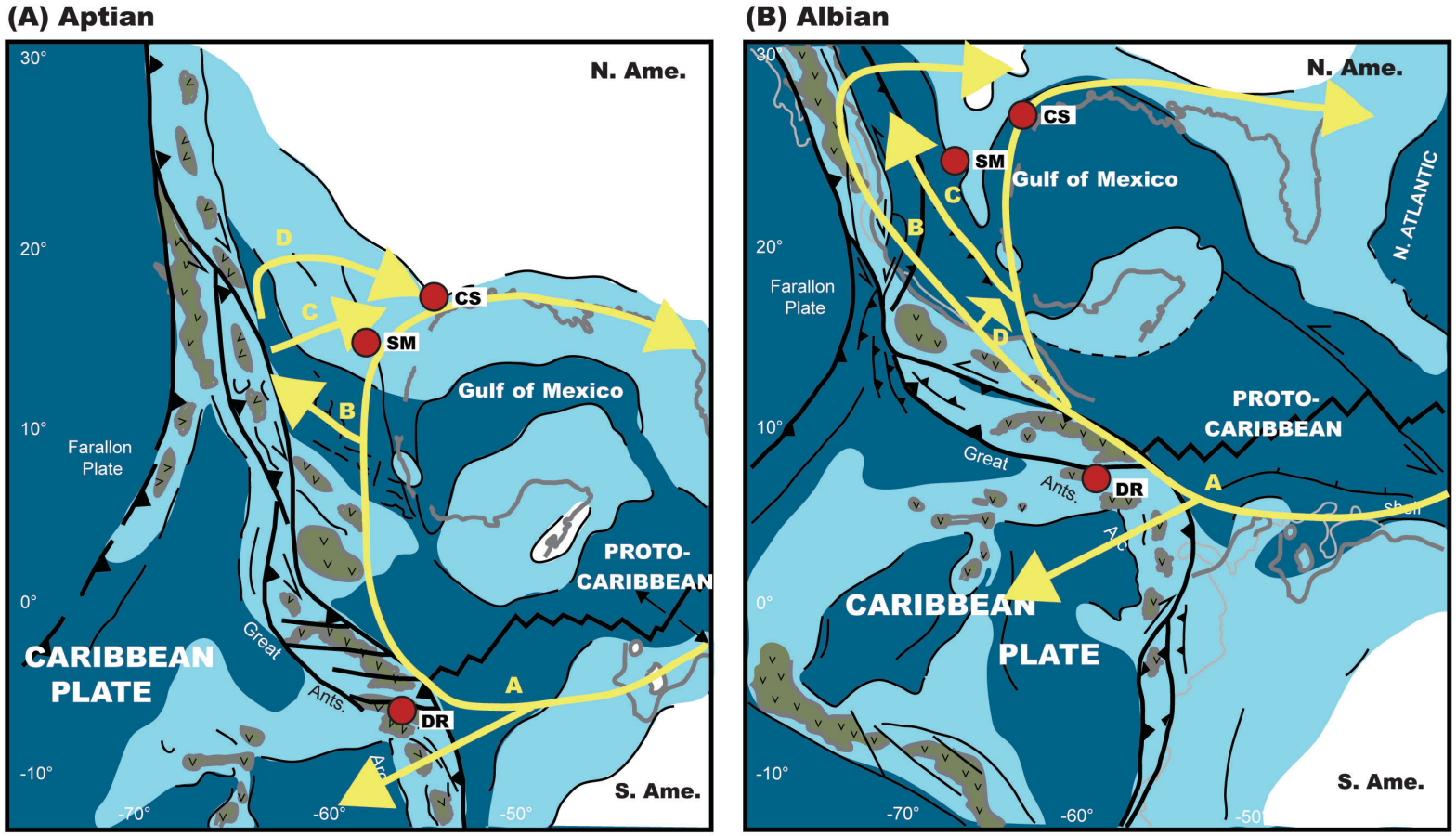

Figure 3.11 (A) Aptian and (B) Albian plate-tectonic and paleogeographic reconstructions (after: Pindell and Kennan, 2009) showing the surface oceanic current flows (yellow arrows) in the Caribbean and Gulf of Mexico regions (after: Johnson, 1999). This figure shows better oceanic current connection between the Caribbean and Gulf of Mexico during the Albian. DR – Dominican Republic (this study); SM – Sierra Madre in Mexico (Bralower et al., 1999); CS – Comanche Shelf in Texas (Phelps, 2011).

Chapter 4 - Stratigraphy and paleoceanographic conditions of the Cotui Limestone Late Cretaceous of southwestern Puerto Rico

ABSTRACT

This study uses strontium isotope stratigraphy to constrain the depositional age of the Cotui Limestone, and oxygen isotopes and fluid inclusions to investigate the Late Cretaceous paleoceanographic conditions (sea surface paleotemperatures and paleosalinities) in the Greater Antilles region. Although age-diagnostic fossils are absent, the Cotui Limestone rudist assemblage (e.g. *Barrettia coatesi* and the *Torreites tschoppi*) is thought to represent a Santonian depositional age. Strontium isotope ($^{87}Sr/^{86}Sr$) ages derived from hippuritid rudists collected in the Cotui Limestone and Guaniquilla Limestone are consistent with late Santonian deposition (84.8 ± 1.2 Ma) for both carbonate platforms. These results demonstrate that part of the limestone exposure mapped as the Guaniquilla Limestone (84.48 Ma) and the Cotui Limestone (84.75 Ma) have nearly identical depositional ages. Fluid inclusion analyses from marine cements found in the inner cavities of hippuritid rudists yielded salinities that range from 35.3 to 41.2 $ppt_{seawater\text{-}salt\ eq}$. The effect of evaporation to water $\delta^{18}O$ composition and the impact on interpreting temperature from calcite $\delta^{18}O$ was evaluated using temperature and salinity reconstructions based on the Railsback et al. (1989) model. In this model, if equatorial western Atlantic conditions are assumed at constant salinities (37 ppt.) paleotemperatures range from 28°C to 34°C. If the evaporative conditions of the Red Sea and Mediterranean at constant salinity (37 ppt.) are assumed, paleotemperatures range

from 30°C to 37°C. If the same Red Sea and Mediterranean evaporative conditions are assumed with seasonal salinity changes (35.3 to 41.2 ppt.), paleotemperatures range from 34°C to 38°C. These results suggest that enhanced evaporation dominated the paleotropics, and agree with global circulation and mass balance models that predict warmer and more saline conditions for tropical and sub-tropical regions during the middle to Late Cretaceous.

INTRODUCTION

Most of the Cretaceous stages are considered as intervals of major global warmth with higher than present-day atmospheric CO_2 concentrations (e.g. Barron, 1983). Cretaceous climate models based on paleogeographic reconstructions, pCO_2 estimations and stable isotope data predict (1) significantly high thermal gradients in low latitudes, (2) warm high latitudes, and (3) an enhanced hydrologic cycle (Barron and Washington, 1982; Barron, 1983; Fassell and Bralower, 1999; Ludvigson et al., 1998; Ufnar et al., 2004). There are, however, uncertainties concerning the conditions in the tropical oceans during Cretaceous greenhouse conditions. Sellwood et al. (1994), for example, described mean equatorial sea surface temperature close to present day for the middle Cretaceous. In their paper, Sellwood et al. (1994) derived their middle Cretaceous equatorial sea surface temperatures from oxygen isotopes ($\delta^{18}O$) of Albian to Cenomanian foraminifers. Conversely, Johnson et al. (1996) proposed warmer than present day conditions in order to explain the expansion of the middle to Late Cretaceous carbonate platforms in tropical and sub-tropical regions. More recently, Fassell and Bralower (1999) challenged the

Sellwood et al. (1994) "coolest" Cretaceous idea citing the effect of enhanced seawater evaporation on calcite enriched $\delta^{18}O$ values. If seawater $\delta^{18}O$ enrichment due to evaporation is taken into account, temperatures derived from calcitic $\delta^{18}O$ values are more consistent with the equable warmer Cretaceous world (Fassell and Bralower, 1999; Zachos et al., 1994). The problem, however, is that there is no accepted proxy to calculate $\delta^{18}O$ seawater enrichment and most interpretations rely on major assumptions based on indirect evidence (Fassell and Bralower, 1999).

The Cretaceous expansion of carbonate platforms in tropical and subtropical areas during elevated atmospheric CO_2 concentrations also introduces an apparent chemical paradox. This paradox is associated with the concerns about marine calcification during intervals with elevated CO_2 concentrations (IPCC, 2007), where enhanced atmospheric pCO_2 results in ocean acidification and subsequent carbonate dissolution. Yet during the middle Cretaceous, Scott (1990) described the carbonate platforms that encircle the Gulf of Mexico as one of the largest and longest-lived reef tracts of Earth history. In order to explain this paradox, Skelton (2003) introduced the "kettle effect". This effect involves intense heating and evaporation of Cretaceous tropical oceans, which resulted in lower seawater CO_2 solubility due to thermal expulsion of aqueous CO_2 and evaporation with a "salting out effect". The seawater becomes supersaturated with respect to $CaCO_3$ and the carbonate factories undergo a positive feedback that is characterized by pushing the CO_2 from seawater back into the atmosphere, maintaining warmth in the tropics and good conditions for calcification (Skelton, 2003). Johnson et al. (1996) used ocean circulation models of salinity and temperature to describe the areas of establishment of ecologically

diverse rudist reefs in the paleotropics and predicted superheated and hypersaline surface water in this areas. Evaporative conditions are also produced in Cretaceous global coupled atmosphere-ocean simulations and mass balance models (Barron, 1995; Suarez et al., 2011; Ufnar et al., 2004).

The Cotui Limestone is one of the largest and best-preserved Late Cretaceous carbonate platforms in southwestern Puerto Rico (Fig. 4.1). Although a Santonian age is partly based on the rudist fauna, uncertainties remain about the depositional age of this carbonate platform. The calcitic outer shell of hippuritid rudists and fibrous calcitic cements of possible shallow-marine origin were analyzed for trace element (Sr, Mg, Mn and Fe) concentrations, strontium isotopes ($^{87}Sr/^{86}Sr$), stable isotopes ($\delta^{13}C$ and $\delta^{18}O$) and fluid inclusions. The results are used to evaluate the preservation of the collected material, constrain the depositional age of the Cotui Limestone, and investigate the paleoceanographic conditions (sea surface paleotemperatures and paleosalinities) during the deposition of this carbonate platform.

GEOLOGIC SETTINGS

In southwestern Puerto Rico, Late Cretaceous rocks are exposed as volcano-sedimentary successions in three major structural blocks: (1) the Mayagüez-Sabana Grande, (2) the Cabo Rojo-San Germán and (3) the Parguera-Ensenada (Fig.4.1) (Mattson, 1960). These volcano-sedimentary successions are represented by periods of intense volcanism and volcaniclastic sedimentation that are followed by deposition of widespread carbonate platform deposits during volcanic quiescence intervals (Jolly et al.,

1998). Although good biostratigraphic controls are absent in these successions, the rudist associations in southwestern Puerto Rico suggest the existence of at least three Late Cretaceous volcano-sedimentary sequences (Santos, 1999). The carbonate platforms exposed in this area include: (1) the Santonian Cotui Limestone, (2) the Campanian Guaniquilla Limestone and (3) the Maastrichtian El Rayo Limestone member of the El Rayo Formation (Fig. 1) (Laó-Dávila et al., 2012; Santos, 1999; Velez-Juarbe and Santos, 2008).

The absence of informative rudist taxa in some localities, however, has resulted in uncertainties surrounding stratigraphic position. The exposure of the Guaniquilla Limestone, for example, is characterized by rugged terrain with thick vegetation that is usually avoided by developers. Volckmann (1984a, 1984b) mapped the limestone exposed west of downtown Cabo Rojo and north of the Boquerón community as part of the Cotui Limestone and limestone lenses from the Sabana Grande Formation, the lithostratigraphic unit above the Cotui Limestone. Santos (1999), however, suggested a younger depositional period for the same limestone exposure (Guaniquilla Limestone) based on the occurrence of younger rudist taxa. Although key Campanian rudists, e.g. *Macgillavryia nicholasi* (Whitfield) and *Barrettia gigas* (Chubb), do occur in several localities mapped as the Guaniquilla Limestone, the lack of fresh exposure has resulted in the debate of whether the entire Guaniquilla Limestone is contained within the Cotui Limestone or if it is a younger depositional unit.

Cotui Limestone

The Cotui Limestone is exposed in the Cabo Rojo-San Germán structural block (Fig. 4.1). The best exposure of the Cotui Limestone occurs in the municipalities of Cabo Rojo, San Germán and Lajas. This limestone overlies unconformably the volcanic and volcaniclastic rocks of the Boquerón and Lajas formations, and is covered by the Monte Grande Formation (Sampayo, 1992), also mapped as the Sabana Grande Formation by Volckmann (1984a, 1984b, 1984c). The maximum development of the Cotui carbonate platform is characterized by five major environmental facies: (1) shallow tidal, (2) shelf, (3) shelf edge, (4) foreslope, and (5) slope facies (Santos, 1990 and 1999). The deposition of the Cotui Limestone ended when a large portion of the carbonate platform was exposed developing karst topography (Sampayo, 1992). A new transgression drowned the Cotui Limestone and resulted in the deposition of the Monte Grande Formation and Guaniquilla Limestone (Sampayo, 1992; Santos 1999).

Uncertainties about stratigraphic range of the Cotui Limestone are associated with the absence of age-diagnostic fossils (e.g. ammonites and nannofossils), and that the only informative fossil, the rudist bivalves, have broad stratigraphic ranges (Rojas et al., 1996). These uncertainties have resulted in age assignation for the Cotui Limestone within the middle to late Santonian (Skelton, 1996), late Campanian (Volckmann, 1984a), and Maastrichtian (Mattson, 1960). The more precise depositional age, the middle to late Santonian, is based on correlations of the Cotui Limestone rudist taxa, e.g. *Barrettia coatesi* (Chubb) and *Torreites tschoppi* (MacGillavey) (Fig. 4.2), with the Peter's Hill Limestone in Jamaica and Loma Yucatán Formation in Cuba (Skelton, 1996).

These rudists, *B. coatesi* and *T. tschoppi*, have not been recorded in rocks younger than Santonian (Skelton, 1996). Moreover, the middle to late Santonian depositional age for the Peter's Hill Limestone (Jamaica) is also based on nannofossil zonations (Jiang and Robinson, 1987).

MATERIALS AND METHODS

The material used in this study was collected from shelf and shelf edge facies exposed in the Sabana Eneas (Cotui Limestone type locality), and El Cerro (Guaniquilla Limestone) localities (Fig. 4.1). In these localities, these facies are dominated by biocalstic matrix and high-energy rudist morphotypes, e.g. recumbent. The studied material mostly consisted of outer shells of hippuritid rudists. In addition, the calcitic cements precipitated within the inner cavities of these hippuritid rudists proved to be valuable for fluid inclusion analyses. The selected material was characterized initially in thin section using a petrographic microscope. Samples selected for further analysis consisted of texturally preserved mollusk shells, primarily hippuritid rudist, and calcite cements. In order to derive numerical ages from $^{87}Sr/^{86}Sr$ analyses and paleoceanographic conditions from $\delta^{18}O$, primary marine signatures and minor diagenetic effects needed to be established. The main preservation filters consisted of cathodoluminescence (CL) microscopy and trace element concentration analyses.

Cathodoluminescence microscopy

CL microscopy was conducted using a Reliotron III CL cathodoluminoscope attached to an Olympus BX41 research microscope with Diagnostic Instrument SPOT RT

camera. In CL microscopy, luminescence is a function of the Fe^{2+} (inhibitor) and Mn^{2+} (activator) contents from the examined material (Dickson, 1990). Because calcite minerals that preserve the original marine geochemistry are generally non-luminescent (absence of Mn^{2+}), the trace elemental concentration analyses were restricted to non-luminescent areas of the collected rudist shells.

Trace elements concentrations

The preservation evaluation based upon trace element concentration relied on the Sr, Mn and Fe concentrations. High Mn and Fe concentrations in skeletal components composed of low-Mg calcite generally indicate diagenetic alteration (Al-Aasm and Veizer, 1986). Because diagenetic carbonates with low concentration of these trace elements are also common in areas with pure carbonates with scarce Mn and Fe bearing minerals (Steuber et al., 2005), strontium concentrations were also used to evaluate degree of diagenetic alteration of our samples, as low Sr concentrations in low-Mg calcitic shells are also indicative of diagenetic alteration (Veizer, 1983). For the trace element concentration analyses, about 100-200 μg of powdered sample was analyzed by ICP-OES (Perkin Elmer Optima 5300DV) for Mg, Sr, Fe and Mn at the University of Kansas KECK Paleoenvironmental and Environmental Stable Isotope Laboratory (K-PESIL). The samples were extracted from polished surfaces of the rudist specimens using tungsten-carbide drill bits. For $^{87}Sr/^{86}Sr$ analyses only samples that contained high Sr (>900 ppm) concentrations, and low Mn (<60 ppm) and Fe (<250 ppm) concentrations were utilized (modified from: Steuber, 2001, and Masse and Steuber, 2007).

Strontium isotope stratigraphy

For the $^{87}Sr/^{86}Sr$ analyses, about 1 mg of powdered sample was obtained from the same general area of the trace element concentration analyses and then dissolved in 3.5 N HNO_3. Strontium was separated from samples through ion-exchange columns filled with strontium-spec resin at the University of Kansas Isotope Geochemistry Laboratories. All samples were analyzed for high precision $^{87}Sr/^{86}Sr$ ratios on the Sector 54 Thermal Ionization Mass Spectrometer (TIMS) in the same laboratory. The applied isotope fractionation correction was $^{86}Sr/^{88}Sr = 0.1194$ using exponential correction. Isotope ratios were adjusted to correspond to a value of 0.71248 on NBS987 for $^{87}Sr/^{86}Sr$ (external precision was 3ppm on ratio on standards during the duration of analyses) to be consistent with the McArthur et al. (2001) normalization. The precision of the derived numerical ages was calculated by combining the 2-sigma internal error of individual $^{87}Sr/^{86}Sr$ measurements (±0.000015), based upon replicate determinations of the NBS987, and the inferred errors from the McArthur et al. (2001) "look-up" table and $^{87}Sr/^{86}Sr$ seawater curve.

Stable isotopes ($\delta^{13}C$ and $\delta^{18}O$)

The carbon ($\delta^{13}C$) and oxygen ($\delta^{18}O$) isotope analyses were performed at the University of Kansas, KPESIL laboratory. These analyses were used to estimate the paleoceanographic conditions, e.g. sea surface paleotemperature, during the deposition of the Cotui Limestone. For these analyses, about 80-100 μg of powdered carbonate sample was obtained using a dental drill with tungsten-carbide bits from polished surfaces of rudists. The powdered samples were vacuum roasted at 200°C for one hour to remove

volatile organics before the isotopic analyses. The isotopic analyses were conducted using phosphoric acid (H_3PO_4) digestion at 75 °C on a ThermoFinnigan KIEL III attached to a dual inlet system ThermoFinnigan MAT 253 isotope ratio mass spectrometer. All reported $\delta^{13}C$ and $\delta^{18}O$ values refer to the VPDB standard with precision better than ± 0.1 ‰ (VPDB) as calculated from the results of multiple analyses of NBS18 and NBS19.

Fluid inclusions

Fluid inclusion measurements were conducted in calcite cements from the inner cavities of a hippuritid rudist collected in the Sabana Eneas area. Fluid inclusion-rich concentric growth zones alternate with clearer zones and served as evidence for primary origin for fluid inclusions. Additionally, the domination of all liquid inclusions in the fluid inclusion assemblages (FIAs) was used to indicate low temperature of entrapment (less than about 50°C). The generation of "bubbles" through artificial stretching of the fluid inclusions was necessary to measure the temperature of final melting of ice (Tm ice) in inclusions. The stretching was accomplished by heating the samples (~110°C) overnight for several days. The inclusions were frozen and the final melting temperature of the ice (Tm ice) was measured following the method in Goldstein and Reynolds (1994). Salinities were calculated as ppt seawater salt equivalent using the Goldstein and Reynolds (1994) calibration equation: ppt seawater salt = $-0.17 + 19.22\theta - 0.932\theta^2 + 0.34\theta^3$, where θ is the depression of the freezing point (Tm ice) in °C.

RESULTS

Preservation of marine signal

Although the outer shell of hippuritid rudists is frequently thick and composed of low-Mg calcite, most of the collected specimens contain shells with cellular microstructures of polygonal shapes with void-filling sparry calcite cements (Fig. 4.3A). To eliminate contamination with sparry calcite, the analyzed material consisted of hippuritid rudist shells with compact fibrous-prismatic structures (Fig. 4.3B). For this reason, only four of the collected hippuritid rudists were evaluated for preservation using trace element concentrations: one from the Cotui Limestone (Sabana Eneas area) and three from the Guaniquilla Limestone (El Cerro area). From these rudist specimens, only three met the trace element concentration criteria for low diagenetic alteration and were analyzed for strontium isotopes ($^{87}Sr/^{86}Sr$). Diagenetic alteration of our samples is reflected by decreased Sr concentrations and increased Mn concentrations (Fig. 4.4A). The preservation of the analyzed hippuritid rudists is supported by consistent $^{87}Sr/^{86}Sr$ values from samples with strontium concentrations >900ppm (Fig. 4.4B).

$^{87}Sr/^{86}Sr$ derived ages

Using the $^{87}Sr/^{86}Sr$ "look-up" table and reference curve for Late Cretaceous seawater (McArthur et al., 2001), the analyzed specimens for the Cotui Limestone and Guanquilla Limestone indicate late Santonian ages (Fig. 4.5). These results include $^{87}Sr/^{86}Sr$-derived ages of 84.8 Ma for the rudist in the Sabana Eneas locality (Cotui Limestone type section), and 84.4 Ma and 84.5 Ma for the rudists in the El Cerro locality

(Guaniquilla Limestone) (Table 4.1). Although the analyzed rudist yielded consistent late Santonian ages (mean = 84.5 Ma), our analytical error (0.000015 $^{87}Sr/^{86}Sr$) and the inherent age uncertainty from the McArthur (2001) "look-up" table resulted in a mean age uncertainty of ±1.2 Ma; thus while the maximum age remains Santonian, the minimum age is earliest Campanian.

Stable isotopes ($\delta^{13}C$ and $\delta^{18}O$)

Carbon ($\delta^{13}C$) and oxygen ($\delta^{18}O$) isotope values were generated from three rudist shells with compact fibrous-prismatic structures (196 analyses) collected in the El Cerro locality, and fibrous calcite cements (45 analyses) from the inner cavity of rudist shells from the Sabana Eneas and El Cerro localities (Fig. 4.6). The preservation of our samples was evaluated using trace element concentrations (36 analyses). The preserved $\delta^{18}O$ values range from -4.5 to -2.5‰ (values >-4.5‰), and altered samples from -7.3 to -4.0‰ (values < -4.0‰) (Fig. 4.6). All the $\delta^{13}C$ values (1.5 to 3.5‰) are within the typical Cretaceous ranges for molluscan and marine cements (Fassell and Bralower, 1999) (Fig. 4.6). Diagenetic alteration in marine precipitated calcite typically exhibits negative trends of $\delta^{13}C$ and $\delta^{18}O$ (Anderson and Arthur, 1983). Fassel and Bralower (1999) compared the amount of secondary calcite in the interior walls of planktonic foraminifers with their isotopic composition, and suggested that diagenetic alteration was reflected by low $\delta^{18}O$ values (< -3.0‰). Steuber (1995 and 1999) used trace elemental concentrations and scanning electron microscopy (SEM) as preservation criteria, and reported -5.0‰ $\delta^{18}O$ values for preserved calcitic outer shells of hippuritid rudists in Greece and Turkey.

Sclerochronologic profiles were generated by systematically sampling (1 mm) the calcitic outer shells of three hippuritid rudists from El Cerro locality. From these rudists, only one resulted in $\delta^{18}O$ cyclic pattern within the preserved range (Fig. 4.7). The other hippuritid rudists were dominated by high isotopic variability and depleted $\delta^{18}O$ values. The $\delta^{18}O$ cyclic pattern consisted of gradual increases through ~-3.2‰ and decreases to ~-4.2 ‰. The $\delta^{13}C$ values in this sclerochronologic profile range from 2.0 to 2.5‰ with no visible pattern. This profile includes five cycles of approximately 8 mm vertical growth. A comparable isotopic cyclic pattern was observed in Late Cretaceous rudist bivalves from Greece and Turkey (Steuber, 1995 and 1999), where $\delta^{18}O$ cycles were described as annual variations of paleotemperature and/or paleosalinities.

Fluid inclusions

Fluid inclusions were studied in fibrous calcitic cements precipitated within the inner cavities of one hippuritid rudist collected in the Sabana Eneas type locality of the Cotui Limestone. As the cement zones are interstratified with marine internal sediment, these calcite cements likely precipitated in a marine setting close to the sediment-water interface (Fig. 4.8). Inclusions are concentrated within crystal growth-zone boundaries and thus are considered primary fluid inclusions. Many of the inclusions were too small for microthermometric measurement, but measurable inclusions (20-80 μm) were preserved as one-phase all liquid before artificial stretching. The final melting temperatures of ice (Tm ice) were obtained from 16 fluid inclusions in five fluid inclusion assemblages (FIAs) and were used to calculate Cretaceous shallow marine

paleosalinities (Fig. 4.8). The total range of all the Tm ice measurements was -2.2 to -1.9 °C with an average of -2.1°C and derived salinities range from 41.2 to 35.3 ppt seawater-salt eq. The Tm ice data for FIA 1 were obtained from five inclusions to yield Tm ice ranging from -2.2 to -2.1°C (41.2 to 39.2 ppt). For FIA 2, five inclusions were measured with Tm ice ranging from -2.2 to -2.0°C (41.2 to 37.3 ppt). For FIA 3, three inclusions were measured with Tm ice ranging from -2.0 to -1.9°C (37.3 to 35.3 ppt). For FIA 4, the Tm ice of two inclusions were both -2.1°C (39.2 ppt). For FIA 5, the Tm ice of -2.2°C (41.2 ppt) was measured from a single inclusion.

DISCUSSION

Cotui Limestone stratigraphic range

The depositional age derived from the $^{87}Sr/^{86}Sr$ analyses was used to investigate whether the Guaniquilla Limestone represents a younger depositional period than the Cotui Limestone. Our results show that the depositional ages from both the Cotui Limestone in the Sabana Eneas type section and Guaniquilla limestones in the El Cerro locality are consistent with the late Santonian interval (84.45 Ma). The age uncertainty associated with these analyses, however, indicates middle Santonian to earliest Campanian as the possible depositional range for the Cotui and Guaniquilla limestones. These results support Skelton's (1996) comparison of the Cotui Limestone with the Peter's Hill Limestone (Jamaica), where a similar stratigraphic range (middle to late Santonian) was based upon nannofossil zonations (Jiang and Robinson, 1987). We suggest that the sources for the younger rudist taxa in the Guaniquilla localities, e.g.

Barrettia rusae, Barrettia gigas and *Macgillavrya nicholasi*, are the limestone lenses mapped in the lithostratigraphic unit above the Cotui Limestone, e.g. the Monte Grande Formation (Sampayo, 1992), and/or the Sabana Grande Formation (Volckmann, 1984a) (Fig. 4.8). This is supported by reports of similar younger rudist taxa in the Monte Grande limestone lenses exposed above the Cotui Limestone in the Cerro Buena Vista locality (the Monte Grande Formation type locality - Sampayo, 1992).

Shallow seawater temperatures and salinities

The $\delta^{18}O$ from preserved calcitic shells of hippuritid rudists and cements should reflect the shallow seawater temperatures and the seawater $\delta^{18}O$ compositions at the time of precipitation (Woo et. al, 1992). Shackleton and Kennet (1975) suggested -1.0 ‰ for the Cretaceous $\delta^{18}O$ seawater composition based upon calculations with negligible high latitude ice volume. The Anderson and Arthur (1983) equation: $T°C = 16.0 - 4.14 (\delta^{18}Oc - \delta^{18}Ow) + 0.13 (\delta^{18}Oc - \delta^{18}Ow)^2$, where $\delta^{18}Oc$ is the isotopic composition of the analyzed specimens (-4.5 to -2.5‰) and the $\delta^{18}Ow$ is the isotopic composition of Cretaceous seawater (-1.0 ‰) as calculated by Shackleton and Kennet (1975) was used to calculate the Late Cretaceous Antillean shallow seawater temperatures. The resulting paleotemperatures range from 23 to 32°C and are comparable to the present-day ranges of sea surface temperatures recorded in the modern carbonate shelf in southwestern Puerto Rico (26°C to 31°C; Winter et al., 1998 and 2000). On the basis of the fluid inclusion data, the temperature range derived from the isotopic analyses is known to be incorrect. The incorrectly cooler Cretaceous paleotemperatures can be explained by

seawater $\delta^{18}O$ enrichment associated with enhanced evaporation (e.g. Fassell and Bralower, 1999; Zachos et al., 1994). Climate simulations based on general circulation models at enhanced pCO_2 predict sea surface temperatures up to 5°C warmer than present day for the Cretaceous paleotropics (Barron and Washington, 1982). These warmer temperatures are consistent with the Albian to Santonian sea surface temperatures (31 to 35°C) based upon the organic geochemical proxy TEX_{86} from the equatorial western Atlantic (Forster et al., 2007).

The Railsback et al. (1989) model provides temperature and salinity relationships used by several authors to study the role of evaporation on Cretaceous $\delta^{18}O$ calcite values (e.g. Fassell and Bralower, 1999; Huber et al., 2011; Steuber, 1999; Woo et al., 1992). In this model (Railsback et al., 1989), the calcite $\delta^{18}O$ values are represented by linear trends (isopleths) of possible combinations of temperatures and salinities for calcite precipitation in equilibrium with $\delta^{18}O$ seawater composition. The estimated slopes of these isopleths are based on the seawater $\delta^{18}O$ compositions and salinity variations from the Red Sea and Mediterranean (0.35‰ isotopic enrichment of calcite/ppt increase in salinity; Fassell and Bralower, 1999; Huber et al., 2011; Railsback et al., 1989; Woo et al., 1992), and equatorial Atlantic (0.18‰ isotopic enrichment of calcite/ppt increase in salinity; Steuber, 1999). These studies, however, lack Cretaceous empirical data and had to assume either temperatures or salinities. Woo et al. (1992), for example, assumed temperatures of 23 to 30°C for their $\delta^{18}O$ calcite values, which resulted in predicted salinities of 37 to 41 ppt. Fassell and Bralower (1999) assumed a high salinity range (36.5 to 40.0 ppt.) to calculate warmer than present-day, equatorial sea surface temperatures in

the equatorial western Atlantic. In our study, the Railsback et al. (1989) model was applied using the salinities derived from fluid inclusion analyses (35.3 to 41.2 ppt) and marine $\delta^{18}O$ calcite values (-4.5 to -2.5‰) as the inputs to constrain the maximum range of Late Cretaceous paleotemperatures in the Greater Antilles (Fig. 4.10). Paleotemperatures based on equatorial Atlantic evaporation resulted in a temperature range from 23.8 to 39.4°C (Fig. 4.10A), and for Red Sea and Mediterranean evaporation, from 24.8 to 46.3°C (Fig. 4.10B). Both scenarios resulted in broad paleotemperature ranges that most likely reflect the maximum possible, with underestimation and overestimation of Late Cretaceous sea surface temperatures likely.

In order to better evaluate the ranges of Late Cretaceous sea surface paleotemperatures from the Antillean region, temperatures were calculated from the $\delta^{18}O$ cyclic pattern recorded in the rudist bivalve collected in the El Cerro section (Fig. 4.7) assuming: (1) temperature oscillations with constant salinities, (2) salinity oscillations but no temperature oscillations, and (3) temperature ranges with seasonally variable salinity derived from fluid inclusions. For the constant salinity calculations, temperature ranges were calculated using the Barron (1995) predicted salinity (37 ppt.), which is within the salinity ranges obtained from the fluid inclusion analyses. These calculations resulted in temperature oscillations that range from 28°C to 34°C based upon equatorial western Atlantic conditions (slope 0.18‰/ppt.; Fig 4.11A and 4.12A), and 30°C to 37°C based upon the Red Sea and Mediterranean conditions (0.35‰/ppt; 4.11B and 4.12A). These paleotemperatures approximate the ones derived from the TEX_{86} geochemical proxy (31 to 35°C) for the equatorial western Atlantic during the Albian to Santonian interval

(Forster et al., 2007). At constant temperatures, the salinity ranges calculated for the western Atlantic conditions require 6.9 ppt oscillations (Fig. 4.11C) and for the Red Sea and Mediterranean conditions require 3.6 ppt oscillations (Fig. 4.11D). For the temperature range and seasonal salinities derived from fluid inclusion analyses, the maximum $\delta^{18}O$ calcite value (-3.04‰) of our sclerochronologic profile was inferred to be associated with summer seasons dominated by evaporation (41.2 ppt.), and the minimum $\delta^{18}O$ calcite value of (-4.28‰) was inferred to be associated with rainy seasons with higher precipitation that resulted in dilution and lower salinities (35.3 ppt.). The Red Sea and Mediterranean scenario resulted in the projected high temperatures (38°C) for the intervals with enhanced evaporation and low temperatures (34°C) during the intervals with reduced evaporation (Fig. 4.11B and 4.12A). Steuber (1999) described similar ranges from calcite $\delta^{18}O$ cyclic pattern from the calcitic outer shells of Late Cretaceous hippuritid rudists in Greece and Turkey. The Steuber (1999) study included winter seasons of lower temperatures and salinities, and summer seasons with higher temperatures and salinities. The western Atlantic scenario (Fig. 4.11C), however, resulted in unreasonably low temperatures during intervals with enhanced evaporation and high temperatures during intervals of reduced evaporation.

Despite the potential for errors and uncertainties in these calculations, our results suggest that high seawater temperatures and evaporative conditions dominated carbonate deposition in the Greater Antilles during the Late Cretaceous. This agrees with proposed evaporative tropical oceans during this interval (Barron, 1995; Johnson et al., 1996; Skelton, 2003; Suarez et al., 2011; Ufnar et al., 2004). Moreover, the relationship

between the salinity and $\delta^{18}O$ seawater composition from the Red Sea and Mediterranean model resulted in seawater $\delta^{18}O$ compositions as high as 1.5‰, for salinities of 41.2 ppt. This seawater $\delta^{18}O$ composition is comparable with Suarez et al. (2011) estimations (1.45 to 1.52‰), which were required to adequately simulate isotopic data from pedogenic carbonate into their global hydrology cycle model for the middle Cretaceous. We propose that during summer seasons background conditions of tropical oceans dominated the shallow water shelf environments and that the influx of freshwater from the winter/rainy seasons diluted these salinities and lowered the temperatures.

CONCLUSIONS

Strontium isotope stratigraphy from Upper Cretaceous limestone in southwestern Puerto Rico has confirmed the practical uses of this technique in tectonically complex areas without good stratigraphic controls. Although diagenetic alteration within the cellular microstructures of most of the collected hippuritid rudists limited the $^{87}Sr/^{86}Sr$ analyses to a few specimens with compact fibrous-prismatic structure, the derived ages from these rudists resulted in consistent late Santonian ages (Cotui Limestone 84.8 Ma, and Guaniquilla Limestone 84.4 and 84.5 Ma). These derived ages suggest that part of the limestone exposure mapped as the Campanian Guaniquilla Limestone in southwestern Puerto Rico (Santos, 1999) should be included as part of the Santonian Cotui Limestone. These results are the first step in resolving the debate of whether the limestone exposed in the Guaniquilla area, west of downtown Cabo Rojo and north of the Boquerón community, represents a younger depositional period relative to the Cotui Limestone.

The paleoceanographic conditions based on oxygen isotopes ($\delta^{18}O$) and fluid inclusion analyses resulted in warm and saline conditions during the deposition of the Cotui Limestone. The fluid inclusion paleosalinities (45.3 to 41.2 ppt.) were used to investigate the effect of enhanced evaporation on the calcite $\delta^{18}O$ values by applying three different scenarios to the Railsback et al., (1989) model; (1) equatorial western Atlantic conditions and constant salinities (37 ppt.) resulting in 28°C to 34°C paleotemperatures, (2) Red Sea and Mediterranean conditions with constant salinities (37 ppt.) resulting in 30°C to 37°C paleotemperatures, and (3) seasonal salinity changes (35.3 to 41.2 ppt.) and the Red Sea and Mediterranean conditions resulting in 34°C to 38°C paleotemperatures. These results suggest that the deposition of the Cotui Limestone occurred during enhanced evaporation and support global circulation and mass balance models that predict evaporative conditions in tropical and subtropical oceans during the middle to Late Cretaceous intervals (Barron, 1995; Johnson et al., 1996; Suarez et al., 2011; Ufnar et al., 2004).

REFERENCES

Al-Aasm, I. S., Veizer, J., 1986. Diagenetic stabilization of aragonite and low-Mg calcite; I. Trace elements in rudist. Journal of Sedimentary Petrology 56, 138-153.

Anderson, T. F., Arthur, M. A., 1983. Stable isotopes of oxygen and carbon and their application to sedimentology and paleoenvironmental problems. In: Arthur, M. A., Anderson, T. F. (Eds.), Stable isotopes in sedimentary geology: SEPM Short Course 10, Tulsa, pp. 1.1-1.151.

Barron, E. J., 1983. A warm, equable Cretaceous: the nature of the problem. Earth Science Review 19, 305-338.

Barron, E. J., 1995. Tropical climate stability and implications for the distribution of line. In: Stanley, S. M. (Eds.), Effect of Past Global Change in Life: National Research Council, Studies in Geophysics, 108-117.

Barron E. J., Washington, W. M., 1982. Cretaceous climate: a comparison of atmospheric simulations with the geologic record. Paleogeography, Paleoclimatology, Palaeoecology 40, 103-133.

Fassell, M. L., Bralower, T. J., 1999. Warm, equable mid-Cretaceous: Stable isotope evidence. In: Barrera, E., Johnson, C. C. (Eds.), Evolution of the Cretaceous Ocean-Climate System: Geological Society of America Special Publication 332, 121-142.

Forster, A., Schouten, S., Baas, M., Sinninghe-Damsté, J. S., 2007. Mid-Cretaceous (Albian–Santonian) sea surface temperaturerecord of the tropical Atlantic Ocean. Geology 35, 919-922.

Goldstein, R. H., Reynolds, T. J., 1994. Systematic of fluid inclusions in diagenetic minerals. SEPM Short Course31, Tulsa, 199 pp.

Huber, B. T., MacLeod, K. G., Gröcke, D. R., Kucera, M., 2011. Paleotemperature and paleosalinity inferences and chemostratigraphy across the Aptian/Albian boundary in the subtropical North Atlantic. Paleoceanography 26, 1-20.

IPCC, 2007, Climate Change 2007. The Physical Science Basis. In: Solomon, S., Qin, D., Manning, M., Chen, Z., Marquis, M., Averyt, K. B., Tignor, M., Miller, H. L.

(Eds.) Contribution of Working Group I to the Fourth Assessment Report of the Intergovernmental Panel on Climate Change. Cambridge University Press, Cambridge, United Kingdom and New York, NY, USA.

Jiang, M. J., and Robinson, E., 1987. Calcareous nannofossils and larger foraminifera in Jamaican rocks of Cretaceous to early Eocene age. In: Ahmad, R. (Eds.), Proceedings of a workshop on the status of Jamaican geology. Geological Society of Jamaica, Special Issue, p. 24-51.

Johnson, C. C., Barron, E. J., Kauffman, E. G., Arthur, M. A., Fawcett, P. J., Yasuda, M. K., 1996, Middle Cretaceous reef collapse linked to ocean heat transport. Geology 24, 376-380.

Jolly, W. T., Lidiak, E. G., Schellekens, J. H., Santos, H., 1998. Volcanism, tectonics, and stratigraphic correlations in Puerto Rico. In: Lidiak, E. G. (Eds.), Tectonics and Geochemistry of the Northeastern Caribbean, Geological Society of America (GSA), Special Paper 322, 1-34.

Laó-Dávila, D. A., Llerandi-Román, P. A., Anderson, T., 2012. Cretaceous-Paleogene thrust emplacement of serpentinite in southwestern Puerto Rico: Geology 124, p. 1169-1190.

Ludvigson, G. A., González, L. A., Metzger, R. A., Witzke, B. J., Brenner, R. L., Murillo, A. P., White, T. S., 1998, Meteoric sphaerosiderite lines and their use for paleohydrology and paleoclimatology: Geology, v. 26, p. 1039-1042.

Lyman, J., Fleming, R. H., 1940, The composition of seawater: Journal of Marine Research, v. 3, p.134-146.

McArthur, J. M., Howarth, R. J., Bailey, T. R., 2001, Strontium isotope stratigraphy: LOWESS version 3: Best fit to the marine Sr-isotope curve for 0-509 Ma and accompanying look-up table for deriving numerical age: The Journal of Geology, v. 109, p. 155-170.

Mattson, P. H., 1960, Geology of the Mayagüez area, Puerto Rico: Geological Society of America Bulletin, v. 7, p. 319-362.

Railsback, L. B., Anderson, T. F., Ackerly, S. C., Cisne, J. L., 1989, Paleoceanographic modeling of temperature-salinity profiles from stable isotopic data: Paleoceanography, v. 4, p. 585–591,

Rojas, R., Iturralde-Vinent, M., Skelton, P.W., 1996. Stratigraphy, composition and age of Cuban rudist-bearing deposits. Revista Mexicana de Ciencias Geológicas 12, 272-291.

Santos, H., 1990, The stratigraphy, paleoenvironments, and biofacies of the Cotui Limestone: Cretaceous of southwestern Puerto Rico: M.S. thesis, University of Colorado.

Santos, H., 1999, Stratigraphy and depositional history of the upper Cretaceous strata in the Cabo Rojo-San German structural block, southwestern Puerto Rico: Ph.D. thesis, University of Colorado.

Sampayo, M. M., 1992, Stratigraphy and sedimentology of the Monte Grande Formation, southwestern Puerto Rico: M.S. thesis, University of Colorado.

Scott, R. W, 1990, Models and stratigraphy of mid-Cretaceous reef communities, Gulf of Mexico: Concepts in Sedimentology and Paleontology (SEPM), v. 2. SEPM Society for Sedimentary Geology, Tulsa.

Shackleton NJ, Kennett JP (1975), Paleotemperature history of the Cenozoic and the initiation of Antarctic glaciation: oxygen and carbon isotope analyses in DSDP sites 277, 279, and 281: Init Rep DSDP, v. 29, p. 743–755

Sellwood, B. W., Prlce, G. D., Valdes, P. J., 1994, Cooler estimates of Cretaceous temperatures: Nature, v. 370, p. 453-455.

Skelton, P.W., 1996, IGCP Project 364: Correlation of Caribbean ophiolites and volcanic arcs – field meeting: Episodes, v. 19, p. 27-28.

Skelton, P.W., 2003, The Cretaceous World. Cambridge University Press and The Open University, Cambridge.

Steuber, T., 1995, Stable isotope sclerochronology of *Vaccinites cornuvaccinum* (Hippuritidae) from Beotia (Greece): Revista Mexicana de Ciencias Geológicas, v. 12, p. 307-314.

Steuber, T., 1999, Isotopic and chemical intra-shell variations in low-Mg calcite of rudist bivalves (Mollusca-Hippuritacea): disequilibrium fractionations and late Cretaceous seasonality: Int Journ Earth Sciences, v. 88, p. 551-570.

Suarez, M.B., González, L.A., and Ludvigson, G.A., 2011, Quantification of a greenhouse hydrologic cycle from equatorial to polar latitudes: The mid-Cretaceous water bearer revisited: Paleogeography, Paleoclimatology, Palaeoecology, v.307, p. 301-312.

Ufnar, D. F., González, L. A., Ludvigson, G. A., Brenner, R. L., Witzke, B. J., 2004, Evidence for increased latent heat transport during the Cretaceous (Albian) greenhouse warming, Geology, v. 32, p. 1049-1052.

Velez-Juarbe, J., Santos, H., 2008, Fossil Echinodermata from Puerto Rico. In: Ausich, E. I., Webster, G. D. (Eds.), Echinoderm Paleontology: Indiana University Press, Bloomington, Indiana, p. 368-394.

Volckmann, R. P., 1984a, Upper Cretaceous stratigraphy of southwest Puerto Rico. In: Stratigraphic Notes, 1983. U.S. Geological Survey Bulletin 1537-A, 73-83.

Volckmann, R. P., 1984b, Geologic map of the Puerto Real Quadrangle, southwest Puerto Rico. U.S. Geological Survey, Miscellaneous Investigation Series, Map 1-1559, scale 1:20,000.

Volckmann, R. P., 1984c, Geologic map of the San Germán Quadrangle, southwest Puerto Rico. U.S. Geological Survey, Miscellaneous Investigation Series, Map 1-1558, scale 1:20,000.

Volckmann, R. P., 1984d, Geologic map of the Cabo Rojo and Parguera Quadrangles, southwest Puerto Rico. U.S. Geological Survey, Miscellaneous Investigation Series, Map 1-1557, scale 1:20,000.

Winter A., Appeldoorn, R., Bruckner, A., Williams, E., Goenaga, C., 1998, Sea surface temperatures and coral reef bleaching off La Parguera, Puerto Rico (northeastern Caribbean Sea): Coral Reefs, v. 17, p. 377-382.

Winter, A., Ishioroshi, H., Watanabe, T., Oba, T., Christy, J., 2000, Caribbean sea surface temperatures: two-to-three dergrees cooler than present during the Little Ice Age: Geophysical Research Letters, v. 27, p. 3365-3368.

Woo KS, Anderson TF, Railsback LB, Sandberg PA, 1992, Oxygen isotope evidence for high salinity surface seawater in the mid-Cretaceous Gulf of Mexico: implications for warm, saline deepwater formation: Paleoceanography, v. 7, p. 673–685

Zachos, J. C., Stott, L. D., Lohmann, K. C., 1994, Evolution of early Cenozoic marine temperatures: Paleoceanography, v. 9, p. 353-387.

TABLES AND FIGURES

Table 4.1
Analytical results of calcitic shells from the Cotui Limestone in southwestern Puerto Rico

Locality Sample ID	$^{87}Sr/^{86}Sr$	±2 s.e. $\times 10^{6}$	Sr	Mg	Fe	Mn	Age (Ma)		
CL-01	0.707454	15	1347	2551	bdl	bdl	86.03	84.86	83.50
GL01-02	0.707464	15	1974	43	bdl	22			
GL01-04	0.707456	15	2005	bdl	bdl	27			
GL01 (Mean)	0.707460	21					86.03	84.31	82.86
GL02-01	0.707454	15	1716	2008	139	55			
GL02-02	0.707464	15	1600	1915	186	37			
GL02 (Mean)	0.707458	21					86.01	84.45	82.99
Cotui Limestone	**0.707458**	**13**					**86.04**	**84.45**	**83.41**

Numerical ages are derived from McArthur et al. (2001); bdl – below detection limit (average 190 ppm Fe); ±2 s.e. – 2 standard error.

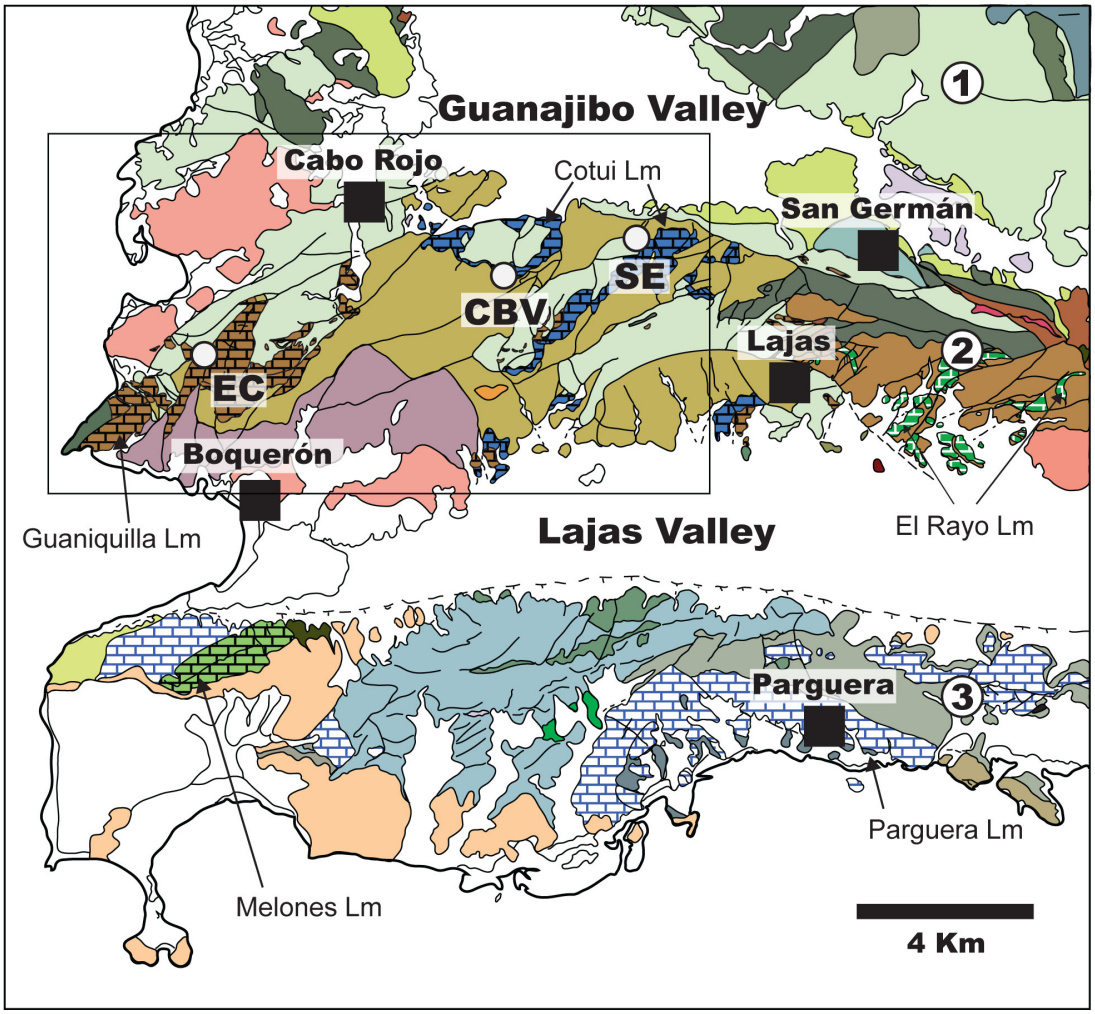

Figure 4.1. Geologic map of southwestern Puerto Rico showing the distribution of Upper Cretaceous volcano-sedimentary successions in the (1) Mayagüez-Sabana Grande, (2) Cabo Rojo-San Germán and (3) Parguera-Ensenada structural blocks (Volckmann, 1984a, 1984b and 1984c; Santos, 1999). SE – Sabana Eneas type locality (Cotui Limestone); CBV – Cerro Buena Vista (Cotui Limestone); PR-100 (Guaniquilla Limestone); EC – El Cerro (Guaniquilla Limestone).

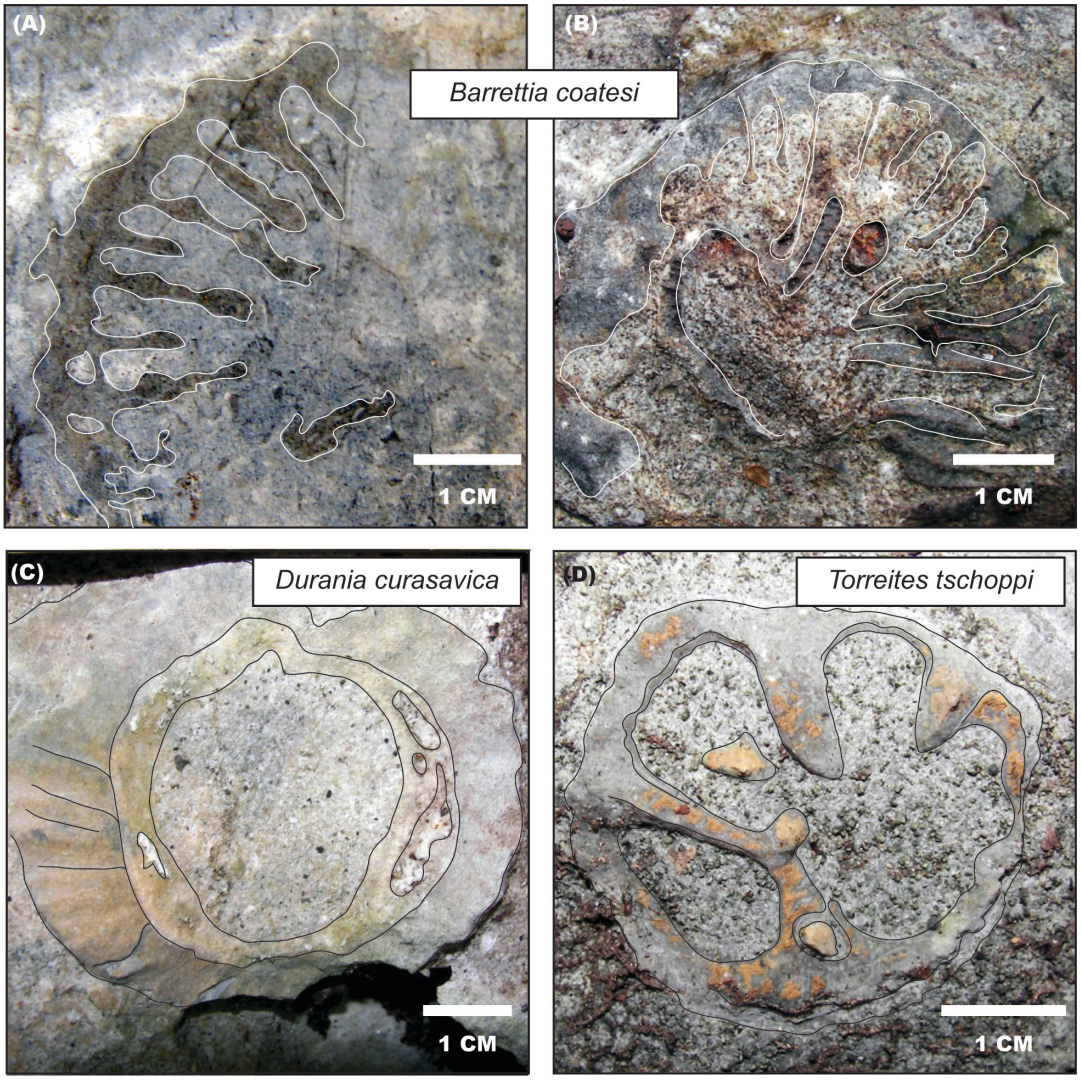

Figure 4.2. Key rudist taxa reported in the Cotui Limestone. (A) *Barrettia coatesi* – Cerro Buena Vista section. (B) *Barrettia coatesi* – Sabana Eneas type section. (C) *Durania curasavica* – Sabana Eneas type section. (D) *Torreites tschoppi* – Sabana Eneas type section.

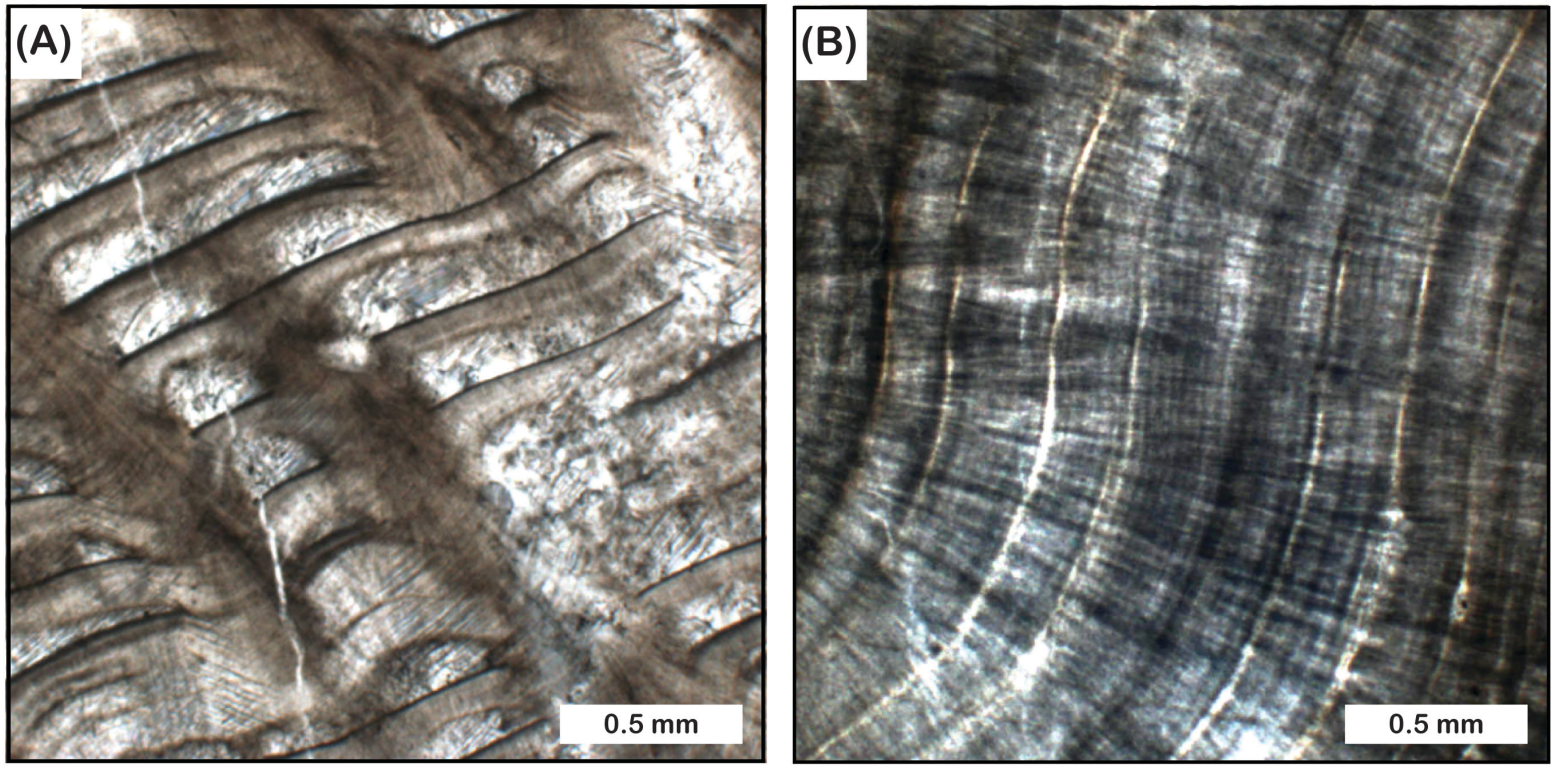

Figure 4.3. Shell structures of hippuritid rudists collected in southwestern Puerto Rico. (A) Rudist shell with cellular microstructure of polygonal cells with void filling sparry calcite cements (Sabana Eneas section – Cotui Limestone type locality). (B) Rudist shell with compacted fibrous prismatic structure (El Cero section – Guaniquilla Limestone).

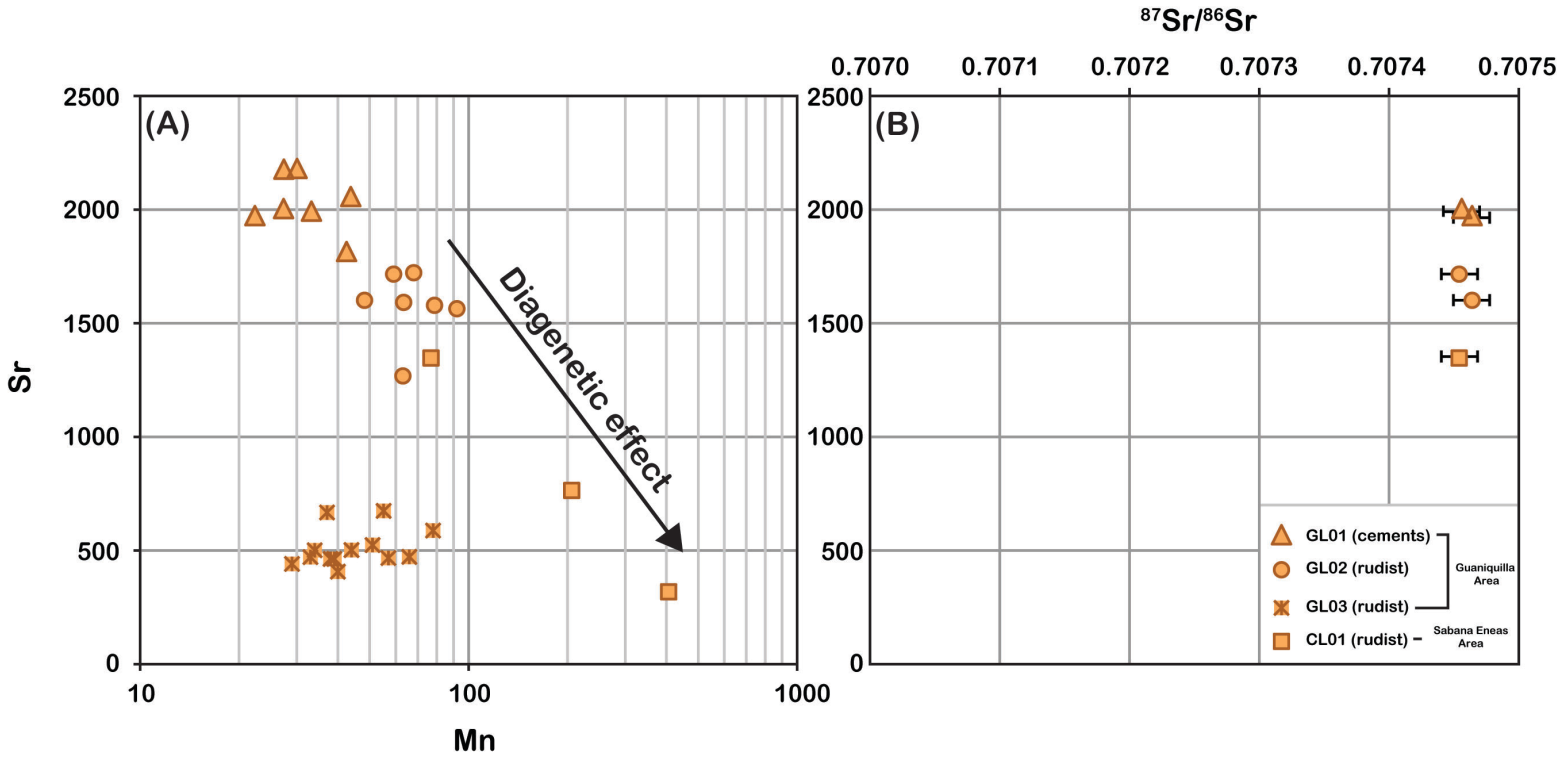

Figure 4.4. (A) Mn vs. Sr concentrations cross-plot from the collected hippuritid rudists in southwestern Puerto Rico. The diagenetic alteration in these samples followed by the decrease of Sr and increase of Mn. (B) Strontium isotopes vs Sr concentrations of selected preserve samples (Sr >900 ppm) showing consistent $^{87}Sr/^{86}Sr$.

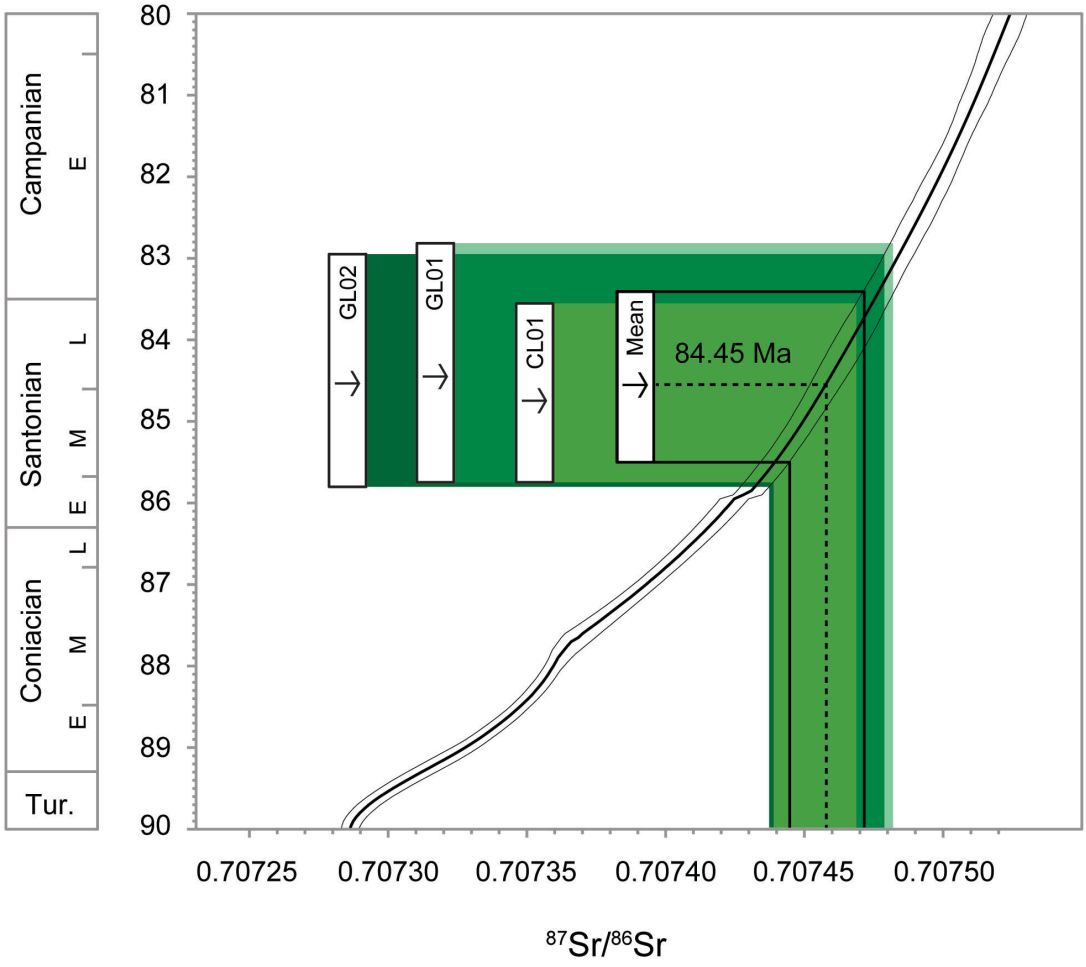

Figure 4.5. Numerical ages derived from $^{87}Sr/^{86}Sr$ analyses of least-altered hippuritid rudists collected in the Cotui Limestone (84.86 Ma), and Guaniquilla Limestone (84.31 and 84.45 Ma). The vertical bars indicate the maximum and minimum ages associated with uncertainties from analytical precision and the McArthur et al. (2001) "look-up" table.

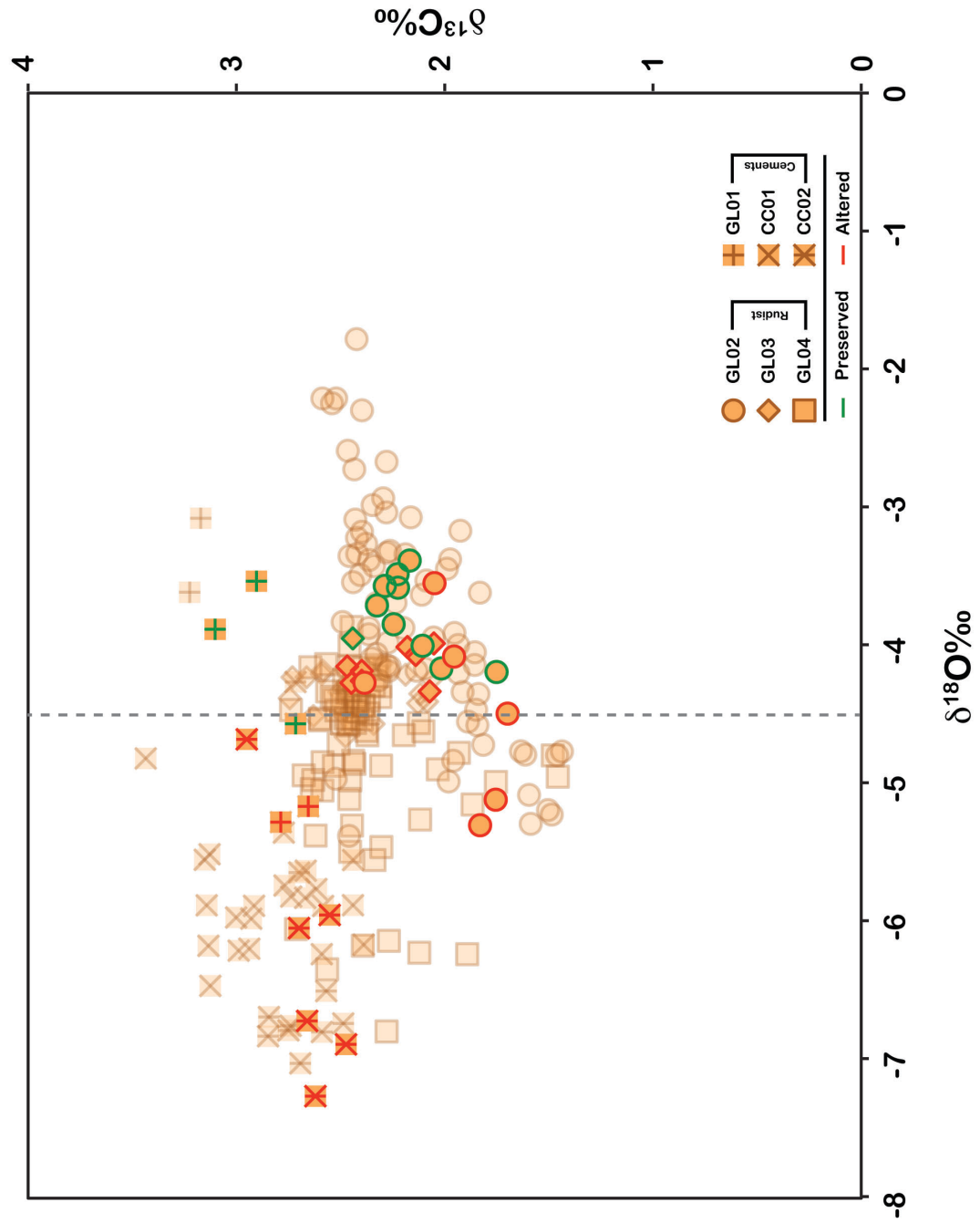

Figure 4.6. $\delta^{13}C$ vs. $\delta^{18}O$ cross-plot from the calcitic outer shell of hippuritid rudists (dots, diamonds and squares) and cements (squares with asterisks) from the Sabana Eneas type locality and El Cerro area. Green outline shows the samples that passed the preservation criteria; red outline are the diagenetically altered samples; dashed -4.5 ‰ line represent the assumed preservation limit.

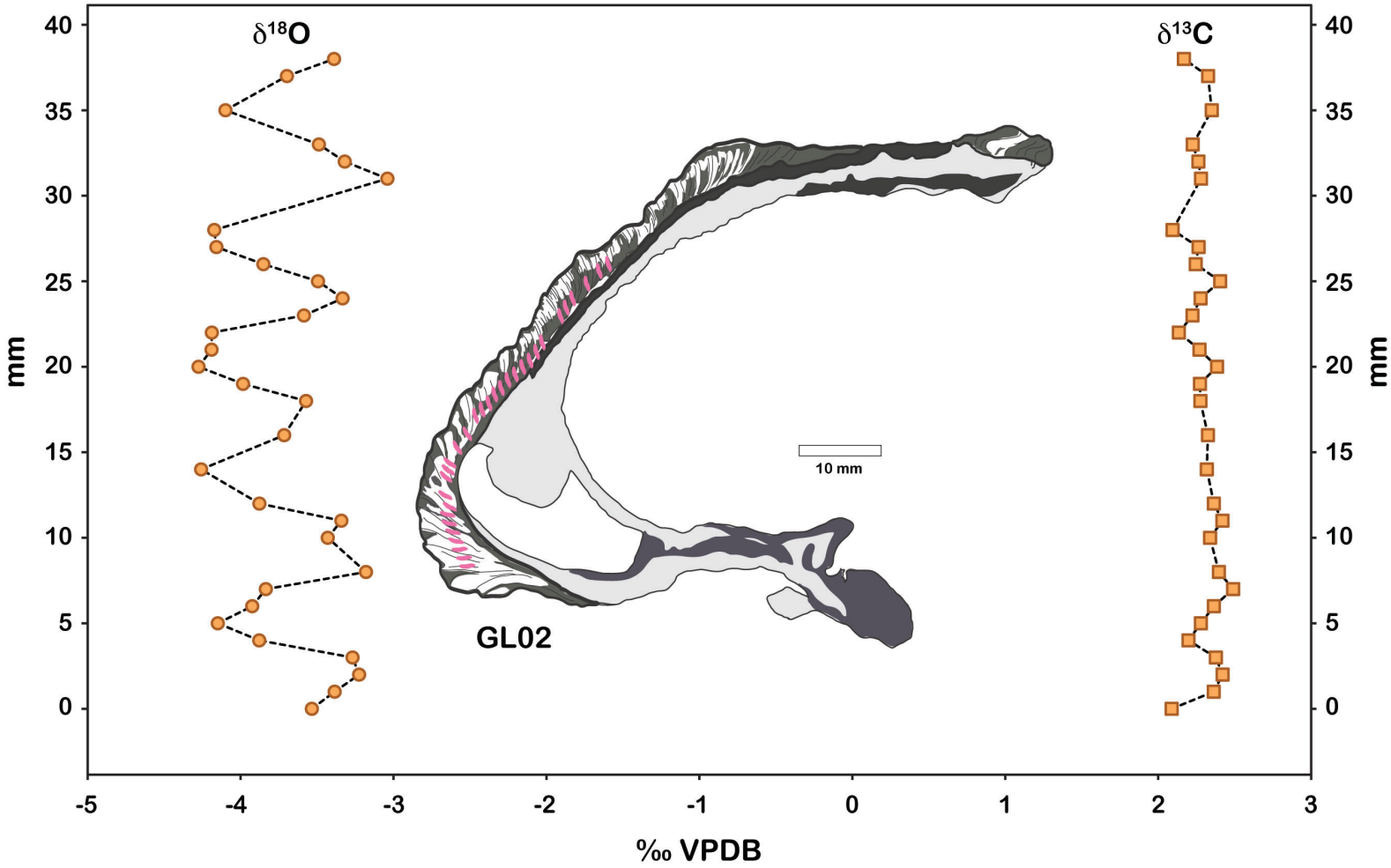

Figure 4.7. Sclerochronological $\delta^{13}C$ and $\delta^{18}O$ profiles from the calcitic outer shell of the hippuritid rudist collected in the EL Cerro area. The pink dots show sampled track for stable isotope analyses.

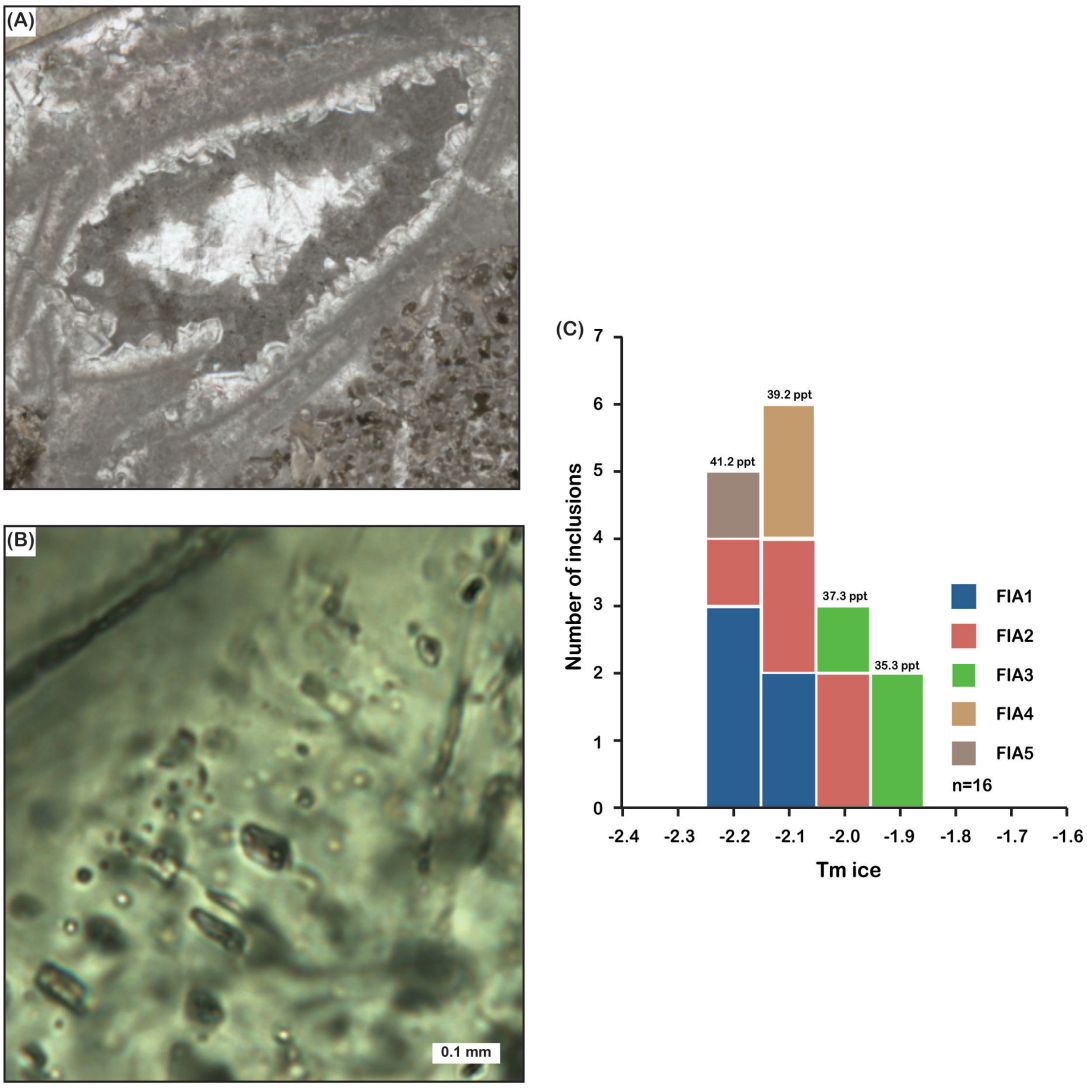

Figure 4.8. (A) Inner-cavity of the hippuritid rudist collected in the Sabana Eneas showing calcite cement interstratified with marine internal sediment. (B) Photomicrograph of fluid inclusions in FIA 1. (B) Frequency histogram of final melting temperatures (Tm ice) from the measured inclusions.

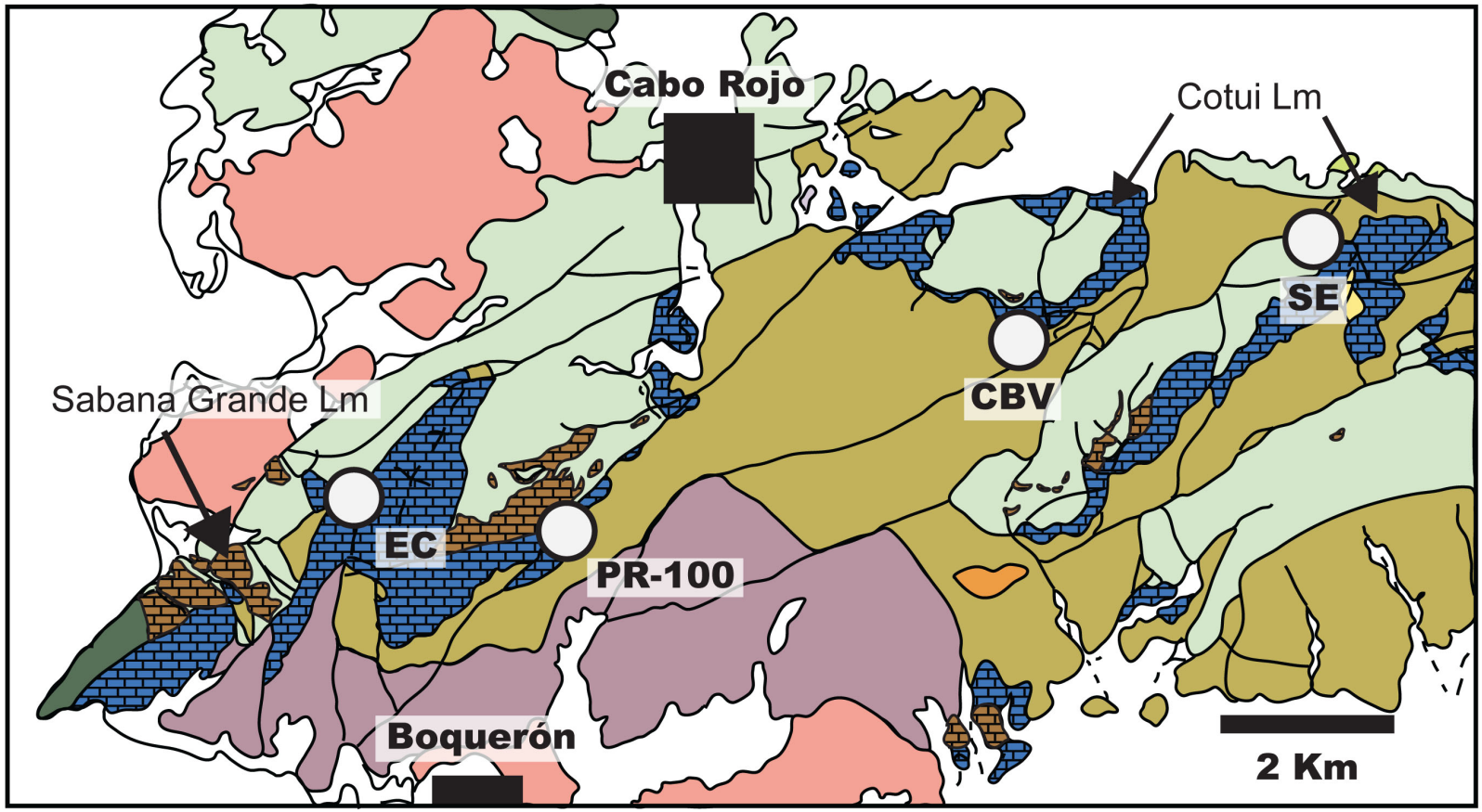

Figure 4.9. Geologic map of the Cabo Rojo-San Germán structural block showing the distribution of the Cotui Limestone and the Sabana Grande limestone lenses exposures as mapped by Volckmann (1984a and 1984b).

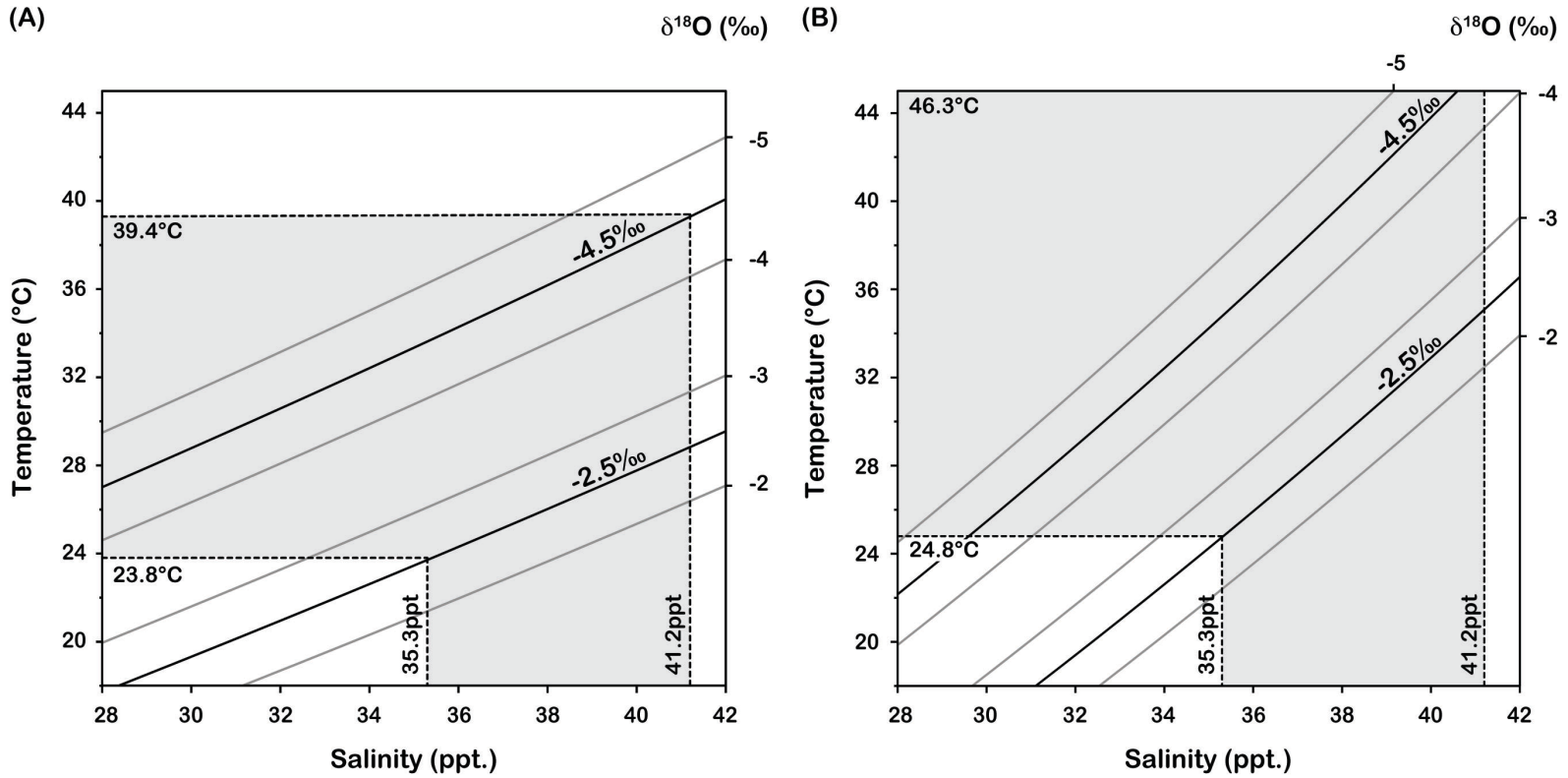

Figure 4.10 Variations of marine calcite δ18O values in relation to salinity and temperature (after Railback et al., 1989). (A) Equatorial Atlantic conditions (0.18‰/ppt.). (B) Red Sea and Mediterranean conditions (0.35‰/ppt.).

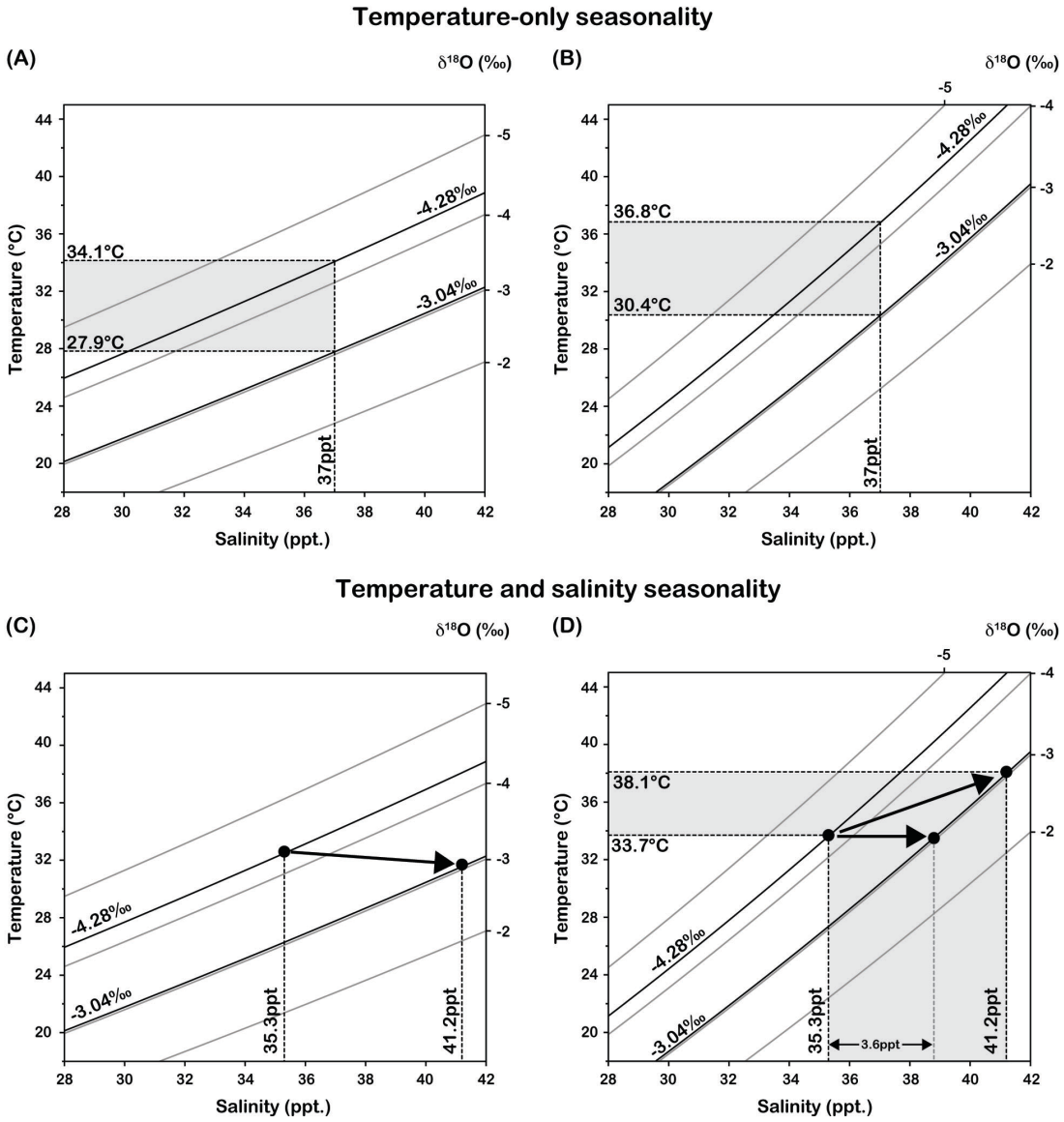

Figure 4.11. Temperatures estimated from Barron predicted salinity (37 ppt.) for (A) equatorial Atlantic (0.18‰/ppt), and (B) Red Sea and Mediterraneans conditions (0.35‰/ppt). Temperatures estimated from $\delta^{18}O$ cyclic values associated with temperature and salinity seasonality for (C) equatorial Atlantic (0.18‰/ppt), and (D) Red Sea and Mediterraneans conditions (0.35‰/ppt).

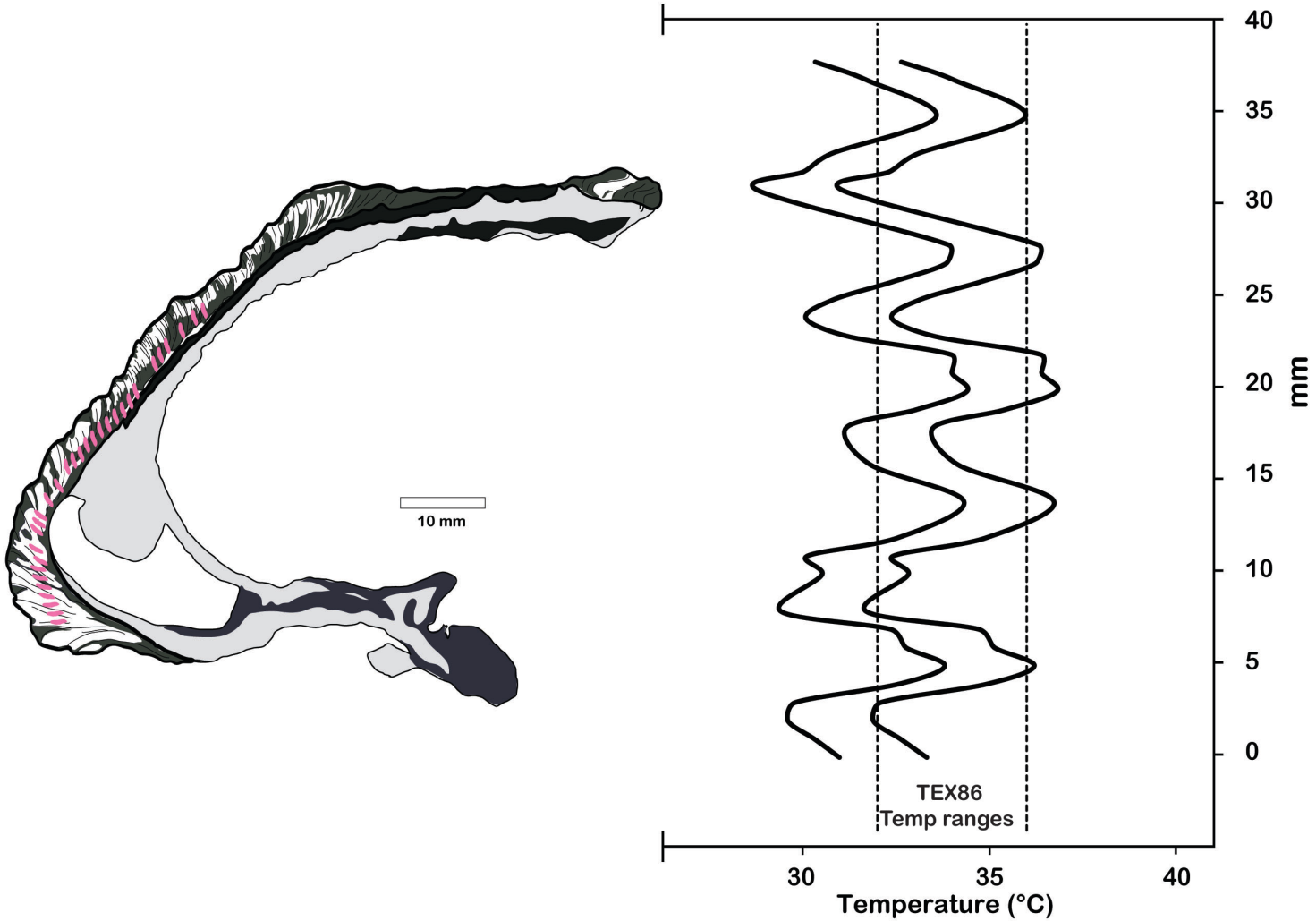

Figure 4.12A. Possible temperature ranges estimated from the $\delta^{18}O$ cyclic pattern at constant salinities (37 ppt.) recorded in the rudist bivalve collected in the El Cerro section. The minimum temperature profile was calculated from equatorial Atlantic conditions (0.18‰/ppt.), and maximum temperature profile from the Red Sea and Mediterranean conditions (0.35‰/ppt.).

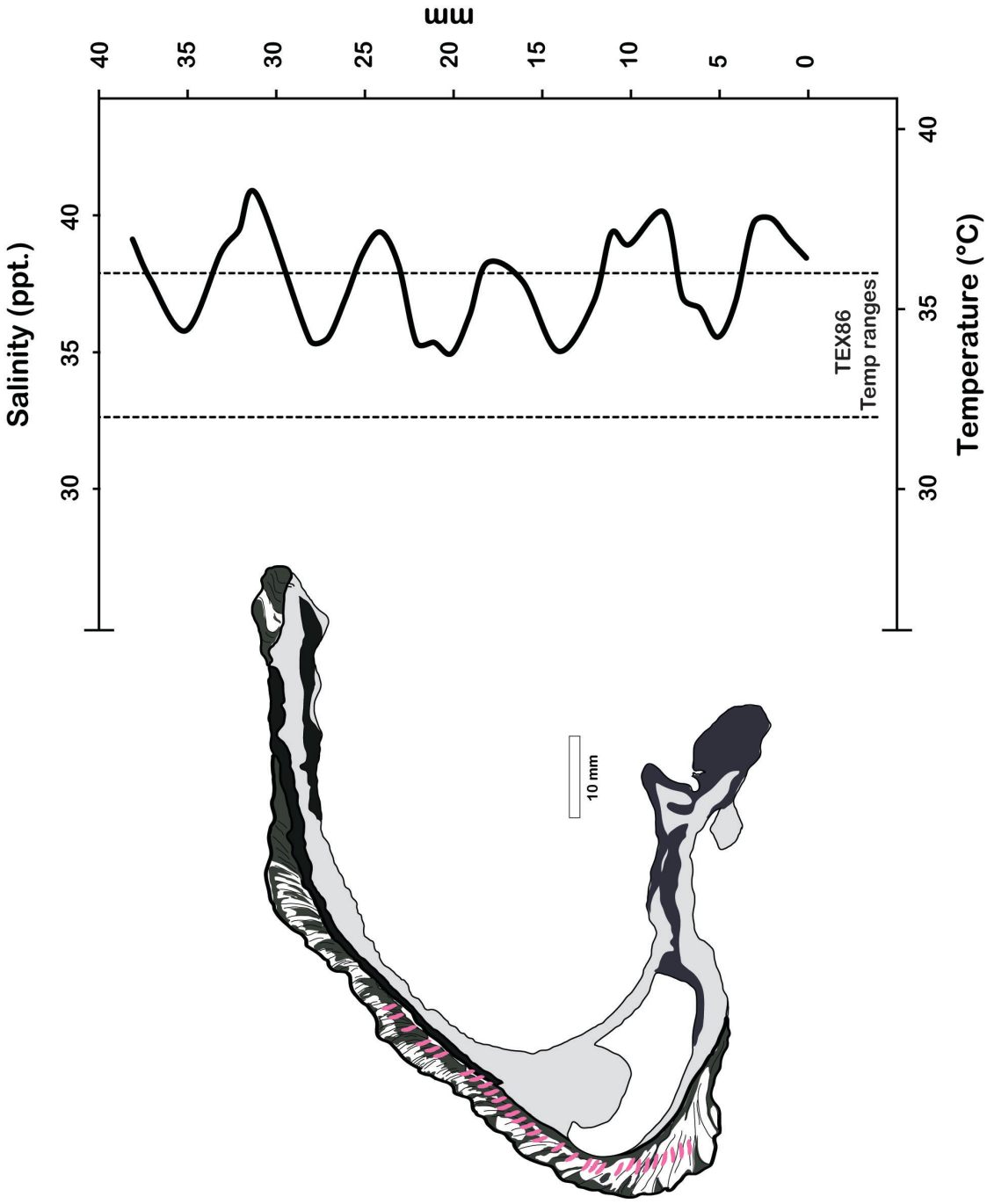

Figure 4.12B. Possible temperature and salinity ranges estimated for the $\delta^{18}O$ cyclic pattern recorded in the rudist bivalve collected in the El Cerro Section. For these calculations, the assumption was made that the maximum calcite $\delta^{18}O$ values reflect intense evaporation conditions and the minimum calcite $\delta^{18}O$ values reduced evaporation intervals.

Chapter 5 - The Socioeconomic impact of degradation of Caribbean reefs

ABSTRACT

Recent coral cover estimations suggest that Caribbean reefs are experiencing net declines of 21% due to anthropogenic stressors and the increased frequency of natural disturbance. The Caribbean reef degradation could have major socioeconomic impact in many Caribbean nations, in particular, by the gradual loss of diving tourism, which currently provides approximately $2.1 billion to the annual economic revenue in the Caribbean region. Current policy and management practices on coral reef protection center efforts in the creation of Marine Protected Areas (MPAs) and No-Take MPAs. These efforts, however, have failed to reverse regional coral reef declines. The documented failure of MPAs calls for drastic changes in practices and policies on coral reef conservation. In this study, we use understanding from the Cretaceous to propose a bold approach to mitigate the present impacts of Caribbean reef degradation. During the Cretaceous, reef ecosystems experienced a major ecological shift that included the domination of rudist bivalves (an extinct group) and scleractinian corals during the Early Cretaceous and the domination of only rudist bivalves during the middle to Late Cretaceous. This ecological shift took approximately 30 Ma, while the current warming rates for tropical oceans suggest that the temperature tolerance of corals will be exceeded within only a few decades. Because the timing for genetic adaptation is most likely to take longer than the rate of change of climate, the genome of corals and mollusks (mostly bivalves) should be mapped in order to produce heat resistant stocks. This bold approach

focuses on mitigation and adaptation, rather than preservation, and could sustain or even enhance the socioeconomic revenue provided by coral reefs for Caribbean nations.

INTRODUCTION

Coral reefs are very important ecosystems for nature and humankind. In the Caribbean over 116 million people live near coastal areas and depend on coral reefs as a source of food and income (Burke and Maidens, 2004; Cesar et al., 2003). Moreover, the carbonate sand beaches and live reefs lure more than 10 million visitors every year to many of the Caribbean countries (Caribbean Tourism Organization, 2013: www.onecaribbean.org). Other benefits of coral reef ecosystems include coastal protection, commercial fishing and high marine biodiversity (Moberg and Folke, 1999). The annual revenue generated by industries related to Caribbean coral reefs is estimated at $3.1 to $4.6 billion range (Burke and Maidens, 2004). The bulk of this revenue comes from dive tourism with approximately $2.1 billion, followed by shoreline protection with approximately $700 million to $2.2 billion, and fisheries with approximately $300 million (Burke and Maidens, 2004). Unfortunately the Caribbean reefs are in serious degradation with net declines of 21% due to anthropogenic stressors and the increased frequency of natural disturbance (Perry et al., 2008, 2013).

The World Resource Institute estimates future economic losses from Caribbean reef degradation at around $350 to $870 million per year (Burke and Maidens, 2004). For this reason, this chapter reviews the science and public policies that are being considered and/or implemented to mitigate the socioeconomic impact of the degradation of

Caribbean reefs. The subjects discussed in this chapter include: (1) reef perturbations and disturbances, (2) climate change projections, (3) historic overview, (4) current policy, (5) mariculture, and (6) bold approach to Caribbean reef conservation. This chapter is the outcome of two years of training from the National Science Foundation (NSF) Integrated Graduate Education and Research Traineeship (IGERT) program, Climate Change Humans and Nature in the Global Environment (C-CHANGE), at the University of Kansas.

REEF PERTURBATIONS AND DISTURBANCES

Anthropogenic stressors

Human induced perturbations include overfishing, tourism overuse, and land-based pollution. Overfishing, for example, has changed the reefs ecological balance in the Caribbean region. The loss of functional groups such as sea grazers and predators due to overfishing has reduced reef's resilience to natural disturbances and in some places resulted in a rapid phase shift from coral-dominated to fleshy macroalgae-dominated reef systems (Bellwood et al., 2004; Hughes, 1993; Moberg and Folke, 1999). Similarly, tourism overuse has resulted in the decline of coral cover in the Caribbean region (Cesar et al., 2003). In many diving destinations, corals are damaged and killed due to direct contact with the living portion of the corals (Needham and Szuster, 2011). In Grand Cayman, for example, the coral cover is considerably lower at high intensity diving sites (Tratalos and Austin, 2001). Most of the impact of land-based pollution comes from unregulated coastal development, land clearance and agriculture. This usually results in

intense sedimentation and pollution of coastal water (Cesar et al., 2003). High sedimentation contributes to the increase of turbidity of coastal waters therefore decreasing the light levels needed for the growth and survival of some coral species (Rogers, 1990). Most of the current reef management initiatives try to reduce these negative human impacts and/or anthropogenic stressors to increase coral resilience to natural disturbance such as hurricanes and coral bleaching events (e.g. Bellwood et al., 2004).

Natural disturbances

Natural disturbances on reef ecosystems include major tropical storms, such as hurricanes and cyclones, and coral bleaching events. In reef ecosystems, hurricanes play a similar role to fire in terrestrial systems (Hughes and Connell, 1999). Hurricane disturbances create empty spaces in the reef and prevent the monopolization by a small group of coral species and improve the coral diversity in the reef (Hughes, 1994; Bythell et al., 1993). Similarly, the coral bleaching phenomenon is believed to be a natural mechanism for the adaptation of corals to a new environmental parameters by expelling their symbiotic zooxanthellae algae and changing the coral-algal configuration (Fautin and Buddemeier, 2004). Although these natural disturbances are thought to be an important parts of reef dynamics (Fautin and Buddemeier, 2004; Hughes, 1994), the increasing frequency and severity of the events is believed to be associated with climate change and lowered reef resilience due to anthropogenic stressors (Bellwood et al., 2004; IPCC AR4, 2007).

CLIMATE CHANGE

The increasing rate of widespread coral bleaching events and subsequent mass mortalities in the Caribbean region are likely to create a serious socioeconomic impact. These disturbances in the Caribbean region could result in annual losses of $100 to $300 million due to reductions in diving tourism (Burke and Maidens, 2004). The IPCC Fourth Assessment Report (2007) centers their concerns about coral reefs on the impact of changing sea surface temperature leading to increased coral bleaching events, increases in frequency and intensity of tropical storms, and on ocean acidification.

Coral bleaching

In recent decades, the increase in sea surface temperatures has resulted in major impacts on Caribbean reefs. High sea surface temperatures often result in widespread coral bleaching events and coral mortalities in the Caribbean region (Cesar et al., 2003; Glynn, 1993). Coral bleaching events often coincide with periods of abnormally high atmospheric and sea surface temperatures (Glynn, 1993). Current projections of sea surface temperatures suggest that the temperature tolerance of corals will be exceeded within a few decades (IPCC FAR, 2007). This would result in more frequent widespread coral bleaching events in the Caribbean region. These projections are complicated by episodes of enhanced oceanic warmth associated with the El Niño oscillations, and coral bleaching events tend to be more frequent during these intervals (IPCC FAR, 2007).

Intense tropical storms

The IPCC Fourth Assessment Report (2007) predicts an increase in the intensity and frequency of tropical storms driven by climate change. The effects of this prediction could result in major decreases in Caribbean coral cover. Gardner et al. (2005) used historical data (from 1977 to 2001) to study the changes of coral cover after a hurricane and showed that in many Caribbean reefs the coral cover is reduced by approximately 17% in the year following hurricane disturbance. Many of these reefs did not recover before the onset of the following hurricane season suggesting a general impairment of the regeneration potential of Caribbean reefs (Gardner et al., 2005).

Ocean acidification

Much attention has been paid to the future impact of elevated atmospheric CO_2 concentration on the oceanic system. Feely et al. (2004) described some of these impacts as the lowering of the oceanic pH and reduced calcification by organisms. Experimental data indicate that doubling of the atmospheric CO_2 concentration could result in the reduction of coral calcification by 20 to 60% (Kleypas et al., 1999; Kleypas and Langdon, 2002; Reynaud et al., 2003). However, the evidence in nature for lower calcification due to ocean acidification is currently non-existent (IPCC AR4, 2007). In the previous chapter the Cretaceous paradox of high calcification during periods of elevated atmospheric CO_2 concentrations was addressed. Although ocean acidification could become a major disturbance in the future, more emphasis should be given to research on seawater supersaturation with respect to $CaCO_3$ and positive calcification

feedbacks in tropical oceans during periods of elevated atmospheric CO_2 concentration, e.g. Cretaceous greenhouse periods.

HISTORICAL OVERVIEW

Historical data suggest that the Caribbean reefs have lost architectural structure since the late 1970s (Alvarez-Filip et al., 2009). Early disturbances, however, date back to the 1960s, when overfishing resulted in the depletion of important keystone species. By this time, the reefs along the northern coast of Jamaica experienced the loss of 80% of fish stocks due to unsustainable commercial fisheries techniques (Hughes, 1994). This pattern was repeated in many reef areas throughout the Caribbean region (Sadovy, 1995). Although coral reefs appeared to be healthy, the depletion of coral fish stocks had a profound impact on reef ecological dynamics from the 1950s through the 1970s (Hughes, 1994). The paucity of herbivorous fish resulted in the proliferation of a single reef herbivore, the grazer echinoid *Diadema antillarum* (Hughes, 1994; Bellwood et al. 2004). With virtually non-existent predators, due to overfishing, the numbers of *D. antillarum* was as high as 10 individuals per square meter in shallow water by the 1960s and 1970s (Bellwood et al., 2004). Although *D. antillarum* substituted for the fish role in consuming algae, preventing benthic algal blooms, echinoids are far more destructive, as they burrow into and erode into the reef matrix (Bellwood et al., 2004). By 1983/1984 a mass mortality of *D. antillarum,* from an outbreak of disease throughout the Caribbean region, reduced this echinoid's numbers by two orders of magnitude (Hughes, 1994; Bellwood et al., 2004). The earlier loss of herbivorous fishes combined with the new loss of *D.*

antillarum left the Caribbean reef in a precarious position. Without reef grazers, macro-algae blooms became frequent since 1983 (Bellwood et al., 2004). Prior to the decimation of *D. antillarum*, shallow water coral cover was around 50% and fleshy macro-algae 4% (Bellwood et al., 2004). These values experienced a rapid shift in more recent decades, with coral covers below 10% and the fleshy macro-algae greater than 90% (Bellwood et al., 2004). This coral cover reduction also coincided with the outbreaks of crown-of-thorns starfish and the widespread occurrence of coral bleaching events that resulted in major coral mass mortalities in the Caribbean by the end of the last century (Bellwood et al. 2004).

CURRENT POLICY

Current preservation efforts are concentrated in management to sustain coral reef goods and services (e.g., fisheries, tourism and cultural values), and to promote the estishment of Marine Protected Areas (MPAs) and in some areas, the creation of No-Take Reserve MPAs. These efforts, however, are locally imposed policies that have failed to reverse regional coral reef declines (Hughes et al., 2003). The intent of these policies is to limit human stressors to the reef ecosystem and in turn improve the reef resilience to natural disturbances. There are seven U.S. reef jurisdictions (American Samoa, Commonwealth of the Northern Mariana Islands, Florida, Guam, Hawaii, Puerto Rico and the U.S. Virgin Islands) that have formally implemented MPAs and No-Take MPAs to manage and conserve their coral reef ecosystems. The percentages of the mapped benthic habitat areas that consist of MPAs and No-Take Reserves in these

jurisdictions are presented in Table 5.1 (NOAA Coral Reef Conservation Program – Assessment February 2009: http://www.coris.noaa.gov/activities/habitat_assessment/). These data show that the preservation efforts are restricted to small portions of local reefs. If these MPAs and No-Take MPAs are to make any difference, the emphasis and implementation of coral reef management must undergo major changes (e.g. the protection of larger portions of reefs).

MARICULTURE

Mariculture could represent another way to mitigate the negative socioeconomic impact of Caribbean reefs degradation. On one hand, the production of desired seafood through mariculture would reduce the fishing pressure on some of these organisms (e.g. the queen conch) and on the other hand, the market price for their meat would result in high revenue for farmers. There are some successful operations in the Caribbean region including the mariculture of the queen conch mollusk, and cobia and snapper fishes.

Queen Conch (Strombus gigas)

The queen conch has been commercially fished since the 1970s due to high demand for their meat, and now is considered one of the most important fisheries in the Caribbean, second only to the spiny lobster (Davis, 2005). The high demand for their meat, however, has resulted in the depletion of the queen conch stock. In order to reduce fishing pressure, some governments (e.g. Puerto Rico, Bahamas, and Florida) have established MPAs to preserve the queen conch and other important organisms (Davis, 2005). In Puerto Rico, for example, the Department of Natural Resources has

implemented a no-harvest season that goes from August 1 to October 31 in addition to their MPAs to relieve the fishing pressure on the local queen conch stocks.

Early queen conch aquaculture research dates back to the late 1970s (e.g. Berg, 1976) and focused on the growth of the larvae. In 1984 the first commercial culture farm was established in the Turks and Caicos Islands (The Caicos Conch Farm) and additional culture laboratories exist in Mexico and Florida that are conducting active conch research and education programs (Davis, 2005). The Caicos Conch Farm operates on a 10 acre facility with 65 acres of subsea pastures and includes facilities for the development of larval and post-larval stages (for more information: www.caicosconchfarm.net). Davis (2005) discussed the economic revenue of the queen conch based on the yearly culture of 500,000 specimens as juvenile and full legal size conch. The production of 500,000 juvenile for the food industry would represent a yearly annual gross revenue of about $350,000 and full-size specimens, an annual gross revenue of approximately $2,000,000, based on the early 2000s market for queen conch meat.

Cobia (Rachycentrum canadum) and snapper (Lutjanus analis)

In the past decade, much of the mariculture research was concentrated in the development of environmentally friendly designs and one particular area was the moving of cage aquaculture operation further offshore (Benetti et al., 2006). The University of Miami in collaboration with the University of Puerto Rico and the private companies of Snapperfarm, Inc. and AquaSense, LLC successfully implemented environmentally friendly mariculture operations in Puerto Rico and Bahamas that produced cobia and snapper. In Puerto Rico, Snapperfarm, Inc was able to implement a program that

produced 50 tons of cobia with an approximate annual gross revenue of $500,000. Snapperfarm, Inc., however, left Puerto Rico in 2009 due to permitting process delays and complexities by the Puerto Rican government in their quest to expand their operations. This company, now with the named of Open Blue, moved their operations to Panamá and is producing approximately 10,000 tons of cobia annually in Panamanian waters.

BOLD APPROACH – THE CRETACEOUS ANALOG

The effect of increasing sea surface temperatures on coral reef ecosystems is still poorly understood. The Cretaceous period, however, provides some analogs of what ecological pattern reef ecosystems and corals could follow as sea surface temperatures and sea level keep rising. During the Cretaceous, rudist bivalves were not the only reef building organisms (Johnson, 2002). Rudists initially shared reef ecosystems with the same type of corals that dominate today's reef ecosystems, scleractinian corals. During the middle Cretaceous, at the peak of the Cretaceous Greenhouse World, reef ecosystems experienced a major ecological shift in which rudist bivalves became the dominant organism and frame builder in reef ecosystems (Johnson 2002; Kauffmann and Johnson, 1988). During this interval, rudist bivalves proliferated in shallow water environments with elevated temperatures and salinities, while scleractinian corals migrated to deeper environments with lower temperatures and quieter waters (Kauffmann and Johnson, 1988; Scott, 1984). This ecological shift was associated with an increase of 3 to 5°C in surface water temperatures of open oceans in the tropics. The timing for this Cretaceous

ecological shift took much longer than the projection of the effect of future climate change and global warming on tropical oceans. During the Cretaceous, rudist bivalves and scleractinian corals shared reef ecosystems during the Barremian (~130 Ma), and the domination of rudist bivalves occurred during the Albian (~100 Ma). In other words, it took approximately 30 Ma for this ecological shift to happen, while the current warming rates for tropical oceans suggest that the temperature tolerance of corals will be exceeded within a few decades (IPCC FAR, 2007).

The documented failure of MPAs to produce effective protection or recovery of modern coral reefs and the apparent inevitability of rapid climate change calls for drastic changes in our practices/policies on coral reef conservation. Recent studies suggest that some coral species could adapt to moderate global warming through genetic adaptation, acclimatization and symbiotic shuffling (Logan et al., 2013; Oliver and Palumbi, 2011). This knowledge should be used to implement a large-scale management program for Caribbean reefs. Counterpart International, for example, has successfully implemented coral garden programs in Caribbean reefs in order to restore degraded reef ecosystems (Counterpart International - http://www.counterpart.org). This approach, however, should not try to save coral species from extinction, but instead produce gardens of heat-resistant coral species to be transplanted to degraded areas and revitalize the coral reef.

As described earlier, mollusks and in particular bivalves were the organisms that successfully adapted to survive during the peak of the Cretaceous greenhouse conditions. The geologic record clearly indicates that these organisms already have the information in their genes needed to adapt to global warmth and occupy or share the reef ecosystem.

Because the timing for genetic adaptation is most likely to take longer than the rate of change of climate change and global warming, mollusks should be studied in greater detail and mapping of their genome be prioritized. If complete eradication of scleractinian corals is to happen, we could envision the Caribbean reef ecosystems as sustainable gardens of heat-tolerant mollusks produced through aquaculture and genetic engineering. This could be a viable addition or replacement for fisheries associated with coral reefs where the reef builder would be a major food source. This bold approach that focuses on mitigation and adaptation, rather than preservation, and could sustain or even enhance the socioeconomic revenue provided by coral reefs for the Caribbean nations.

CONCLUSIONS

The degradation of the Caribbean reefs could have major socioeconomic impacts on many Caribbean nations. In particular, by the gradual loss of diving tourism, which currently provides approximately $2.1 billion annually to the economy of the Caribbean region. The causes for the degradation of the Caribbean reefs are associated with human stressors (overfishing, direct contact, and land-based pollution) and natural disturbances (tropical storms and coral bleaching events). The combination of these stressors and disturbances in association with the loss of the reefs' resilience has resulted in a decrease in Caribbean coral cover and in some areas resulted in a rapid phase shift from coral-dominated to fleshy macroalgal-dominated reef systems. Climate change projections of enhanced sea-surface temperatures, intense hurricane seasons and ocean acidification also have major negative implications for the future of Caribbean reefs. Current reef

management initiatives center on the creation of MPAs and No-Take reserve MPAs. This implementation, however, is restricted to a small portion of the Caribbean reefs, and is failing to reverse the overall regional reef declines. This chapter explored the used of mariculture as an alternative to mitigate the socioeconomic impact of the Caribbean reef degradation and provided two examples of successfully implemented culture programs, the queen conch mollusk, and the cobia and snapper fishes in the Caribbean region.

The main contribution of this chapter is the use of the knowledge from the Cretaceous interval to propose a bold approach to mitigate the impact of Caribbean reef degradation. During the Cretaceous, reef ecosystems experienced a major ecological shift that included the domination of rudist bivalves and scleractinian coral during the Early Cretaceous and the domination of only rudist bivalves during the middle to Late Cretaceous. The Cretaceous ecological shift, however, took approximately 30 Ma to happen, while the current warming rates for tropical oceans suggest that the temperature tolerance of corals will be exceeded within a few decades. Because the timing for genetic adaptation is most likely to take longer than the rate of change of climate change and global warming, the genomes of mollusks (mostly bivalves) should be mapped in order to produce heat-resistant stocks. This bold approach focuses on mitigation and adaptation, rather than preservation, and could sustain or even enhance the socioeconomic revenue provided by coral reefs for the Caribbean nations.

REFERENCES

Alvarez-Filip, L., Dulvy, N. K., Gill, J. A., Côté, I. M., Watkinson, A. R., 2009, Flattening of Caribbean coral reefs: region-wide declines in architectural complexity: Proc. R. Soc., v. 276, p. 3019-3025.

Bellwood, D. R., Hughes, T. P., Folke, C., 2004, Confronting the coral reef crisis: Nature, v. 429, p. 827–833.

Benetti, D., Brand, L., Collins, J., Orhun, R., Benetti, A., O'Hanlon, B., Danylchuk, A., Alston, D., Rivera, J., Cabarcas, A., 2006, Can offshore aquaculture of carnivorous fish be sustainable? Case studies from the Caribbean: World Aquaculture, p. 44-47.

Berg, C. J. Jr., 1976, Growth of the queen conch *Stronbus gigas*, with a discussion of the practicality of its mariculture: Marine Biology, v. 34, p. 191-199.

Burke, L., Maidens, J., 2004, Reefs at Risk in the Caribbean.:World Resources Institute, Washington, DC.

Bythell, J. C., Gladfelter, E. H., Bythell, M., 1993, Chronic and catastrophic natural mortality of three common Caribbean reef corals: Coral Reefs, v. 12, p. 143–152.

Cesar, H., Burke, L., Pet-Soede, L., 2003, The economics of worldwide coral reef degradation: Cesar Environmental Economics Consulting (CEEC), Arnhem, The Netherlands.

Davis, M., 2005. Species Profile: Queen Conch, *Strombus gigas*: Southern Regional Aquaculture Center (SRAC) Publication No. 7203.

Fautin, D. G., Buddemeier, R. W., 2004, Adaptive bleaching: a general phenomenon: Developments in Hydrobiology, v. 178, p. 459-467.

Gardner, T. A., Côté, I. M., Gill, J. A., Grant, A., Watkinson, A. R., 2005, Hurricanes and Caribbean reefs: Impacts, recovery patterns and role in long-term decline: Ecology, v. 86, p. 174-184.

Glynn, P. W., 1993, Coral reef bleaching: Ecological perspective: Coral Reefs, v. 12, p. 1-17.

Hughes, T. P., 1994, Catastrophes, phase shift, and large-scale degradation of a Caribbean coral reef: Science, v. 265, p. 1547-1551.

Hughes, T. P., Connell, J. H., 1999, Multiple stressors on coral reefs: A long-term perspective: Limnol. Oceanogr., v. 44, p. 932-940.

Hughes, T. P., Baird, A. H., Bellwood, D. R., Card, M., Connolly, S. R., Folke, C., Grosberg, R., Hoegh-Guldberg, O., Jackson, J. B., Kleypas, J., 2003, Climate change, human impacts, andthe resilience of coral reefs: Science, v. 301, p. 929–933

IPCC WG I, 2007, Climate Change 2007: The physical science basis: Contribution of Working Group I to the Fourth Assessment Report of the Intergovernmental Panel on Climate Change: Cambridge University Press.

Johnson, C. C., 2002, The rise and fall of rudist reefs: Reef of the dinosaur era were dominated not by corals but by odd mollusk, which died off at the end of the Cretaceous from causes yet to be discovered: American Scientist, v. 90, p. 148-153.

Kauffman, E. G., Johnson, C. C., 1988, The morphological and ecological evolution of middle to Upper Cretaceous reed-building rudistids: PALAIOS, v. 3, p. 194-216.

Klevpas, J. A., Buddemeier, R. W., Archer, D., Gattuso, J. P., Langdon, C., Opdyke, B. N., 1999, Geochemical consequences of increased atmospheric carbon dioxide on coral reefs: Science, v. 284, p. 118-120.

Kleypas, J., Langdon, C., 2002, Overview of CO sub (2)-induced changes in seawater chemistry: Proceedings of the 9th Interna- tional Coral Reef Symposium, Bali, Indonesia, p. 1085–1089.

Logan, C. A., Dunne, J. P., Eakin, C. M., Donner, S. D., 2013, Incorporating adaptive response into future projections of coral bleaching: Global Change Biology, in press.

Moberg, F., Folke, C., 1999, Ecological goods and services of coral reef ecosystems: Ecological Economics, v. 29, p. 215-233.

Needham, M., Szuster, B., Bell, C., 2011, Encounter norms, social carrying capacity indicators, and standards of quality at a marine protected area: Ocean and Coastal Management, v. 54, p. 633–641.

Oliver, T. A., Palumbi, S. R., 2011, Many corals host thermally resistant symbionts in high-temperature habitat: Coral Reefs, v. 30, p. 241-250.

Perry, C. T., Spences, T., Kench, P.S., 2008, Carbonate budget and reef production states: A geomorphic perspective on the ecological phase-shift concept: Coral Reefs, v. 27, p. 853-866.

Perry, C. T., Murphy, G. N., Kench, P. S., Smithers, S. G., Edinger, E. N., Steneck, R. S., Mumby, P. J., 2013, Caribbean-wide decline in carbonate production threatens coral reef growth: Nature Communications, v. 4, p. 1-7.

Reynaud, S., Leclercq, N., Romaine-Lioud, S., Ferrier-Pages, C., Jaubert, J., Gattuso, J. P., 2003, Interacting eVects of CO_2 partial pressure and temperature on photosynthesis and calciWcation in a scleractinian coral: Global Change Biol, v. 9, p. 1660–1668.

Rogers, C. S., 1990, Reponses of coral reefs and reef organism to sedimentation: Mar. Ecol. Prog. Ser., v. 62, p. 185-202.

Sadvoy, Y. 1995, The case of the disappearing grouper Epinephelus striatus, the Nassau grouper, in the Caribbean and western Atlantic: Proceedings of the Gulf and Caribbean Fisheries Institute, v. 45, p. 6-22.

Scott, R .W., 1984, Evolution of Early Cretaceous reefs in the Gulf of Mexico: Palaeontographica Americana, v. 54, p. 406-412.

Tratalos, J. A., Austin, T. J., 2001, Impacts of recreational SCUBA diving on coral communities of the Caribbean island of Grand Cayman: Biological Conservation, v. 102, p. 67-75.

TABLES

Table 5.1.

U.S. Jurisdiction	All MPAs	No-Take Reserves
American Samoa	24%	15%
Commonwealth of the Northern Marina Island	6%	3%
State of Florida	99%	7%
Territory of Guam	28%	22%
Commonwealth of Puerto Rico	29%	3%
U.S. Virgin Islands	64%	13%
Total Average	**43%**	**9%**

Table 1. Calculated percentages of the coral reef coverage areas in MPAs and No-Take Reserves for the seven U.S. coral jurisdictions (NOAA Coral Reef Conservation Program – Assessment February 2009).

Chapter 6 - Conclusions

The first part of this dissertation (Chapters 2 and 3) addressed the uncertainties surrounding Antillean rudist biostratigraphy that are associated with the scarcity of age diagnostic fossils (e.g., ammonites) in the Greater Antilles. This research discusses the middle Cretaceous Antillean biostratigraphic record (rudist bivalves and orbitolinid foraminifers), and uses chemostratigraphic proxies ($^{87}Sr/^{86}Sr$ and $\delta^{13}C$) to constrain the depositional age of the *Coalcomana-Caprinuloidea* rudist assemblage in Puerto Rico (Río Matón and Barrancas limestones), the Dominican Republic (Hatillo Limestone) and Jamaica (Seafield Formation).

In Chapter 2, the $^{87}Sr/^{86}Sr$-derived ages from the *Coalcomana-Caprinuloidea* rudist assemblage confirmed the validity of correlations with related rudist taxa in Texas and Mexico (e.g. *Coalcomana* interval zone), even though the correlations were drawn using a limited number of biostratigraphic markers. The derived $^{87}Sr/^{86}Sr$ numerical ages were close to the Aptian/Albian boundary for the *Coalcomana-Caprinuloidea* rudist assemblage in Puerto Rico (112.43 Ma), the Dominican Republic (112.62 Ma) and Jamaica (112.68 Ma). Furthermore it is proposed that the *Coalcomana-Caprinuloidea* rudist assemblage extended up into the middle Albian. This proposal is based on subtle but important differences in the biostratigraphic record. These include, an uppermost Aptian to lower Albian that is characterized by the presence of the rudist *Coalcomana ramosa,* a primitive form of the rudist *Caprinuloidea,* and the orbitolinid foraminifers *Orbitulina texana* and *Paracoskinolina sunnilandensis.* The depositional age for this

lower fossil assemblage was constrained using the $^{87}Sr/^{86}Sr$ derived dates from the Hatillo Limestone in the Hato Mayor area (112.62 Ma) and the Rio Matón Limestone (112.43 Ma). Conversely, the early to middle Albian fossil assemblage is characterized by the presence of *C. ramosa,* the advanced *Caprinuloidea* form and the orbitolinid foraminifer *C. texanus*. The depositional age for the upper fossil assemblage was constrained using good chronostratigraphic controls reported in the Hatillo Limestone exposed in the Pueblo Viejo area. These include published reports of fossils from the upper lower Albian *Douvilleiceras mammillatum* ammonite subzone at the base of the Hatillo Limestone and early Albian zircon dates in the upper Los Ranchos Formations, the lithostratigraphic unit directly below the Hatillo Limestone (Kesler et al., 2005a, 2005b), and the identification of the middle Albian orbitolinid foraminifer *Coskinolinoides texanus* occurring toward the upper part of the limestone succession.

In Chapter 3, the first Antillean carbon isotope ($\delta^{13}C$) chemostratigraphic record from the Central and Oriental cordilleras of the Dominican Republic was used to improve the correlations established in chapter 2. Our chemostratigraphic record included a borehole core (T82 section) section of approximately 100m from the Pueblo Viejo area. While none of the analyzed rudist samples from the Pueblo Viejo area had appropriate preservation for $^{87}Sr/^{86}Sr$ analyses (Chapter 2), the $\delta^{13}C$ chemostratigraphic record from the T82 section was used to establish local and regional correlations. The Hatillo Limestone $\delta^{13}C$ chemostratigraphy was correlated to $\delta^{13}C$ profiles from the Comanche Shelf in Texas (Phelps, 2011), the Sierra Madre in Mexico (Bralower et al., 1999) and the Vocontian Basin in France (Gale et al., 2011; Herrle et al., 2004). These $\delta^{13}C$ correlations

indicate a depositional age close to the Aptian/Albian boundary for the Hatillo Limestone in the Hato Mayor area as reported by the $^{87}Sr/^{86}Sr$ derived ages (Chapter 2) and lower to middle Albian the depositional range in the Pueblo Viejo area. The $\delta^{13}C$ correlation in the Pueblo Viejo area to the lower and middle Albian intervals is supported by early Albian zircon dates from the upper Los Rancho Formation, the lithostratigraphic unit directly below the Hatillo Limestone (Kesler et el., 2005a, 2005b), the presence of fossils from the upper lower Albian *D. mammillatum* ammonite subzone at the base of the Hatillo Limestone (Myczyński and Iturralde-Vinent, 2005) and the presence of *C. texanus* towards the upper part of the limestone succession in the T82 section. The documented similarities and differences between the Antillean and Gulf of Mexico chemostratigraphic records suggest a major paleoceanographic change during the Aptian/Albian transition. During the Aptian, the proposed dominance of westward oceanic current from the Mediterranean Tethys through the Caribbean and the Pacific realm are used to explain the better chemostratigraphic correlations between the Antillean chemostratigraphic record in the Dominican Republic and the Mediterranean $\delta^{13}C$ profiles in southern France. Similarly, the improved Albian chemostratigraphic correlations between the Caribbean and Gulf of Mexico suggest a better connection of the surface oceanic current for this region. The dominance of a northward split surface current, as modeled by Johnson (1999), is proposed to be the driving mechanism for the better oceanic current connection and chemostratigraphic correlations between the Greater Antilles and Gulf of Mexico during the Albian interval. This paleoceanographic change also coincides with major paleobiogeographic divergence between the Tethys and Pacific record (Iba and Sano,

2008; Iba et al., 2011). The more eastward position of the Greater Antilles volcanic arc and/or the origination of the Panama-Costa Rica arcs between the Americas, coupled with lower relative sea level (or arc emergence) acted as a barrier for the Caribbean-Pacific ocean circulations and the intensification of the northward oceanic surface current that flowed from the Greater Antilles through the Gulf of Mexico.

The second part of this dissertation (Chapter 4) addressed the uncertainties surrounding the response of tropical oceans to Cretaceous greenhouse conditions and the role of enhanced evaporation into Cretaceous calcite $\delta^{18}O$ values. In order to answer these questions, this part of the research focused on the Late Cretaceous exposures in southwestern Puerto Rico (the Cotui and Guaniquilla limestones) because of the presence of well-preserved rudist shells. Paleosalinities (35.3 to 41.2 ppt.) derived from fluid inclusions were used to investigate the effect of enhanced evaporation into the calcite $\delta^{18}O$ values from our Antillean rudist shells by applying three different scenarios to the Railsback et al. (1989) model: (1) equatorial western Atlantic conditions (0.18‰/ppt.) and constant salinities (37 ppt.) that resulted in a paleotemperature range from 28°C to 34°C, (2) Red Sea and Mediterranean conditions (0.35‰/ppt.) with constant salinities (37 ppt.) resulting in 30°C to 37°C paleotemperatures, and (3) Red Sea and Mediterranean conditions (0.35‰/ppt.) conditions with seasonal salinity changes (35.3 to 41.2 ppt.) that resulted in paleotemperatures ranging from 34°C to 38°C. The modeled paleoceanographic conditions suggest that areas with enhanced evaporation dominated the deposition of the Antillean limestones. In this chapter, $^{87}Sr/^{86}Sr$ data were also used to derive numerical ages and constrain the depositional age of the Cotui and Guaniquilla

limestones. The derived ages from the hippuritid rudists collected in southwestern Puerto Rico resulted in consistent late Santonian ages (Cotui Limestone 84.75 Ma, and Guaniquilla Limestone 84.40 and 84.55 Ma) and suggest that part of the limestone exposure mapped as the Guaniquilla Limestone (Campanian – Santos, 1999) should be included as part of the Santonian Cotui Limestone.

The final chapter of this dissertation explores the socioeconomic effect of Caribbean reef degradation and utilizes the knowledge gained in this and other studies to provide ideas on how to mitigate the impacts from Caribbean reef decline. The degradation of Caribbean reefs could have major socioeconomic impact in many Caribbean nations due to the gradual loss of diving tourism. The causes for the degradation of the Caribbean reefs are associated with human stressors and natural disturbances that when coupled to the loss of the reefs resilience has resulted in the diminished Caribbean coral cover and a shift from coral-dominated to fleshy macroalgal dominated reef systems. The problem is projected to be exacerbated by projected climate change that will produce elevated sea surface temperatures, more intense hurricane seasons, and increased ocean acidification. Current reef management initiatives centered on the creation of the MPAs and No-Take reserve MPAs presently are restricted to small portion of Caribbean reefs and are failing to reverse the overall regional reef declines. The main contribution of the chapter, however, is the use of the knowledge from the Cretaceous interval to propose a bold approach to mitigate the present impacts of the Caribbean reefs degradation. During the Cretaceous, reef ecosystems experienced a major ecological shift that included the domination of rudist bivalves and scleractinian coral

during the Lower Cretaceous and the near exclusive domination of rudist bivalves during the middle to Late Cretaceous. The Cretaceous ecological shift, however, took approximately 30 Ma to happen, while the current warming rates for tropical oceans suggest that the temperature tolerance of corals will be exceeded within a few decades. Because the timing for genetic adaptation is most likely to take longer than the rate of change of climate change, it is suggested that the mapping of the genome of corals and mollusks (mostly bivalves) be expedited in order to facilitate the production of heat resistant stocks. This bold approach focuses on mitigation and adaptation, rather than preservation, and could sustain or even enhance the socioeconomic revenue provided by reefs for the Caribbean nations.

REFERENCES

Bralower, T. J., CoBabe, E., Clement, B., Sliter, W. V., Osburn, C. L., and Longoria, J., 1999, The record of global change in Mid-Cretaceous (Barremian-Albian) sections from the Sierra Madre, northeastern Mexico: Journal of Foraminiferal Research, v. 29, p. 418-437.

Gale, A. S., Bown, P., Caron, M., Crampton, J., Crowhurst, S. J., Kennedy, W. J., Petrizzo, M. R., and Wray, D. S., 2011, The uppermost Middle and Upper Albian succession at the Col de Palluel, Hautes-Alpes, France: An integrated study (ammonites, inoceramid bivalves, planktonic foraminifera, nannofossils, geochemistry, stable oxygen and carbon isotopes, cyclostratigraphy): Cretaceous Research, v. 32, p. 59-130.

Herrle, J. O., Kössler, P., Friedrich, O., Erlenkeuser, H., and Hemleben, C., 2004, High-resolution carbon isotope records of the Aptian to Lower Albian from SE France and the Mazagan Plateau (DSDP Site 545): a stratigraphic tool for paleoceanographic and paleobiologic reconstruction: Earth and Planetary Science Letters, v. 218, p. 149-161.

Johnson, C. C., 1999, Evolution of Cretaceous surface current circulation patterns, Caribbean and Gulf of Mexico, *in* Barrera, E., and Johnson, C. C., ed., Evolution of the Cretaceous ocean-climate systems: Geological Society of America, Special Paper 332, p. 329-343.

Kesler, S. E., Campbell, I. H., and Allen, C. M., 2005a, Age of the Los Ranchos Formation, Dominican Republic: Timing and tectonic setting of primitive island arc volcanism in the Caribbean region: Geological Society of America Bulletin, v. 117, p. 987.

Kesler, S. E., Campbell, I. H., Smith, C. N., Hall, C. M., and Allen, C. M., 2005b, Age of the Pueblo Viejo gold-silver deposit and its significance to models for high-sulfidation epithermal mineralization: Society of Economic Geologists, v. 100, p. 253–272.

Myczyński, R., and Iturralde-Vinent, M., 2005, The late lower Albian invertebrate fauna of the Río Hatillo Formation of Pueblo Viejo, Dominican Republic: Caribbean Journal of Science, v. 41, p. 782-796.

Phelps, R. M., 2011, Middle-Hauterivian to lower-Campanian sequence stratigraphy and stable isotope geochemistry of the Comanche Platform, south Texas; unpublished Ph.D. thesis, The University of Texas, Austin, Texas, 198 p.

Railsback, L. B., Anderson, T. F., Ackerly, S. C., Cisne, J. L., 1989. Paleoceanographic modeling of temperature-salinity profiles from stable isotopic data. Paleoceanography 4, 585–591.

Santos, H., 1999. Stratigraphy and depositional history of the upper Cretaceous strata in the Cabo Rojo-San German structural block, southwestern Puerto Rico. Ph.D. thesis, University of Colorado.

Appendix A - Analytical results of trace elements and strontium isotope from the middle Cretaceous low-Mg calcite of Antillean rudist bivalves

Puerto Rico Sample no.	Sr (ppm)	Mg (ppm)	Fe (ppm)	Mn (ppm)	$^{87}Sr/^{86}Sr$
PRCH-1	697	1829	-	281	-
PRCH-2	612	2044	-	353	-
PRCH-3	470	2066	-	303	-
PRCH-4	478	2085	-	203	-
PRCH-5	603	1865	-	67	-
RM01-1	139	2721	-	114	-
RM01-2	591	1719	-	133	-
RM01-3	1124	630	bdl	34	0.707254
RM01-4	812	2095	-	109	-
RM01-5	43	332	-	235	-
RM02-1	939	803	710	56	-
RM02-2	1097	674	-	39	-
RM02-3	1270	387	bdl	32	0.707262
RM02-4	633	2043	-	159	-
RM02-5	397	1488	bdl	154	0.707185
RM03-1	465	2240	-	188	-
RM03-2	396	1891	-	260	-
RM03-3	467	1530	-	140	-
RM03-4	317	2044	-	232	-
RM04-1	315	1622	-	244	-
RM04-2	275	1740	-	218	-
RM04-3	302	1808	-	244	-
RM05-1	1031	480	-	61	-
RM05-2	900	1549	-	93	-
RM05-3	400	2271	-	141	-
RM05-4	370	1661	-	239	-
RM05-5	317	1878	-	313	-
RM01	673	2668	-	75	-
RM02	687	2264	400	54	-
RM03	916	2677	349	55	-
RM04	1106	1437	bdl	35	0.707298
RM05	362	2779	-	126	-

RM06	419	2992	-	81	-
RM07	1213	2014	bdl	31	0.707277
RM08	608	2897	-	74	-
RM09	897	2581	-	46	-
RM10	965	2714	-	58	-
RM11	524	2294	-	84	-
RM12	246	1507	-	73	-
BA01-1	107	2210	349	69	-
BA01-2	201	3594	-	109	-
BA01-3	524	3937	-	104	-
BA01-4	578	6966	-	283	-

D. Republic Sample no.	**Sr (ppm)**	**Mg (ppm)**	**Fe (ppm)**	**Mn (ppm)**	**$^{87}Sr/^{86}Sr$**
DA01	673	2833	-	45	-
DA02	951	2575	bdl	67	-
DA03	1267	1029	bdl	28	0.707285
DA04	1075	2120	bdl	31	0.707285
DA05	1296	1532	234	32	0.707262
DA06	1362	930	220	33	0.707262
DA01-1	1154	2436	bdl	38	0.707258
DA01-2	856	1105	bdl	28	0.707211
DA01-3	860	3254	bdl	36	0.707228
DA01-4	567	3749	bdl	72	0.707200
DA01-5	1268	1254	bdl	25	-
DA01-6	142	1188	-	131	-
DA01-7	1266	843	bdl	20	-
DA02-1	1030	1143	bdl	27	0.707244
DA02-2	653	3578	bdl	32	0.707235
DA02-3	1032	1270	bdl	20	0.707250
DA02-4	1198	912	bdl	19	0.707254
DA02-5	389	3989	bdl	37	0.707132
DA02-6	644	1375	bdl	37	0.707213
DA03-1	536	2739	-	185	-
DA03-2	916	3172	-	84	-
DA03-3	897	4090	-	86	-
DA03-4	1080	3630	-	68	-

DRCH-1	1028	2713	-	72	-
DRCH-2	1168	3406	-	79	-

Jamaica Sample no.	**Sr (ppm)**	**Mg (ppm)**	**Fe (ppm)**	**Mn (ppm)**	**$^{87}Sr/^{86}Sr$**
JAM-01	886	2777	-	102	-
JAM-02	770	2119	-	200	-
JAM-03	594	1740	-	201	-
JAM-04	1116	3009	-	71	-
JAM-05	1077	2941	-	85	-
JAM-06	1321	3020	205	58	0.707264
JAM-07	1039	2808	bdl	24	-
JAM-08	1119	3016	-	73	-

Appendix B - Analytical results of systematic $\delta^{13}C_{CARB}$, $\delta^{13}C_{OM}$, total organic matter (%TOM), and percentage of carbonate (%CARB)

T82 core Sample no.	Depth (m)	$\delta^{13}C_{OM}$ (‰)	$\delta^{13}C_{CARB}$ (‰)	$\delta^{18}O_{CARB}$ (‰)	TOM	%CARB
T82-1	124.90	-26.45	-	-	0.04	9.90
T82-2	124.65	-26.28	-	-	0.04	10.39
T82-3	124.40	-24.61	-	-	0.02	9.12
T82-4	124.15	-25.75	-	-	0.02	9.80
T82-5	123.90	-26.64	-	-	0.03	13.10
T82-6	123.65	-26.48	-	-	0.03	13.52
T82-7	123.40	-26.98	-	-	0.01	10.98
T82-8	123.15	-22.37	-	-	0.02	5.81
T82-9	123.00	-26.46	-	-	0.02	11.12
T82-10	122.75	-25.47	-	-	0.04	5.27
T82-11	122.50	-34.09	-	-	0.03	6.30
T82-12	122.25	-31.43	-	-	0.06	7.93
T82-13	122.00	-23.86	-	-	0.01	2.98
T82-14	121.75	-27.93	-	-	0.05	5.61
T82-15	121.50	-25.27	-	-	0.02	5.36
T82-16	121.25	-30.27	-	-	0.03	9.09
T82-17	121.00	-26.41	-	-	0.02	9.26
T82-18	120.75	-26.87	-	-	0.04	17.52
T82-19	120.50	-26.33	-	-	0.02	10.08
T82-20	120.25	-27.98	-	-	0.03	12.14
T82-21	120.00	-27.43	-	-	0.03	13.42
T82-22	119.75	-27.38	-	-	0.03	14.76
T82-23	119.50	-27.36	-	-	0.03	11.21
T82-24	119.25	-27.46	-	-	0.03	11.49
T82-25	119.00	-27.34	-	-	0.03	12.37
T82-26	118.75	-26.72	-	-	0.03	8.29
T82-27	118.50	-	-	-	0.03	-
T82-28	118.25	-27.32	-	-	0.03	4.17
T82-29	118.00	-27.34	-	-	0.04	17.38
T82-30	117.75	-30.75	-	-	0.03	10.12
T82-31	117.50	-27.50	-	-	0.04	12.46
T82-32	117.25	-26.56	-	-	0.02	10.00
T82-33	117.00	-	-	-	-	-
T82-34	116.75	-26.69	-	-	0.05	9.40
T82-35	116.50	-27.68	-	-	-	-
T82-36	116.25	-27.18	-	-	0.04	14.74
T82-37	116.00	-27.10	-	-	-	-

T82-38	115.75	-29.98	-	-	0.03	9.89
T82-39	115.50	-27.02	-	-	0.04	15.51
T82-40	115.25	-27.05	-	-	0.04	16.17
T82-41	115.00	-27.70	-	-	0.02	14.40
T82-42	114.75	-27.25	-	-	0.03	10.66
T82-43	114.50	-27.30	-	-	0.01	13.11
T82-44	109.00	-	-	-	-	-
T82-45	108.50	-27.39	-	-	0.03	12.43
T82-46	108.00	-26.94	-	-	0.02	17.91
T82-47	107.50	-26.32	-	-	0.05	13.46
T82-48	107.00	-30.15	-	-	0.04	28.08
T82-49	106.50	-30.31	-	-	0.02	40.51
T82-50	106.00	-	-	-	-	-
T82-51	105.50	-	-	-	-	-
T82-52	105.00	-27.99	-	-	0.02	14.90
T82-53	104.50	-28.06	-	-	0.04	10.19
T82-54	104.00	-26.12	-	-	0.02	19.24
T82-55	103.50	-27.20	-	-	0.05	-
T82-56	103.00	-28.82	-	-	0.05	11.71
T82-57	102.50	-26.24	-	-	0.02	17.81
T82-58	102.00	-26.96	-	-	0.03	6.89
T82-59	101.50	-26.99	-	-	0.02	24.07
T82-60	101.00	-28.52	-	-	0.03	20.22
T82-61	100.50	-26.47	-	-	0.04	5.99
T82-62	100.00	-27.70	-	-	0.01	25.04
T82-63	99.50	-29.51	-	-	0.03	18.77
T82-64	99.00	-27.46	-	-	0.03	17.68
T82-65	98.50	-	-	-	-	-
T82-66	98.00	-32.70	-	-	0.05	18.81
T82-67	97.50	-27.84	-	-	0.02	16.94
T82-68	97.00	-28.87	-	-	0.02	8.42
T82-69	96.50	-32.29	-	-	0.09	9.73
T82-70	96.00	-28.46	-	-	0.05	13.45
T82-71	95.50	-26.46	-	-	0.03	11.69
T82-72	95.00	-29.30	-	-	0.05	15.95
T82-73	94.50	-28.30	-	-	0.05	8.97
T82-74	94.00	-30.88	-	-	0.05	6.81
T82-75	93.50	-32.07	-	-	0.06	3.90
T82-76	93.00	-27.41	-	-	0.06	2.54
T82-77a	92.75	-24.10	-	-	5.05	6.50
T82-77b	92.50	-23.48	-	-	1.42	11.31
T82-77c	92.25	-24.39	-	-	5.04	6.45
T82-77d	92.00	-23.48	-	-	1.43	12.31
T82-78	91.50	-26.10	-	-	0.06	3.28

T82-79	91.00	-24.70	0.93	-17.07	0.22	65.19
T82-80	90.75	-25.27	-0.18	-17.22	0.17	39.53
T82-81	90.50	-25.34	-0.96	-15.83	0.20	13.69
T82-82	90.25	-25.49	-	-	-	-
T82-83	90.00	-22.82	-	-	0.38	6.70
T82-84	89.75	-24.23	0.75	-16.13	0.34	70.85
T82-85	89.50	-23.96	1.19	-16.65	0.40	59.88
T82-86	89.25	-24.18	0.83	-16.45	0.23	35.76
T82-87	89.00	-25.29	0.46	-16.43	-	-
T82-88	88.75	-24.23	0.67	-16.41	0.05	78.44
T82-89	88.50	-24.61	1.27	-15.16	0.20	55.53
T82-90	88.25	-24.36	1.74	-14.02	0.23	41.62
T82-91	88.00	-23.87	1.39	-14.70	0.08	77.01
T82-92	87.75	-24.41	1.51	-13.50	0.17	38.20
T82-93	87.50	-23.85	1.32	-13.54	-	-
T82-94	87.25	-23.65	1.02	-11.02	0.10	51.03
T82-95	87.00	-22.81	1.79	-13.34	0.26	31.41
T82-96	86.75	-23.89	1.57	-14.35	0.32	60.38
T82-97	86.50	-23.79	2.36	-13.96	0.27	46.48
T82-98	86.25	-23.20	2.56	-14.01	0.20	61.84
T82-99	86.00	-24.34	1.38	-10.83	0.15	88.81
T82-100	85.75	-23.89	2.45	-12.73	-	-
T82-101	85.50	-23.94	2.55	-12.91	0.16	69.23
T82-102	85.25	-23.69	3.03	-13.06	0.14	86.14
T82-103	85.00	-20.83	1.73	-10.70	0.02	96.94
T82-104	84.75	-23.05	2.25	-10.86	0.01	97.68
T82-105	84.50	-29.07	2.32	-10.54	-	-
T82-106	84.25	-23.73	2.84	-12.48	-	-
T82-107	84.00	-22.93	2.92	-11.56	0.02	96.84
T82-108	83.75	-22.96	1.97	-8.88	0.32	74.35
T82-109	83.50	-23.39	2.84	-9.58	0.29	62.47
T82-110	83.25	-23.68	2.84	-9.87	0.01	98.81
T82-111	83.00	-22.71	2.00	-9.06	0.03	92.11
T82-112	82.75	-22.29	2.32	-9.89	-	-
T82-113	82.50	-25.80	2.52	-9.52	0.01	99.54
T82-114	82.25	-	3.16	-10.37	-	-
T82-115	82.00	-24.96	1.78	-9.34	-	-
T82-116	81.75	-22.90	3.16	-8.59	0.06	99.04
T82-117	81.50	-21.14	2.87	-10.17	0.01	99.52
T82-118	81.25	-21.89	3.04	-9.10	0.01	99.57
T82-119	81.00	-	3.07	-10.53	-	-
T82-120	80.75	-23.35	2.78	-9.75	0.02	98.89
T82-121	80.50	-23.84	2.59	-9.13	0.00	99.85
T82-122	80.25	-23.33	2.22	-9.06	0.02	99.32

T82-123	80.00	-	2.82	-8.92	-	-
T82-124	79.75	24.47	2.90	-9.30	0.02	99.39
T82-125	79.50	-27.34	-	-	0.02	97.51
T82-126	79.25	-27.91	1.50	-8.72	-	-
T82-127	79.00	-23.11	1.32	-8.79	0.01	98.33
T82-128	78.75	-25.32	0.89	-8.97	0.01	98.82
T82-129	78.50	-29.77	-0.22	-7.73	0.04	99.04
T82-130	78.25	-26.73	2.55	-8.83	-	-
T82-131	78.00	-29.05	3.16	-8.27	0.07	99.51
T82-132	77.75	-27.79	3.07	-7.27	0.02	95.41
T82-133	77.50	-22.47	2.62	-8.82	-	-
T82-134	77.25	-22.98	3.24	-9.47	0.06	97.01
T82-135	77.00	-28.23	2.35	-8.88	0.02	99.07
T82-136	76.75	-24.24	1.90	-8.32	-	-
T82-137	76.50	-23.26	2.91	-8.53	0.17	89.41
T82-138	76.25	-23.35	3.18	-8.04	0.15	88.82
T82-139	76.00	-25.80	2.82	-7.76	0.17	86.65
T82-140	75.75	-23.24	2.99	-7.78	0.16	89.77
T82-141	75.50	-22.63	-	-	0.14	88.48
T82-142	75.25	-23.87	3.52	-8.84	0.12	90.95
T82-143	75.00	-23.34	3.21	-9.19	0.09	92.12
T82-144	74.75	-23.10	3.26	-8.44	0.13	90.35
T82-145	74.50	-23.48	3.42	-7.75	0.03	97.55
T82-146	74.25	-23.64	3.19	-8.06	0.07	89.83
T82-147	74.00	-22.14	1.39	-6.35	0.09	95.29
T82-148	73.75	-21.91	-	-	-	-
T82-149	73.50	-22.93	-	-	0.06	92.04
T82-150	73.25	-23.19	3.58	-7.94	0.10	85.41
T82-151	73.00	-23.12	1.24	-5.87	-	-
T82-152	72.75	-23.85	2.81	-7.66	-	-
T82-153	72.50	-22.27	3.14	-7.73	-	-
T82-154	72.25	-23.42	3.33	-8.24	0.13	66.67
T82-155	72.00	-23.56	3.35	-8.04	0.17	49.86
T82-156	71.75	-23.63	3.23	-7.98	0.16	66.20
T82-157	71.50	-23.57	3.07	-8.08	0.09	83.40
T82-158	71.25	-23.73	3.44	-7.92	0.19	55.08
T82-159	71.00	-23.40	3.39	-7.85	0.23	61.34
T82-160	70.75	-23.30	3.51	-7.96	0.20	62.48
T82-161	70.50	-23.36	3.28	-8.08	-	-
T82-162	70.25	-23.44	2.70	-7.20	0.07	94.03
T82-163	70.00	-23.79	3.42	-6.87	0.13	85.28
T82-164	69.75	-23.03	3.50	-7.61	0.11	84.23
T82-165	69.50	-23.50	3.33	-7.48	0.11	66.32
T82-166	69.25	-23.92	3.41	-8.64	0.07	77.49

T82-167	69.00	-	3.41	-7.33	-	-
T82-168	68.75	-22.93	2.74	-7.11	0.05	84.88
T82-169	68.50	-22.68	3.38	-7.06	-	-
T82-170	68.25	-24.14	3.51	-7.00	0.08	87.32
T82-171	68.00	-22.14	2.51	-5.63	0.08	87.03
T82-172	67.75	-23.18	3.38	-6.66	0.09	88.82
T82-173	67.50	-	3.59	-7.08	-	-
T82-174	67.25	-22.94	3.57	-6.68	0.08	90.12
T82-175	67.00	-23.66	3.46	-6.37	0.03	93.49
T82-176	66.75	-23.21	3.22	-6.49	0.02	81.83
T82-177	66.50	-22.33	3.37	-6.59	0.03	92.97
T82-178	66.25	-22.72	3.05	-6.27	0.04	95.04
T82-179	66.00	-23.50	3.22	-6.19	0.02	96.74
T82-180	65.75	-23.61	3.27	-5.96	0.05	94.85
T82-181	65.50	-23.38	2.41	-5.30	0.03	95.89
T82-182	65.25	-23.18	3.53	-5.58	0.03	96.49
T82-183	65.00	-23.13	3.45	-5.78	0.03	95.68
T82-184	64.75	-23.86	3.27	-5.51	0.02	97.01
T82-185	64.50	-25.36	3.24	-5.40	0.04	95.70
T82-186	64.25	-23.92	3.38	-5.37	0.02	95.30
T82-187	64.00	-23.90	3.04	-5.40	0.02	95.85
T82-188	63.75	-24.01	3.23	-5.46	0.03	96.01
T82-189	63.50	-23.82	3.29	-5.27	0.02	97.15
T82-190	63.25	-24.38	3.25	-5.52	0.03	97.18
T82-191	63.00	-25.20	2.96	-5.21	0.03	97.55
T82-192	62.75	-24.00	3.07	-5.13	0.03	97.63
T82-193	62.50	-23.64	2.93	-5.11	0.13	81.75
T82-194	62.25	-24.92	2.81	-5.05	0.03	96.95
T82-195	62.00	-23.62	2.74	-4.87	0.02	97.31
T82-196	61.75	-	-	-	-	-
T82-197	61.50	-24.91	3.08	-5.26	0.02	98.54
T82-198	61.00	-24.78	3.18	-4.82	0.02	98.30
T82-199	60.50	-	-	-	-	-
T82-200	60.00	-24.28	3.11	-5.08	0.03	98.01
T82-201	59.50	-24.37	3.03	-4.83	0.02	91.81
T82-202	59.00	-22.84	3.08	-5.35	0.02	99.09
T82-203	58.50	-24.03	3.14	-6.06	0.01	99.74
T82-204	58.00	-25.13	3.27	-6.46	0.01	99.67
T82-205	57.50	-25.23	2.69	-6.08	0.03	99.16
T82-206	57.00	-24.68	-	-	0.05	99.14
T82-207	56.50	-23.68	3.18	-7.85	0.03	99.44
T82-208	56.00	-23.18	2.95	-7.35	0.02	98.72
T82-209	55.50	-24.16	3.05	-6.73	0.03	97.67
T82-210	55.00	-26.27	2.97	-6.26	0.16	99.71

T82-211	54.50	-24.30	2.88	-6.10	0.01	98.96
T82-212	54.00	-25.05	3.10	-5.84	0.02	99.76
T82-213	53.50	-23.80	2.48	-5.95	0.01	99.45
T82-214	53.00	-25.72	2.51	-6.16	0.01	99.87
T82-215	52.50	-25.16	2.67	-6.26	0.05	99.25
T82-216	52.00	-25.58	2.54	-6.51	0.02	99.83
T82-217	51.50	-25.66	2.65	-6.43	0.02	99.72
T82-218	51.00	-25.15	-	-	0.01	99.83
T82-219	50.50	-24.47	2.54	-6.60	0.01	99.59
T82-220	50.00	-	2.35	-6.51	0.09	98.99
T82-221	49.50	-24.43	2.43	-6.16	0.02	99.83
T82-222	49.00	-25.13	2.42	-6.60	0.06	99.15
T82-223	48.50	-	2.33	-6.29	-	-
T82-224	48.00	-	2.26	-6.31	-	-
T82-225	47.50	-25.53	2.48	-5.73	0.02	99.81
T82-226	47.00	-25.04	-	-	0.01	99.82
T82-227	46.50	-	2.19	-5.81	-	-
T82-228	46.00	-25.66	2.56	-6.43	0.08	98.86
T82-229	45.50	-24.61	1.51	-6.13	0.02	99.74
T82-230	45.00	-24.14	2.48	-6.32	0.02	99.75
T82-231	44.50	-24.70	-	-	0.01	99.95
T82-232	44.00	-25.38	2.53	-6.63	0.01	99.87
T82-233	43.50	-25.56	2.43	-6.48	0.02	99.79
T82-234	43.00	-26.07	2.43	-6.40	0.01	99.81
T82-235	42.50	-23.39	2.56	-6.73	0.08	99.34
T82-236	42.00	-25.94	2.27	-6.40	0.10	98.77
T82-237	41.50	-23.93	2.60	-7.02	0.01	99.93
T82-238	41.00	-24.38	2.55	-6.57	0.04	99.59
T82-239	40.50	-24.83	2.64	-6.97	0.01	99.89
T82-240	40.00	-24.25	2.51	-6.59	0.03	99.78
T82-241	39.50	-24.58	2.52	-6.86	0.01	99.71
T82-242	39.00	-	2.33	-7.04	-	-
T82-243	38.50	-25.06	2.61	-6.97	0.01	99.93
T82-244	38.00	-25.33	2.44	-6.77	0.01	99.92
T82-245	37.50	-25.61	2.21	-6.78	0.00	99.98
T82-246	37.00	-25.62	2.11	-6.85	0.01	99.95
T82-247	36.50	-25.44	2.58	-6.85	0.01	99.92
T82-248	36.00	-25.74	2.49	-6.87	0.01	99.88
T82-249	35.50	-25.60	2.58	-6.69	0.02	99.92
T82-250	35.00	-22.49	1.90	-6.63	0.01	99.93
T82-251	34.50	-25.42	2.27	-6.98	0.01	99.86
T82-252	34.00	-	2.60	-7.62	-	-
T82-253	33.50	-24.95	2.61	-7.69	0.02	99.86
T82-254	33.00	-25.06	2.63	-7.67	0.03	99.83

T82-255	32.50	-23.31	2.53	-8.01	0.01	99.89
T82-256	32.00	-23.97	2.61	-7.93	0.02	99.82
T82-257	31.50	-25.00	2.74	7.58	0.04	99.63
T82-258	31.00	-	-	-	-	-
T82-259	30.50	-25.07	2.65	-7.72	0.02	99.86
T82-260	30.00	-24.10	2.85	-7.86	0.01	99.85

BarrickGold Sample no.	**Thick-ness (m)**	**$\delta^{13}C_{OM}$ (‰)**	**$\delta^{13}C_{CARB}$ (‰)**	**$\delta^{18}O_{CARB}$ (‰)**	**TOM**	**%CARB**
BG_01	0.25	-27.86	2.73	-6.98	-	-
BG_02	0.5	-26.04	2.82	-6.75	-	-
BG_03	0.75	-26.02	2.69	-7.11	-	-
BG_04	1	-26.50	2.76	-7.06	-	-
BG_05	1.25	-24.34	2.65	-7.38	-	-
BG_06	1.5	-25.10	2.48	-7.40	-	-
BG_07	1.75	-26.88	2.80	-6.86	-	-
BG_08	2	-25.94	2.75	-6.75	-	-
BG_09	2.25	-28.10	2.88	-6.98	-	-
BG_10	2.5	-26.59	2.62	-7.23	-	-
BG_11	2.75	-	2.74	-6.81	-	-
BG_12	3	-26.97	2.86	-6.95	-	-
BG_13	3.25	-25.03	2.78	-6.86	-	-
BG_14	3.5	-26.88	2.82	-6.84	-	-
BG_15	3.75	-26.13	2.80	-7.00	-	-
BG_16	4	-24.59	2.63	-6.85	-	-
BG_17	4.25	-25.08	2.77	-6.87	-	-
BG_18	4.5	-22.68	2.29	-6.63	-	-
BG_19	4.75	-27.02	2.79	-7.21	-	-
BG_20	5	-	2.97	-7.09	-	-
BG_21	5.25	-26.67	2.70	-6.73	-	-
BG_22	5.5	-26.28	2.87	-6.95	-	-
BG_23	5.75	-25.76	-	-	-	-
BG_24	6	-	3.03	-7.31	-	-
BG_25	6.25	-27.04	2.94	-7.26	-	-
BG_26	6.5	-26.56	2.92	-7.34	-	-
BG_27	6.75	-	-	-	-	-
BG_28	7	-25.37	2.60	-7.18	-	-
BG_29	7.25	-28.33	2.77	-7.01	-	-
BG_30	7.5	-25.76	-	-	-	-
BG_31	7.75	-26.02	2.54	-7.22	-	-
BG_32	8	-25.66	2.60	-7.29	-	-
BG_33	8.25	-25.87	1.47	-6.77	-	-

BG_34	8.5	-25.16	2.17	-7.78	-	-
BG_35	8.75	-	-	-	-	-
BG_36	9	-24.31	2.41	-7.34	-	-
BG_37	9.25		2.33	-7.80	-	-
BG_38	9.5	-26.87	1.30	-6.79	-	-
BG_39	9.75	-25.57	2.40	-7.68	-	-
BG_40	10	-25.18	2.51	-7.45	-	-
BG_41	10.25	-26.56	-	-7.01	-	-
BG_42	10.5	-25.39	2.60	-7.59	-	-
BG_43	10.75	-	2.40	-6.25	-	-
BG_44	11	-25.08	2.44	-6.70	-	-
BG_45	11.25	-26.47	2.40	-6.82	-	-
BG_46	11.5	-24.61	2.31	-6.52	-	-
BG_47	11.75	-26.41	-	-	-	-
BG_48	12	-25.81	2.36	-6.41	-	-
BG_50	12.5	-26.06	2.22	-6.51	-	-
BG_51	12.75	-23.45	2.25	-6.64	-	-
BG_52	13	-25.32	2.35	-6.51	-	-
BG_53	13.25	-25.50	-	-	-	-
BG_54	13.5	-25.38	2.30	-6.56	-	-
BG_55	13.75	-25.75	2.28	-6.67	-	-
BG_56	14	-24.93	2.36	-6.43	-	-
BG_57	14.5	-27.15	2.35	-7.04	-	-
BG_59	14.75	-23.80	2.09	-7.31	-	-
BG_60	15	-25.26	2.35	-6.70	-	-
BG_61	15.25	-	-	-	-	-
BG_62	15.5	-	-	-	-	-
BG_63	15.75	-25.12	2.23	-6.84	-	-
BG_64	16	-25.95	2.38	-6.77	-	-
BG_65	16.25	-25.96	2.42	-6.89	-	-
BG_66	16.5	-25.96	2.35	-6.22	-	-
BG_82	16.75	-25.72	2.29	-7.00	-	-
BG_83	17	-25.83	2.15	-6.74	-	-
BG_84	17.25	-24.32	2.17	-6.93	-	-
BG_85	17.5	-25.78	2.20	-6.88	-	-
BG_86	17.75	-26.21	2.20	-6.90	-	-
BG_87	18	-25.00	2.37	-6.75	-	-
BG_88	18.25	-25.89	2.29	-6.86	-	-
BF_90	18.5	-	-	-	-	-

103 Sample no.	Depth (m)	$\delta^{13}C_{OM}$ (‰)	$\delta^{13}C_{CARB}$ (‰)	$\delta^{18}O_{CARB}$ (‰)	TOM	%CARB
HM_01	0.25	-23.78	3.19	-4.39	94.35	0.09
HM_02	0.50	-23.24	2.93	-4.47	97.43	0.04
HM_03	0.75	-22.76	2.82	-4.28	95.76	0.05
HM_05	1.25	-22.62	3.08	-4.43	95.38	0.05
HM_06	1.50	-22.04	3.20	-5.09	95.93	0.05
HM_07	1.75	-22.66	3.21	-4.62	98.10	0.04
HM_08	2.00	-23.26	3.19	-5.15	98.65	0.03
HM_09	2.25	-22.72	3.18	-4.60	99.27	0.02
HM_10	2.50	-23.26	3.05	-4.82	98.96	0.03
HM_11	2.75	-22.47	3.21	-4.85	99.20	0.03
HM_12	3.00	-23.32	3.20	-5.37	98.80	0.04
HM_13	3.25	-23.40	3.11	-4.58	99.35	0.04
HM_14	3.50	-23.14	3.10	-5.53	99.37	0.03
HM_15	3.75	-	-	-	-	-
HM_16	4.00	-23.32	2.95	-4.94	99.29	0.03
HM_17	4.25	-23.36	2.95	-4.90	99.28	0.03
HM_18	4.50	-23.78	2.87	-6.36	98.43	0.04
HM_19	4.75	-23.75	2.77	-4.79	99.02	0.04
HM_20	5.00	-23.84	2.67	-6.64	98.27	0.04
HM_21	5.25	-22.62	2.99	-5.09	98.44	0.03
HM_22	5.50	-22.82	2.96	-4.63	99.28	0.03
HM_23	5.75	-23.14	1.54	-5.16	97.04	0.02
HM_24	6.00	-24.21	2.41	-4.97	97.73	0.05
HM_25	6.25	-24.36	2.30	-5.21	98.53	0.04
HM_26	6.50	-23.29	2.31	-5.17	98.17	0.05
HM_27	6.75	-23.67	2.16	-6.99	95.62	0.03
HM_28	7.00	-23.33	2.49	-5.88	98.04	0.05
HM_29	7.25	-23.74	2.20	-5.70	97.14	0.06
HM_30	7.50	-24.53	2.16	-5.88	99.27	0.02
HM_31	7.75	-23.99	1.94	-5.77	99.44	0.04
HM_32	8.00	-	2.30	-	-	-
HM_33	8.25	-23.34	2.24	-6.14	98.95	0.04
HM_34	8.50	-23.76	2.10	-6.14	99.37	0.03
HM_35	8.75	-	-	-	-	-
HM_36	9.00	-24.13	2.16	-6.56	99.24	0.04
HM_37	10.00	-	1.86	-	-	-
HM_38	10.25	-23.77	1.37	-5.41	97.98	0.05
HM_39	10.50	-24.89	2.56	-4.79	98.59	0.07
HM_41	10.75	-23.78	2.39	-6.01	98.54	0.04
HM_42	11.00	-23.76	2.41	-7.46	99.36	0.02
HM_44	11.25	-24.08	2.05	-6.65	98.85	0.04

HM_45	11.50	-24.14	2.00	-5.17	99.37	0.04
HM_46	11.75	-23.07	2.40	-5.12	99.73	0.03
HM_47	12.00	-23.55	2.35	-4.98	99.50	0.05

Appendix C - Analytical results of trace elements and strontium isotope from the low-Mg calcite of Late Cretaceous rudist bivalves

Puerto Rico Sample no.	Sr (ppm)	Mg (ppm)	Fe (ppm)	Mn (ppm)	$^{87}Sr/^{86}Sr$
CL-01-1	1347	2551	bdl	bdl	0.707454
CL-01-2	764	3219	-	206	-
CL-01-3	318	1739	-	406	-
GL01-01	2057	bdl	bdl	bdl	
GL01-02	1974	43	bdl	bdl	0.707464
GL01-03	2181	bdl	bdl	bdl	-
GL01-04	2005	bdl	bdl	bdl	0.707456
GL01-05	1993	bdl	bdl	bdl	-
GL01-06	1816	465	bdl	bdl	-
GL01-07	2178	bdl	bdl	bdl	-
					-
GL02-01	1716	2008	55	bdl	0.707454
GL02-02	1601	1915	37	bdl	0.707464
GL02-03	1564	1559	92	-	-
GL02-04	1722	2138	68	-	-
GL02-05	1579	1634	79	-	-
GL02-06	1268	668	63	-	-
GL02-07	1592	1141	63	-	-
GL03-01	674	5991	59	330	
GL03-02	667	6464	48	372	
GL03-03	588	5627	78	bdl	
GL03-04	472	4140		bdl	
GL03-05	467	4564		bdl	
GL03-06	501	4088		bdl	
GL03-07	471	4644		bdl	
GL03-08	524	4702		bdl	
GL03-09	407	3916		bdl	
GL03-10	463	4785		319	
GL03-11	502	4790		bdl	
GL03-12	463	4523		bdl	
GL03-13	441	4120			

Appendix D - Analytical results of $\delta^{13}C$ and $\delta^{18}O$ from sclerochronological profiles

Sample Label	$\delta^{13}C$ VPDB	$\delta^{18}O$ VPDB
GL01-01	2.43	-4.86
GL01-02	2.12	-5.27
GL01-03	1.89	-6.24
GL01-04	2.39	-6.18
GL01-05	2.27	-6.15
GL01-06	2.34	-5.56
GL01-07	2.56	-6.35
GL01-08	2.64	-5.05
GL01-09	2.74	-4.47
GL01-10	2.71	-6.06
GL01-11	2.63	-4.98
GL01-12	2.28	-6.80
GL01-13	1.75	-4.99
GL01-14	2.45	-4.98
GL01-15	2.45	-5.50
GL01-16	2.46	-4.58
GL01-17	2.56	-4.34
GL01-18	2.57	-4.14
GL01-19	2.45	-5.31
GL01-20	2.20	-4.66
GL01-21	2.60	-4.54
GL01-22	2.62	-5.38
GL01-23	1.93	-4.78
GL01-24	1.87	-5.16
GL01-25	2.12	-6.23
GL01-26	1.48	-4.80
GL01-28	2.10	-4.63
GL01-29	2.53	-4.88
GL01-30	2.46	-4.01
GL01-31	2.39	-4.44
GL01-32	2.44	-4.54
GL01-33	2.45	-4.33
GL01-34	2.38	-4.62
GL01-35	2.42	-4.48
GL01-36	2.44	-4.84
GL01-37	2.59	-4.85
GL01-38	2.60	-4.55
GL01-39	2.68	-4.95
GL01-40	2.53	-4.40

GL01-41	2.37	-4.66
GL01-42	2.40	-4.54
GL01-43	2.37	-4.50
GL01-44	2.03	-4.90
GL01-45	2.12	-4.57
GL01-46	2.42	-4.31
GL01-47	2.36	-4.41
GL01-48	2.33	-4.18
GL01-49	2.31	-4.38
GL01-50	2.31	-4.88
GL01-51	2.34	-4.30
GL01-52	2.43	-4.37
GL01-53	2.30	-5.47
GL01-54	2.43	-4.26
GL01-55	2.51	-4.72
GL01-56	2.65	-4.16
GL01-57	1.46	-4.96
GL01-58	-	-
GL01-59	2.59	-5.06
GL01-60	2.43	-4.40
GL01-61	2.46	-4.58
GL01-62	2.47	-4.35
GL01-63	2.48	-4.53
GL01-64	2.49	-4.57
GL01-65	2.52	-4.48
GL01-66	2.43	-4.57
GL01-67	2.48	-4.25
GL01-68	2.46	-4.15
GL01-69	2.46	-5.12
GL01-70	2.33	-4.15
GL01-71	2.45	-3.87
GL01-72	2.31	-4.17
GL01-73	2.33	-4.23
GL01-74	2.31	-4.30
GL01-75	2.42	-4.44
GL01-76	2.49	-4.43
GL01-77	2.39	-4.44
GL01-78	2.43	-4.48
GL01-79	2.54	-4.38
GL01-80	2.39	-4.17
GL02-01	2.54	-2.25
GL02-02	2.59	-2.21
GL02-03	2.40	-2.30

GL02-04	2.43	-2.73
GL02-05	2.09	-3.53
GL02-06	2.36	-3.39
GL02-07	2.42	-3.23
GL02-08	2.38	-3.27
GL02-09	2.20	-3.88
GL02-10	2.28	-4.15
GL02-11	2.36	-3.92
GL02-12	2.49	-3.84
GL02-13	2.40	-3.18
GL02-14	2.34	-3.43
GL02-15	2.42	-3.34
GL02-16	2.36	-3.88
GL02-17	2.32	-4.26
GL02-18	2.33	-3.72
GL02-19	2.28	-3.57
GL02-20	2.27	-3.98
GL02-21	2.39	-4.28
GL02-22	2.27	-4.19
GL02-23	2.14	-4.19
GL02-24	2.22	-3.59
GL02-25	2.28	-3.33
GL02-26	2.41	-3.49
GL02-27	2.25	-3.85
GL02-28	2.26	-4.16
GL02-29	2.09	-4.17
GL02-30	2.28	-3.04
GL02-31	2.26	-3.32
GL02-32	2.23	-3.49
GL02-33	2.35	-4.10
GL02-34	2.33	-3.70
GL02-35	2.17	-3.39
GL02-36	1.98	-4.99
GL02-37	2.33	-4.07
GL02-38	2.46	-5.39
GL02-39	2.02	-4.17
GL02-40	1.99	-3.45
GL02-41	2.52	-4.97
GL02-42	1.75	-4.20
GL02-43	1.60	-5.09
GL02-44	2.11	-4.01
GL02-45	1.61	-4.80
GL02-46	1.59	-5.30
GL02-47	1.83	-5.31

GL02-48	1.50	-5.20
GL02-49	1.63	-4.77
GL02-50	1.46	-4.80
GL02-51	1.44	-4.77
GL02-52	1.49	-5.23
GL02-53	1.76	-5.12
GL02-54	1.85	-4.47
GL02-55	2.24	-3.70
GL02-56	1.94	-4.00
GL02-57	2.05	-3.55
GL02-58	1.86	-4.15
GL02-59	1.93	-4.21
GL02-60	2.19	-3.34
GL02-61	2.46	-3.36
GL02-62	2.44	-3.55
GL02-63	2.30	-2.94
GL02-64	2.28	-2.67
GL02-65	2.05	-3.95
GL02-66	1.84	-4.58
GL02-67	1.96	-4.09
GL02-68	1.82	-4.73
GL02-69	1.89	-4.56
GL02-70	1.91	-4.34
GL02-71	1.70	-4.50
GL02-72	1.96	-4.84
GL02-73	1.86	-4.05
GL02-74	1.84	-4.36
GL02-75	1.95	-3.91
GL02-76	1.83	-3.62
GL02-77	1.93	-3.17
GL02-78	1.97	-3.38
GL02-79	2.11	-3.64
GL02-80	2.16	-3.08
GL02-81	2.43	-3.09
GL02-82	2.42	-1.78
GL02-83	2.52	-2.21
GL02-84	2.47	-2.59
GL02-85	2.35	-2.99
GL03-01	2.13	-4.42
GL03-02	2.08	-4.41
GL03-03	2.06	-4.25
GL03-04	2.12	-4.36
GL03-05	2.14	-4.07

GL03-06	2.05	-3.99
GL03-07	2.07	-4.34
GL03-08	2.18	-4.02
GL03-09	2.19	-4.22
GL03-10	2.30	-4.14
GL03-11	2.34	-4.57
GL03-12	2.42	-4.23
GL03-13	2.47	-4.16
GL03-14	2.44	-3.95
GL03-15	2.45	-4.28
GL03-16	2.40	-4.19
GL03-17	2.40	-4.26
GL03-18	2.48	-4.18
GL03-19	2.49	-4.46
GL03-20	2.48	-4.52
GL03-21	2.59	-4.21
GL03-22	2.74	-4.39
GL03-23	2.73	-4.24
GL03-24	2.51	-4.34
GL03-25	2.48	-4.67
GL03-26	2.47	-4.33
GL03-27	2.44	-4.31
GL03-28	2.47	-4.36
GL03-29	2.47	-4.28
GL03-30	2.48	-4.48
GL03-31	2.66	-4.24
GL03-32	2.63	-4.52
GL03-33	2.59	-4.19